Targeting FTO Suppresses Cancer Stem Cell Maintenance and Immune Evasion

Article *in* Cancer Cell · June 2020

DOI: 10.1016/j.ccell.2020.04.017

Cancer Cell

Article

Targeting FTO Suppresses Cancer Stem Cell Maintenance and Immune Evasion

Graphical Abstract

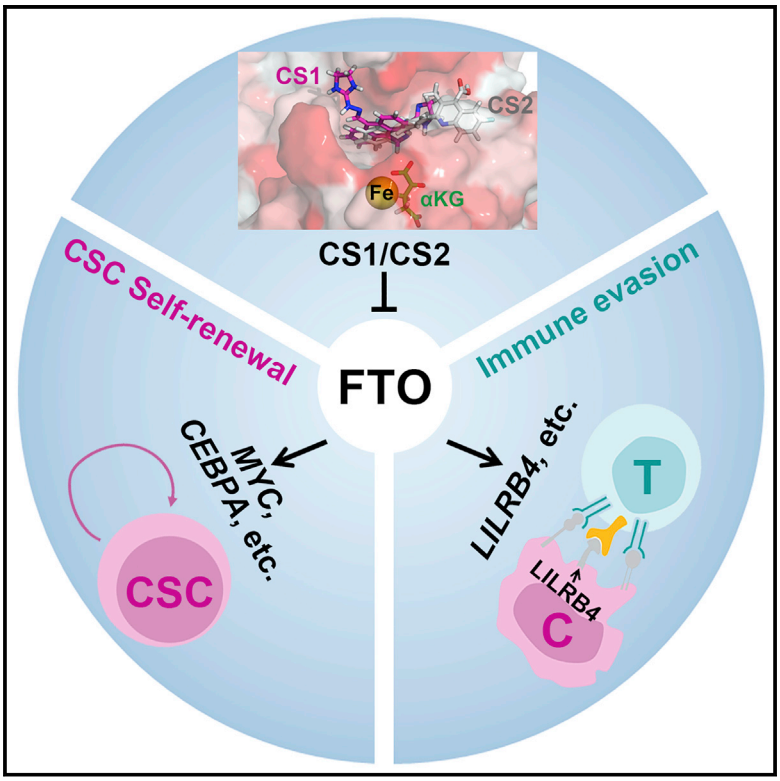

Authors

Rui Su, Lei Dong, Yangchan Li, ..., Minjie Wei, David Horne, Jianjun Chen

Correspondence

jianchen@coh.org

In Brief

Su et al. develop two potent small-molecule inhibitors against an RNA N6-methyladenosine demethylase called FTO. FTO inhibition shows anti-tumor effects in several types of cancers in mouse models by restricting self-renewal of cancer stem cells and suppressing immune evasion.

Highlights

- Development of two potent FTO inhibitors with IC_{50} values in the low nanomolar range
- KD of *FTO* or pharmacological inhibition of FTO suppresses LSC/LIC self-renewal
- Targeting FTO suppresses immune checkpoint gene expression and immune evasion
- Targeting FTO by potent inhibitors holds therapeutic promise against various cancers

Su et al., 2020, Cancer Cell *38*, 79–96
July 13, 2020
https://doi.org/10.1016/j.ccell.2020.04.017

CellPress

Cancer Cell

CellPress

Article

Targeting FTO Suppresses Cancer Stem Cell Maintenance and Immune Evasion

Rui Su,[1,17] Lei Dong,[1,17] Yangchan Li,[1,10,17] Min Gao,[1,11,17] Li Han,[1,2,17] Mark Wunderlich,[3] Xiaolan Deng,[1] Hongzhi Li,[4] Yue Huang,[6] Lei Gao,[1,12] Chenying Li,[1,13] Zhicong Zhao,[1,16] Sean Robinson,[1] Brandon Tan,[1] Ying Qing,[1] Xi Qin,[1] Emily Prince,[1] Jun Xie,[4] Hanjun Qin,[5] Wei Li,[1] Chao Shen,[1] Jie Sun,[7] Prakash Kulkarni,[8] Hengyou Weng,[1] Huilin Huang,[1] Zhenhua Chen,[1] Bin Zhang,[7,9] Xiwei Wu,[5] Mark J. Olsen,[14] Markus Müschen,[1,9] Guido Marcucci,[7,9] Ravi Salgia,[8] Ling Li,[7,9] Amir T. Fathi,[15] Zejuan Li,[12] James C. Mulloy,[3] Minjie Wei,[2] David Horne,[4] and Jianjun Chen[1,9,18,*]

[1]Department of Systems Biology, Beckman Research Institute of City of Hope, Monrovia, CA 91016, USA
[2]School of Pharmacy, China Medical University, Shenyang, Liaoning 110001, China
[3]Division of Experimental Hematology and Cancer Biology, Cincinnati Children's Hospital Medical Center, Cincinnati, OH 45229, USA
[4]Department of Molecular Medicine, Beckman Research Institute of City of Hope, Duarte, CA 91010, USA
[5]The Integrative Genomics Core, Beckman Research Institute, City of Hope Medical Center, Duarte, CA 91010, USA
[6]State Key Laboratory of Drug Research, Shanghai Institute of Materia Medica, Chinese Academy of Sciences, Shanghai 201203, China
[7]Department of Hematologic Malignancies Translational Science, Beckman Research Institute of City of Hope, Monrovia, CA 91016, USA
[8]Department of Medical Oncology and Therapeutics Research, City of Hope, Duarte, CA 91010, USA
[9]City of Hope Comprehensive Cancer Center and Gehr Family Center for Leukemia Research, City of Hope, Duarte, CA 91010, USA
[10]Department of Radiation Oncology, The First Affiliated Hospital of Sun Yat-sen University, Guangzhou, Guangdong 510080, China
[11]School of Pharmaceutical Science and Technology, Tianjin Key Laboratory for Modern Drug Delivery and High Efficiency, and Collaborative Innovation Center of Chemical Science and Engineer (Tianjin), Tianjin University, Tianjin 300072, China
[12]Department of Pathology and Genomic Medicine, Houston Methodist, Houston, TX 77030, USA
[13]Department of Hematology, The First Affiliated Hospital, Zhejiang University, Hangzhou, Zhejiang 31003, China
[14]Department of Pharmaceutical Sciences, College of Pharmacy-Glendale, Midwestern University, Glendale, AZ 85308, USA
[15]Massachusetts General Hospital Cancer Center, Harvard Medical School, Boston, MA 02114, USA
[16]Department of Liver Surgery, Renji Hospital, Shanghai Jiao Tong University School of Medicine, Shanghai 200127, China
[17]These authors contributed equally
[18]Lead Contact
*Correspondence: jianchen@coh.org
https://doi.org/10.1016/j.ccell.2020.04.017

SUMMARY

Fat mass and obesity-associated protein (FTO), an RNA N^6-methyladenosine (m^6A) demethylase, plays oncogenic roles in various cancers, presenting an opportunity for the development of effective targeted therapeutics. Here, we report two potent small-molecule FTO inhibitors that exhibit strong anti-tumor effects in multiple types of cancers. We show that genetic depletion and pharmacological inhibition of FTO dramatically attenuate leukemia stem/initiating cell self-renewal and reprogram immune response by suppressing expression of immune checkpoint genes, especially *LILRB4*. FTO inhibition sensitizes leukemia cells to T cell cytotoxicity and overcomes hypomethylating agent-induced immune evasion. Our study demonstrates that FTO plays critical roles in cancer stem cell self-renewal and immune evasion and highlights the broad potential of targeting FTO for cancer therapy.

INTRODUCTION

Among the >170 modified RNA nucleotides, N^6-methyladenosine (m^6A) represents the most abundant and prevalent internal modification in eukaryotic mRNA (Boccaletto et al., 2018; Frye et al., 2018). Fat mass and obesity-associated protein (FTO) was identified as the first RNA demethylase that can remove m^6A from RNA through an α-ketoglutarate (α-KG) and

Significance

Targeting FTO suppresses cancer stem cell self-renewal and exhibits promising therapeutic effects against acute myeloid leukemia and various solid tumors. Pharmacological inhibition or genetic depletion of FTO reprograms immune response and augments T cell toxicity by targeting *LILRB4*.

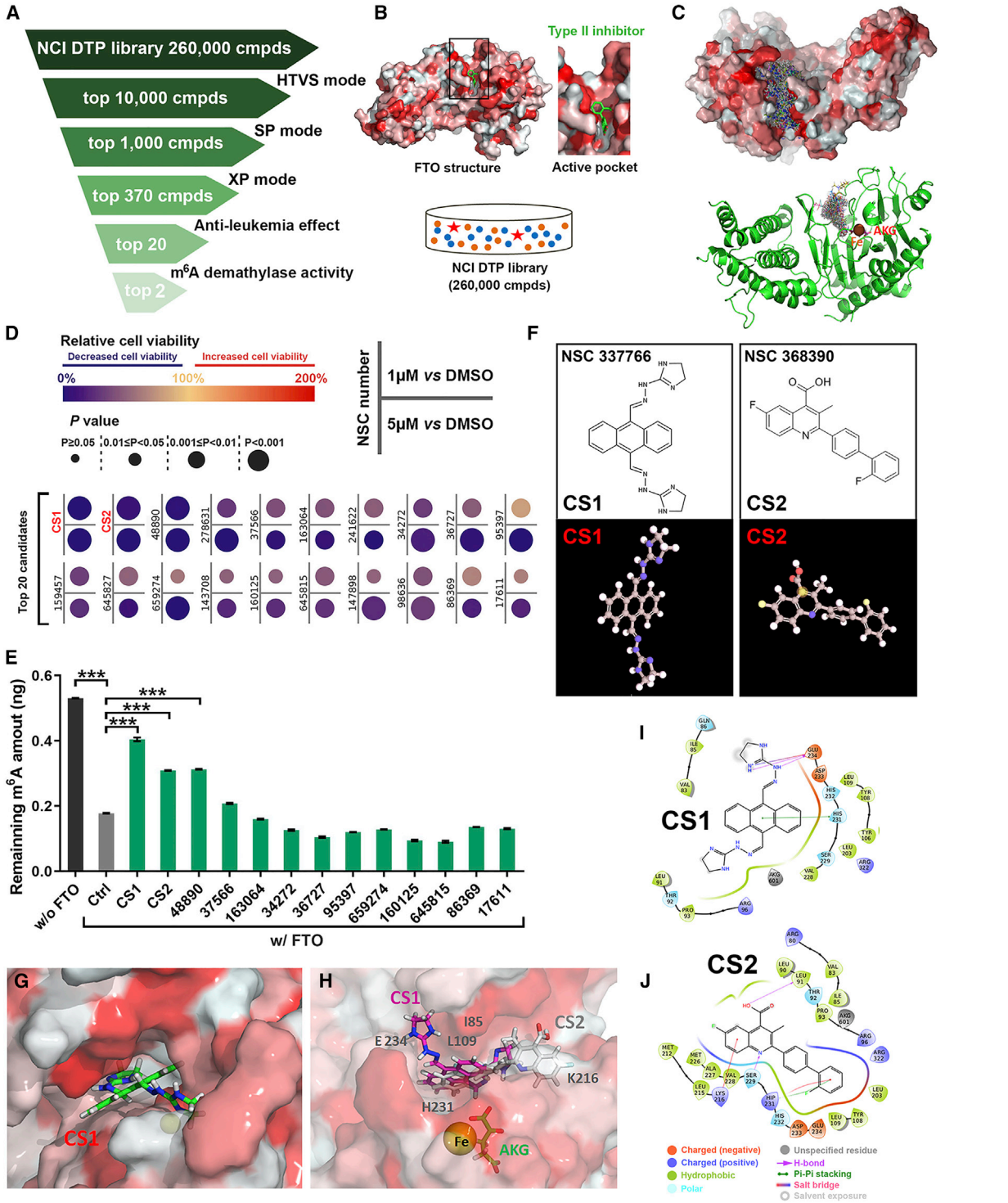

Figure 1. Identification of FTO Inhibitors through Structure-Based Virtual Screening and Validation Assays

(A) Pyramid flowchart of the pipeline to identify FTO inhibitors from the NCI DTP library.

(B) Docking models were developed based on FTO crystal structure and the 260,000 compounds from the NCI DTP library.

(C) Docking pose of the top 370 hits within the catalytic center of FTO protein.

(D) Effects of top 20 compounds on cell viability in MONOMAC 6.

(E) Effects of top 20 compounds on the enzymatic activity of FTO.

(legend continued on next page)

Fe(II)-dependent mechanism (Jia et al., 2011), suggesting that m^6A is a type of reversible and dynamic RNA modification (Jia et al., 2013). Recently, we reported that FTO is overexpressed and plays a critical role in leukemia as an m^6A demethylase (Li et al., 2017). Subsequently, we showed that FTO is a target of R-2-hydroxyglutarate (R-2HG) and by suppression of FTO activity, R-2HG displays intrinsic anti-leukemia effects (Su et al., 2018). In addition, the aberrant overexpression and potential oncogenic roles of FTO have also been reported in multiple solid tumors (Niu et al., 2019; Tang et al., 2019; Yang et al., 2019). Thus, these data suggest that FTO is a promising therapeutic target. Better understanding of the mechanisms underlying FTO's functions in cancers and development of effective targeted therapeutics against FTO are warranted.

A set of specific or non-specific FTO inhibitors, such as rhein, meclofenamic acid (MA), MO-I-500, fluorescein, and R-2HG, have been identified (Chen et al., 2012; He et al., 2015; Huang et al., 2015; Padariya and Kalathiya, 2016; Singh et al., 2016; Su et al., 2018; Toh et al., 2015; Wang et al., 2015; Zheng et al., 2014). However, all these small molecules are limited in clinical potential due to mild biological function and low sensitivity and/or specificity (Huang et al., 2019). More recently, two derivatives of MA, termed FB23 and FB23-2, have been developed, which showed improved efficacy in inhibiting FTO activity and viability of human acute myeloid leukemia (AML) cells. Nonetheless, their IC_{50} values in inhibiting AML cell viability are still >1 μM (FB23-2) or even >20 μM (FB23) (Huang et al., 2019). While FB23-2 showed a statistically significant effect on inhibiting the progression of human primary AML in mice, which provides proof-of-concept evidence indicating the therapeutic potential of pharmacological targeting FTO in treating AML, the inhibitory degree was not satisfactory. Thus, there is still an urgent and unmet need to develop efficacious inhibitors against FTO to treat AML and other cancers.

Here, through a series of screening and validation assays, we identified two potent small-molecule FTO inhibitors. Our further studies revealed the significant effects and the underlying mechanisms of targeting FTO on suppressing cancer stem cell self-renewal and immune evasion, highlighting the broad potential of targeting FTO for cancer therapy.

RESULTS

Identification of Effective FTO Inhibitors

To identify potential FTO inhibitors, we conducted a structure-based virtual screening of the 260,000 compounds from the National Cancer Institute Developmental Therapeutics Program (NCI DTP) library (see STAR Methods for details). We requested from NCI the top 370 candidate compounds that showed the highest scores based on their docking to FTO's catalytic pocket (Figures 1A–1C), but only 213 compounds were available. We then assessed their anti-leukemic efficacy in the human MONOMAC 6 AML cell line (carrying t(9; 11)/*MLL-AF9*) via MTT (3-[4,5-dimethylthiazol-2-yl]-2,5-diphenyltetrazolium bromide) cell proliferation/viability assays (Figure S1A). The top 20 compounds showing the most robust inhibitory effects on MONOMAC 6 cell viability (Figure 1D) were selected and further validated in two additional AML cell lines (NOMO-1 and U937; Figure S1B). We also assessed their efficacy on inhibition of FTO's m^6A demethylase activity through cell-free m^6A demethylase assays (Figure 1E). We identified three compounds (CS1, CS2, and NSC 48890) that display consistently robust effects on inhibition of AML cell viability and FTO's demethylase activity. Due to the overly simplistic structure of NSC 48890 (unlikely a selective inhibitor) (Figure S1C), we decided to focus on CS1 and CS2 (Figure 1F) for further studies.

Our docking models suggest that both CS1 and CS2 bind tightly to FTO protein and block its catalytic pocket (Figures 1G–1J, S1D, and S1E). Additionally, based on the crystal structure of FTO-oligonucleotide complex (Zhang et al., 2019), we found that CS1/2 interact with FTO residues that were known to be involved in the binding of FTO with m^6A modified single-strand DNA (Zhang et al., 2019), such as HIS231 and GLU234 by CS1, and LYS216, SER229, and HIS231 by CS2 (Figures 1H–1J and S1F–S1H). These data suggest that CS1 and CS2 selectively bind to and occupy the catalytic pocket of FTO and thereby block m^6A-modified oligos from entering into FTO's catalytic pocket, which in turn inhibits FTO's demethylase activity and its binding with the target RNA transcripts.

CS1 and CS2 Are Highly Efficacious FTO Inhibitors with Potent Anti-leukemic Efficacy *In Vitro*

Compared with two previously reported FTO inhibitors (FB23-2 and MO-I-500) (Huang et al., 2019; Zheng et al., 2014), CS1 and CS2 displayed a much higher efficacy in inhibiting AML cell viability, with 10- to 30-fold lower IC_{50} (half-maximal inhibitory concentration) values in AML cells (Figures S2A and S2B), indicating their greatly improved efficacy. We then determined their IC_{50} values in a panel of leukemia cell lines with high or low levels of *FTO* expression (Li et al., 2017; Su et al., 2018). As expected, the FTO-high leukemia lines showed lower IC_{50} values than the FTO-low cell lines (Figures 2A and 2B). Knockdown (KD) of *FTO* in FTO-high AML cells reduced their sensitivity to CS1 and CS2 (Figures S2C and S2D). These results suggest that the anti-leukemia effects of CS1 and CS2 are FTO-abundance dependent. Both CS1 and CS2 significantly inhibited the viability of human primary AML cells, but largely spared the healthy control cells (Figures 2C and 2D), highlighting their therapeutic potential in treating leukemia patients.

The direct interactions between CS1/2 and FTO protein were confirmed by a biophysical method, nuclear magnetic resonance (NMR). CS1 and CS2-induced dose-dependent attenuation of signals were observed in Carr-Purcell-Meiboom-Gill (CPMG) NMR titration, and positive saturation transfer signals (STD) were also detected (Figures 2E–2H), demonstrating their direct binding with FTO *in vitro* (i.e., in a cell-free system). Drug

(F) Two-dimensional (2D) structure (upper panel) and three-dimensional (3D) conformer (lower panel) of CS1 and CS2.
(G) Binding model of CS1 in FTO catalytic pocket.
(H) CS1/FTO and CS2/FTO binding models.
(I and J) 2D ligand interaction diagrams for CS1/FTO (I) and CS2/FTO (J).
Data are presented as mean ± SEM from three independent experiments. ***$p < 0.001$. See also Figure S1.

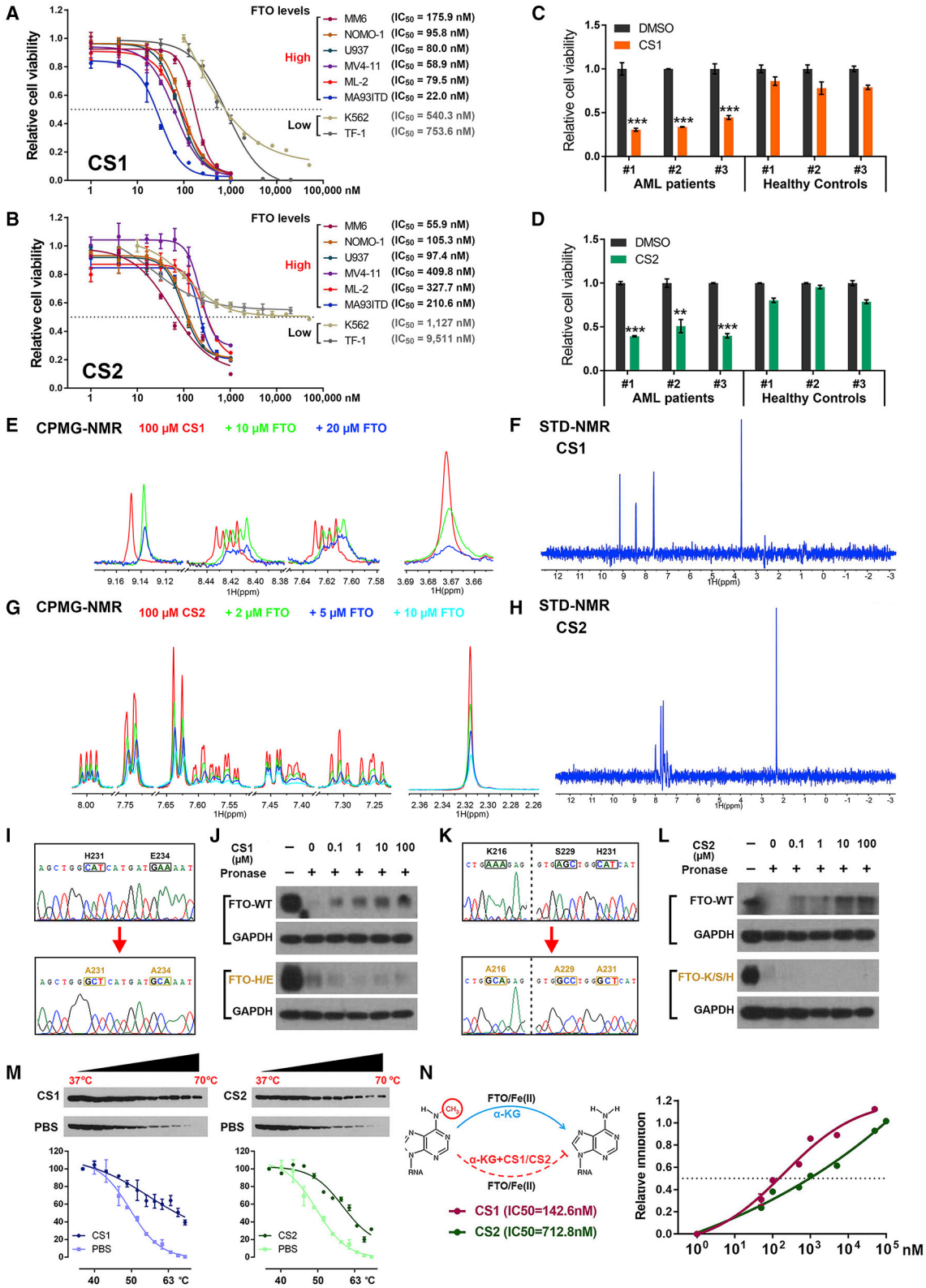

Figure 2. The Anti-leukemic Efficacy of CS1 and CS2 Is FTO Dependent

(A and B) IC_{50} values of CS1 (A) and CS2 (B) on inhibiting cell viability in AML cell lines. The cells were treated for 72 h.

(C and D) Effects of CS1 (100 nM, 48 h; C) and CS2 (200 nM, 48 h; D) on cell viability in $CD34^+$ cells of AML patients and healthy donors.

(legend continued on next page)

affinity responsive target stability (DARTS) (Lomenick et al., 2009) assay and cellular thermal shift assay (CETSA) (Jafari et al., 2014) were conducted to confirm their direct interactions in AML cells. According to the docking poses of CS1/2 and FTO protein (see Figures 1I and 1J), residues H231 and E234 are essential for the binding of FTO with CS1, while K216, S229, and H231 are crucial for its binding with CS2. CS1 and CS2 could block pronase-induced proteolysis of wild-type (WT) FTO but not that of mutant FTO$^{H231A/E234A}$ or FTO$^{K216A/S229A/H231A}$ (Figures 2I–2L). Such data confirmed that FTO bind directly with CS1 and CS2 *in cellulo*, and the mutated amino acids are essential for their interactions. In addition, both CS1 and CS2 treatment led to substantial shifts of the thermal stability of FTO protein (Figure 2M), which further confirmed their direct interactions. Through cell-free m^{6}A demethylase assays, we showed that both CS1 and CS2 efficiently suppressed m^{6}A demethylase activity of FTO, with IC_{50} values in the nanomolar range (Figures 2N and S2E).

Since the residues K216, S229, H231, and E234 of FTO are essential for the bindings of FTO with both CS1/2 (Figures 2I–2L) and m^{6}A-modified oligonucleotides (Zhang et al., 2019), we presumed that CS1 and CS2 could disrupt the binding of FTO with its target RNAs. Indeed, our crosslinking immunoprecipitation-qPCR data confirmed that CS1 and CS2 block the binding of FTO with its known target mRNAs, such as *MYC*, *CEBPA*, and *RARA* (Li et al., 2017; Su et al., 2018) (Figures S2F–S2H). In addition, CS1 and CS2 treatment notably increased global m^{6}A abundance in AML cells (Figure S2I) but had no noticeable effect on the FTO protein level (Figure S2J). Neither CS1 nor CS2 treatment suppressed the enzymatic activity of ALKBH5, another major m^{6}A demethylase (Zheng et al., 2013), or TET1, another α-KG-dependent dioxygenase (Figures S2K and S2L), highlighting the selectivity of CS1 and CS2 against FTO.

Effects of FTO KD and Inhibition on AML Cell Viability and Differentiation and on Leukemia Stem/Initiating Cell Self-Renewal

Consistent with the effects of *FTO* KD (Li et al., 2017), we showed that pharmacological inhibition of FTO by CS1 or CS2 resulted in substantially increased apoptosis and cell-cycle arrest (at the G_0 phase) in human AML cells (Figures 3A–3D and S3A–S3D). Both inhibitors, alone or together with all-*trans* retinoic acid, also significantly promoted myeloid differentiation in human AML cells (Figures S3E and S3F).

Leukemia stem/initiating cells (LSCs/LICs), characterized by their unlimited self-renewal potential, are considered to be the root cause of the treatment failure and relapse of AML; thus, eradication of LSCs/LICs is necessary to achieve a cure (Krause and Van Etten, 2007; Pollyea and Jordan, 2017). Via flow cytometry, we found that FTO is overexpressed in human primary AML patient cells relative to healthy control cells (Figures 3E and S3G). Moreover, in primary AML patient samples, the FTO level is even higher in CD34$^+$ immature AML cells than in CD34$^-$ AML bulk cells (Figures 3F and 3G). Consistent with their higher FTO levels, AML patient samples have a lower m^{6}A abundance compared with healthy controls (Figure S3H), as do CD34$^+$ AML cells compared with CD34$^-$ AML cells (Figure S3I). *FTO* KD substantially promoted apoptosis and myeloid differentiation and suppressed the colony-forming capability of human primary AML CD34$^+$ cells (Figures S3J–S3L), implying that FTO may play a role in self-renewal/repopulation of LSCs/LICs. To test this, we conducted *in vitro* and *in vivo* limiting dilution assays (Krivtsov et al., 2006; Li et al., 2015; Weng et al., 2018). Either KD of *FTO* or pharmacological inhibition of FTO resulted in a remarkable decrease in the frequency of LSCs/LICs in murine AML models (Figures 3H–3L). Notably, 50 nM CS1 could almost completely inhibit the repopulating capacity of AML cells (Figure S3M), further highlighting the potent effect of our FTO inhibitors in suppressing self-renewal of LSCs/LICs.

CS1 and CS2 Treatments Modulate the Signaling Pathways of FTO

RNA sequencing (RNA-seq) was carried out to understand the molecular mechanisms underlying the effects of CS1 and CS2 (Figure S4A). Cluster analysis revealed that CS1, sh*FTO*, and CS2 treated samples can be grouped together, separate from the two control groups (Figure 4A). The dysregulated genes induced by CS1, CS2, and *FTO* KD overlapped well with each other (Figures 4B and 4C). Our RNA-seq and qPCR data showed that CS1 or CS2 treatment substantially decreased *MYC* and *CEBPA* expression while increasing *RARA* and *ASB2* expression (Figures 4D, S4B, and S4C), which are positive and negative targets of FTO, respectively (Li et al., 2017; Su et al., 2018). By targeting FTO, CS1 and CS2 treatment also increased m^{6}A abundance on FTO target RNAs, such as *MYC* and *CEBPA* mRNA (Su et al., 2018) and small nuclear RNAs (snRNAs) (Mauer et al., 2019) (Figures S4D–S4F). Through global gene set enrichment analysis (GSEA) (Subramanian et al., 2005), we identified a set of upregulated or downregulated pathways upon CS1 or CS2 treatment or *FTO* KD. Notably, among the upregulated pathways, CS1, CS2, and sh*FTO* groups shared the majority of their enriched signaling pathways and core-enriched genes (Figures 4E [left panel] and 4F; Table S2). Among the downregulated pathways, all the pathways suppressed by CS1 or CS2 also exist in the pathways suppressed by *FTO* KD (Figures 4E [right panel] and 4G; Table S2). FTO inhibition or KD-mediated cell apoptosis

(E) CPMG spectra for CS1 (red), CS1 in the presence of 10 μM FTO (green), and 20 μM FTO (blue).
(F) STD spectrum for CS1 in the presence of 5 μM FTO protein.
(G) CPMG spectra for CS2 (red), CS1 in the presence of 2 μM FTO (green), 5 μM FTO (blue), and 10 μM FTO (cyan).
(H) STD spectrum for CS2 in the presence of 5 μM FTO protein.
(I) Confirming FTO$^{H231A/E234A}$ mutation via Sanger sequencing.
(J) Western blot analysis of FTO WT (upper panel) and FTO$^{H231A/E234A}$ (lower panel) from DARTS with CS1 in MONOMAC 6 cells.
(K) Confirming FTO$^{K216A/S229A/H231A}$ mutation via Sanger sequencing.
(L) Western blot analysis of FTO WT (upper panel) and FTO$^{K216A/S229A/H231A}$ (lower panel) from DARTS with CS2 in MONOMAC 6 cells.
(M) Western blot analysis (upper panel) and thermal shift curves (lower panel) of FTO from CETSA in MONOMAC 6 pretreated with 200 nM CS1 or CS2.
(N) Inhibitory effects of CS1 and CS2 on FTO demethylase activity via *in vitro* (cell-free) m^{6}A demethylation assays.
Data are presented as mean ± SEM from three independent experiments. **$p < 0.01$; ***$p < 0.001$. See also Figure S2 and Table S1.

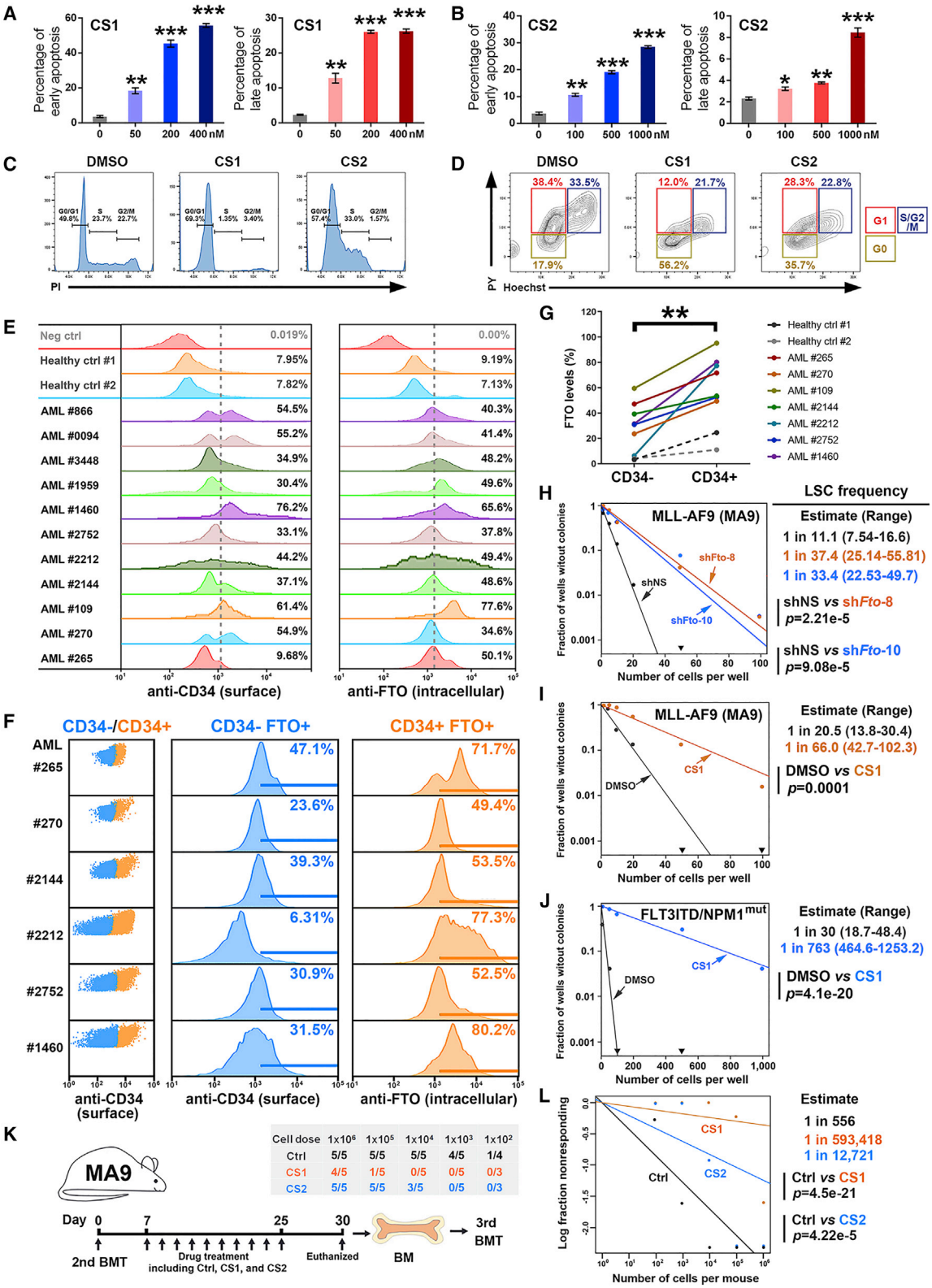

Figure 3. Effects of CS1 and CS2 on Apoptosis, Cell Cycle, and LSCs/LICs Frequency in AMLs

(A and B) Effect of CS1 (A) and CS2 (B) treatment on early apoptosis (left panel) and late apoptosis (right panel) in NOMO-1 AML cells upon 48 h of treatment. (C and D) Effects of CS1 and CS2 treatment on cell-cycle distribution in NOMO-1 cells as detected by propidium iodide (PI) staining (C) and Hoechst 33342/ Pyronin Y staining (D).

(legend continued on next page)

and cell-cycle arrest are likely attributed to the activation of the "Apoptosis" signaling, and suppression of the "MYC targets V1" and "MYC targets V2" pathways (Figure 4H). We also compared the key biological pathways effects by CS1, CS2, and other FTO inhibitors, FB23 and FB23-2 (Huang et al., 2019), and found that the distinct inhibitors shared these crucial signaling pathways and core-enriched gene (Figure S4G and Table S2). Thus, our mechanistic study data suggest that CS1 and CS2 exert their anti-leukemic effects through modulation of the essential signaling pathways of FTO.

CS1 and CS2 Display Potent Anti-leukemic Efficacy *In Vivo*

We next assessed the therapeutic efficacy of CS1 and CS2 *in vivo*. In a patient-derived xenotransplantation (PDX) AML model (with a relapsed AML patient sample, 2017-38), we showed that CS2 treatment dramatically reduced leukemia infiltration (Figure S5A) and doubled the overall survival (Figure 5A). Surprisingly, however, CS1 treatment did not show any significant effects, although CS1 exhibited an equal or even stronger anti-leukemic activity compared with CS2 *in vitro* (see Figures 2A, 2B, and 3A–3D). Further analysis revealed that the poor solubility and uptake of CS1 likely caused its weak effect *in vivo*. To increase bioavailability, we employed mPEG-b-PLA micelles or β-cyclodextrin, both widely used in the clinic (Cho et al., 2016; Hirayama and Uekama, 1999), to deliver hydrophobic CS1 (Figure 5B). We then repeated the treatment with the same PDX AML model by use of micelles packaged CS1 (Micelle_CS1), and demonstrated that delivery of CS1 with micelles markedly improved its anti-leukemia activity *in vivo* (Figure 5C). Similarly, Micelle_CS1 displayed a much more potent anti-leukemic activity than free CS1 in treating mice bearing transplanted murine MLL-AF9 AML, where free CS2 still showed robust anti-leukemic activity (Figures 5D, S5B, and S5C). Both Micelle_CS1 and free CS2 also displayed potent anti-AML efficacy in another PDX AML model (AML 3448), significantly more effective than FB23-2 (Figures S5D–S5F). Similarly, β-cyclodextrin packaged CS1 (β-CD_CS1) and CS2 substantially delayed AML progression and prolonged survival in an additional PDX model (AML, 2016-9) (Figures 5E, 5F, and S5G) accompanied by a significant impact on the expression of FTO targets, including *MYC*, *RARA*, and *ASB2* (Figure S5H). Via bioluminescence imaging, we observed that pharmacological inhibition or KD of *FTO* remarkably inhibited leukemia progression, constantly reduced leukemia burden, and dramatically prolonged survival (Figures 5G, 5H, and S5I–S5K). Thus, our preclinical animal model studies demonstrated the potent therapeutic efficacy of CS1 (packaged by micelles or β-cyclodextrin) or CS2 alone in treating AML, including relapsed AML. As we just tested relatively low dosages of CS1 and CS2 (merely 5 mg/kg once every other day, 10 times), higher dosages may result in more robust therapeutic effects.

The FTO/m^{6}A Axis Regulates Immune Checkpoint Gene Expression

We previously reported that R-2HG-mediated FTO inhibition displayed synergistic effects with hypomethylating agents (HMAs; e.g., azacitidine and decitabine [DAC]) in treating AML (Su et al., 2018). HMAs are wildly used for the treatment of patients with AML or myelodysplastic syndrome (MDS), especially in elderly patients and in those who are not eligible for allogeneic stem cell transplantation (Dombret et al., 2015; Issa et al., 2004; Yun et al., 2016). However, the vast majority of AML or MDS patients treated with HMA eventually developed drug resistance (Yun et al., 2016). The upregulation of immune checkpoint genes, such as *PD-1*, *PD-L1*, and *PD-L2*, and subsequent immune evasion have been assumed to contribute to HMA-induced drug resistance in the treated patients with myeloid malignancies (Orskov et al., 2015; Stahl and Goldberg, 2019; Yang et al., 2014). Since inhibition of FTO by R-2HG could sensitize AML cells to HMA (Su et al., 2018), here we sought to reveal the mechanism(s) underlying their synergistic effect and determine whether FTO signaling contributes to HMA-mediated upregulation of immune checkpoint genes and subsequent immune evasion.

We confirmed the increased expression of *PD-L1*, *PD-L2*, and *PD-1* upon DAC treatment in human AML or T cells (Figure S6A). Strikingly, DAC treatment also resulted in globally decreased m^{6}A abundance in AML cells (Figure 6A). The reduced m^{6}A level is likely the result of the increased expression of m^{6}A eraser *FTO*, as no significant expression changes observed in *ALKBH5*, *METTL3*, or *METTL14* (Figures 6B and S6B). We thus presumed that DAC-induced FTO overexpression may contribute to the increased expression of immune checkpoint genes via an m^{6}A-dependent mechanism. Indeed, FTO KD or inhibition significantly inhibited the expression of *PD-L1* and *PD-L2* in human AML cells with or without DAC treatment (Figures S6C–S6F). Nonetheless, we found that the endogenous expression levels of such immune checkpoint genes in most human AML cell lines are very low (Figures S6G–S6I). Consistently, it was reported that due to their limited expression in AML patients, targeting those immune checkpoint proteins by inhibitors alone showed only limited clinical efficacy in treating AML patients (Berger et al., 2008; Daver et al., 2019).

Besides PD-L1/PD-L2, leukocyte immunoglobulin-like receptor subfamily B (LILRB), including LILRB1, 2, 3, 4, and 5, have also been recognized as immune checkpoint proteins in AML (Chen et al., 2018; Deng et al., 2018a; Kang et al., 2016). We observed that DAC treatment remarkably promoted expression

(E) FTO abundance in the bone marrow-derived mononuclear cells (BMMNCs) of AML patients and healthy donors.
(F) FTO abundance in the CD34$^+$ and CD34$^-$ cells of BMMNCs from AML patients.
(G) FTO levels in CD34$^+$ cells versus CD34$^-$ cells of individual BMMNC samples.
(H) LSC/LIC frequency changes in MA9 primary murine AML cells upon *Fto* KD as estimated by *in vitro* limiting dilution assays (LDAs).
(I and J) LSC/LIC frequency changes in MA9 (I) and FLT3ITD/NPM1^{mut} (J) primary murine AML cells upon CS1 (20 nM) treatment.
(K) Diagram of the *in vivo* LDAs.
(L) LSC/LIC frequency changes in the MA9 AML mouse models upon CS1 or CS2 treatment.
Data are presented as mean ± SEM, n = 3. *p < 0.05; **p < 0.01; ***p < 0.001. See also Figure S3 and Table S1.

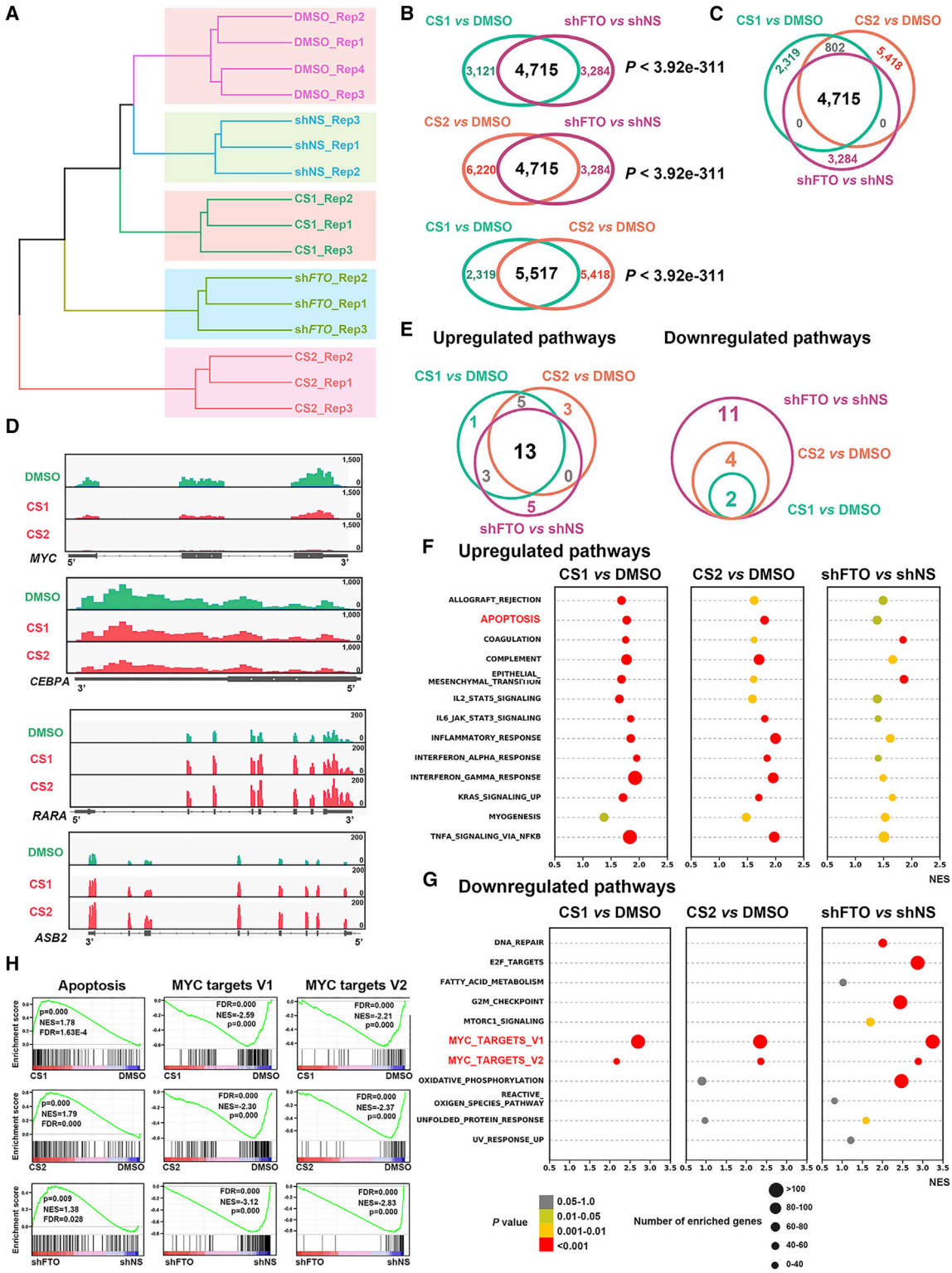

Figure 4. Identifying Signal Pathways Affected by FTO Inhibition and KD via RNA-Seq

(A) Hierarchical clustering dendrogram of RNA-seq data from NOMO-1 cells upon CS1, CS2, DMSO, shNS, or sh*FTO* (sh*FTO*-1) treatment.

(B) Overlapped dysregulated genes between CS1 treatment and *FTO* KD (upper panel), CS2 treatment and *FTO* KD (middle panel), and CS1 and CS2 treatments (lower panel).

(legend continued on next page)

of *LILRB* family members, including *LILRB3*, *LILRB4*, and *LILRB5* (Figure S6J). In particular, the *LILRB4* level was increased over 100-fold upon DAC treatment (Figure 6C), which is 6= to 20-fold greater than the fold changes for *PD-L1* and *PD-L2* (see Figure S6A). Interestingly, among the *LILRB* genes, only expression of *LILRB4* could be significantly downregulated by *FTO* KD (Figure S6K), implying that *LILRB4* might be a target of FTO in AML cells. Notably, *LILRB4* is overexpressed in human AML cell lines relative to normal bone marrow-derived mononuclear cells (MNCs) and T cells (Figures 6D and S6L), with a much higher level than those of *PD-1*, *PD-L1*, and *PD-L2* in AML lines (Figure S6M). Similarly, when analyzing The Cancer Genome Atlas (TCGA) AML dataset (Ley et al., 2013), we found that the median expression level of *LILRB4* is 40- to 50-fold higher than those of *PD-L1* and *PD-L2* in human primary AML samples (Figure 6E).

Consistent with the effect of *FTO* KD, CS1 or CS2 treatment also significantly decreased LILRB4 expression at both RNA and protein levels; conversely, forced expression of FTO WT (but not the catalytically inactive mutant) significantly increased the expression of *LILRB4* (Figures 6F–6L). DAC treatment could partially rescue the suppressed expression of LILRB4 induced by FTO inhibition (Figure 6M). Notably, CS1 and CS2 treatment did not obviously affect LILRB4 level in normal dendritic cells or macrophages (Figures S6N and S6O), likely due to the low level of FTO in such cells. FTO inhibition or KD increased m^6A abundance on *LILRB4* mRNA transcript (Figures 6N and 6O). Moreover, we demonstrated that FTO WT, but not mutant, could significantly increase the stability of *LILRB4* mRNA in AML cells; the opposite is true when *FTO* was knocked down (Figures 6P and 6Q). KD of m^6A reader YTHDF2, which was reported to promote decay of m^6A-modified transcripts (Wang et al., 2014), also increased the half-life of *LILRB4* mRNA (Figure 6R). Together, the results show that FTO positively regulates *LILRB4* expression in AML by suppressing YTHDF2-mediated decay of m^6A-modified *LILRB4* mRNA.

Targeting FTO Sensitizes AML Cells to T Cell Cytotoxicity and Overcomes HMA-Induced Immune Evasion

To determine whether pharmacological inhibition of the FTO/m^6A/LILRB4 axis can reprogram immune response, we pretreated AML cells with CS1 or CS2 and then co-cultured them with activated T cells. We found that FTO inhibition sensitized human AML cells to T cells, accompanied by decreased expression of *LILRB4* in AML cells (Figures 7A–7E). To generate a comprehensive molecular profiling of FTO inhibition in an immune-competent setting, we utilized the MLL-AF9 AML mouse model for RNA-seq. Among the immune checkpoint genes, *Lilrb4* is highly expressed in AML cells and significantly suppressed by FTO inhibitor therapy (Figures 7F, 7G, and S7A). Further flow-cytometry studies validated the downregulation of Lilrb4 by CS1 and CS2 treatment *in vivo* (Figures 7H–7K). *LILRB4* knockout (KO) or KD also significantly inhibited human AML cell growth (Figures 7L and 7M). Consistent with its role in immune surveillance, forced expression of *LILRB4* suppressed T cell killing of human AML cells with or without FTO inhibitor pretreatment (Figures 7N, 7O, S7B, and S7C).

To assess the effect of targeting the FTO/m^6A/LILRB4 axis on AML progression and immune evasion *in vivo*, we employed AML xenograft models with FTO inhibition and T cell treatment. We found that FTO inhibition (by CS1 or CS2) synergized with T cell treatment and substantially suppressed AML progression, resulting in remarkably prolonged survival in the combinational treatment groups (Figures 8A and 8B). Consistent with the role of FTO in mediating HMA-induced upregulation of immune checkpoint genes and subsequent immune evasion, FTO inhibition also synergized with HMAs (e.g., DAC) in inhibiting AML progression in immune-competent BMT recipient mice, and the combinations showed much improved therapeutic efficacy than either treatment alone (Figures 8C, S7D, and S7E). Collectively, FTO inhibition could suppress immune checkpoint gene expression and thereby sensitize AML cells to T cell cytotoxicity and overcome HMA-induced immune evasion.

The Minimal Drug Toxicity, Structure-Activity Relationships, and Broad Anti-cancer Efficacy of FTO Inhibitors

To evaluate the potential drug toxicity of CS1 and CS2 *in vivo*, we injected two doses for each compound (5 mg/kg/day [i.e., the dose used for AML mouse treatment] and 20 mg/kg/day) into C57BL/6 mice once every other day for 20 days, and euthanized all the mice 10 days after the final treatment. We observed no significant difference between the drug-treated groups and control group regarding whole-body or organ weight (Figures S7F–S7K and Table S3). Complete blood count data collected from peripheral blood did not show any significant difference between the treated groups and control group (Table S3). H&E staining also showed no difference between the groups (Figure S7L). These data suggest that the drug toxicity of CS1 or CS2 is minimal.

To explore the structure-activity relationships of CS1 and CS2 chemical scaffolds, we designed and synthesized six analog compounds for CS1 and four analogs for CS2, based on their structures and their binding poses with FTO protein. Among the six CS1 analogs, only CS1-3 and CS1-7 showed anti-leukemic efficacy similar to that of CS1 (Figure S8A). As shown in the docking models, both CS1-3 and CS1-7 display tight binding with FTO protein (Figure S8A). According to the structures of CS1 and its analogs, we conjecture that the planar three-ring structure may be important for their efficacy. Among CS2 analogs, only CS2-2, with the highest similarity to CS2, exhibited an anti-leukemia effect similar to that of CS2 (Figure S8B). Further systematic studies are warranted to develop more effective CS1 and CS2 analogs.

(C) Overlapped dysregulated genes among CS1 treatment, CS2 treatment, and *FTO* KD groups.
(D) Distribution of RNA-seq reads in *MYC*, *CEBPA*, *RARA*, and *ASB2* mRNA.
(E) Overlap of upregulated pathways (left panel) or downregulated pathways (right panel) induced by *FTO* KD, CS1, and CS2 based on the GSEA.
(F and G) Scattergrams of the upregulated pathways (F) and downregulated pathways (G) based on GSEA.
(H) GSEA of shared upregulated apoptosis and downregulated MYC pathways by inhibition of FTO (CS1 or CS2) and KD of *FTO* (sh*FTO*).
All RNA-seq experiments were conducted with at least three independent biological replicates. See also Figure S4 and Table S2.

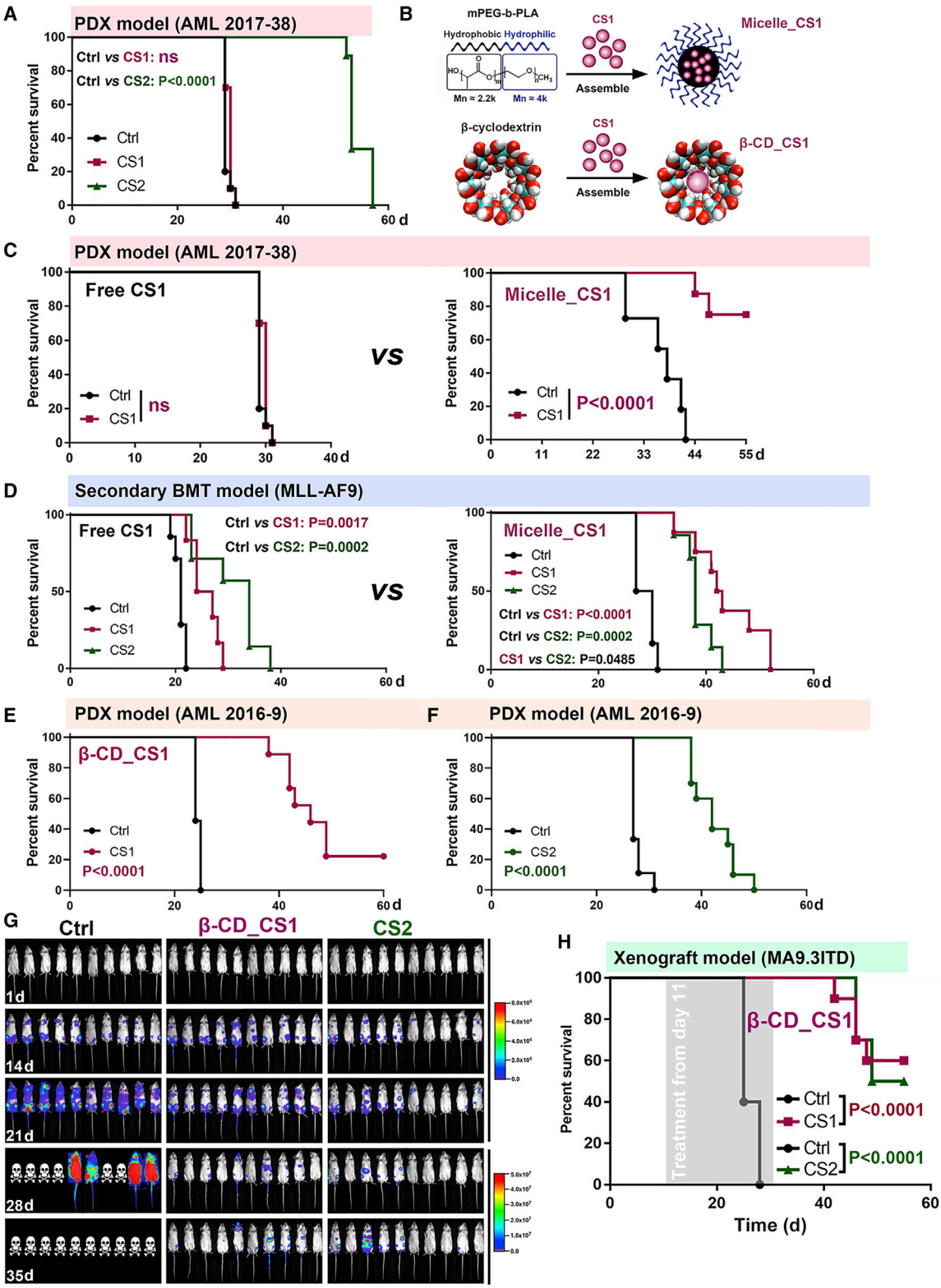

Figure 5. FTO Inhibition Substantially Delayed AML Progression and Improved Survival *In Vivo*

(A) Kaplan-Meier survival curves of AML PDX mouse model (AML, 2017-38) treated with free CS1 or CS2.

(B) Polymeric micelles of mPEG-*b*-PLA (upper panel) and β-cyclodextrin (lower panel) were utilized to deliver CS1.

(C) Kaplan-Meier survival curves of AML PDX mouse model (AML, 2017-38) treated with free CS1 or Micelle_CS1.

(legend continued on next page)

In addition to hematopoietic malignancies, FTO has also been reported to play oncogenic roles in many types of solid tumors (Huang et al., 2020a; Niu et al., 2019; Tang et al., 2019; Yang et al., 2019). To test the therapeutic potential of targeting FTO in treating solid tumors, we chose glioblastoma, breast cancer, and pancreatic cancer as representative models, in which *FTO* expression is comparable with that in AML (Figure S8C). FTO KD or inhibition significantly suppressed the proliferation of these cancer cells (Figures S8D–S8G). Further *in vivo* studies confirmed the potent anti-tumor efficacy of FTO inhibitors in treating breast cancer (Figures 8D and 8E). Together, our results demonstrate the broad therapeutic potential of FTO inhibitors in treating various types of cancers.

DISCUSSION

While m^6A modification and the machinery have been implicated in the initiation, progression, maintenance, and drug resistance of various types of cancers (Deng et al., 2018b, 2018c; Huang et al., 2020b), the development of effective inhibitors to target m^6A regulators for cancer therapy is still in its infancy (Huang et al., 2020a). In the present study, by *in silico* virtual screening and subsequent validation assays, we have identified two effective small-molecule compounds (CS1 and CS2) that specifically target FTO and efficiently suppress its m^6A demethylase activity by occupying the catalytic pocket and interfering with the binding of FTO with m^6A-modified RNAs. CS1 and CS2 treatment significantly inhibited the viability/growth of human AML cells with IC_{50} values at low nanomolar levels, which are at least 10-fold more effective than previously reported FTO inhibitors (e.g., FB23-2 and MO-I-500) (Huang et al., 2019; Zheng et al., 2014). Mechanistically, CS1 and CS2 exert anti-leukemic effects by suppression of FTO activity and signaling, leading to the activation of apoptosis signaling and inhibition of MYC pathways. Notably, CS1 (NSC337766, also named bisantrene) has been introduced into clinical trials since the 1980s as an anthracene compound for various types of cancer therapy, and some patients responded to such treatment (Cowan et al., 1986; Miller et al., 1986; Myers et al., 1984; Pratt et al., 1986; Rothman, 2017; Yap et al., 1983). This agent was originally thought to be similar to doxorubicin in activity (Yap et al., 1983); however, unlike doxorubicin, bisantrene does not exhibit anthracycline-associated cardiotoxicity and was generally well tolerated by most patients (Rothman, 2017; Yap et al., 1983). Indeed, aside from functioning as a DNA-reactive agent, its immune-activating and telomerase-inhibiting activities have also been reported (Rothman, 2017), suggesting that the mechanisms of its action have yet to be fully investigated. CS2 (NSC368390, also named brequinar) was previously reported to inhibit the enzyme dihydroorotate dehydrogenase and thereby block *de novo* pyrimidine biosynthesis (Peters et al., 1992). Brequinar has also been tested in clinical trials for cancer therapy (Burris et al., 1998; de Forni et al., 1993; Noe et al., 1990; Schwartsmann et al., 1990). In the present study, we demonstrated that CS1 and CS2 bind directly to FTO protein as detected by NMR, DARTS, and CETSA assays, and our mutagenesis assays also confirmed the essential amino acids for their binding. In addition, we showed that FTO-high AML samples are more sensitive to CS1 and CS2, while FTO depletion reduced their sensitivity. Collectively, although further systematic studies are warranted to evaluate whether other reported mechanisms of their actions also contribute to the overall anti-cancer efficacy of CS1 and CS2, we have provided compelling evidence that FTO is a direct and essential drug target of both CS1 and CS2. Thus, future clinical trials of these two compounds should focus on cancer patients with a high level of FTO.

Moreover, we showed that FTO is particularly overexpressed in LSCs/LICs, and pharmacological inhibition or KD of FTO significantly suppressed LSC/LIC self-renewal. Thus, pharmacologically targeting FTO holds potent therapeutic potential because it can eradicate LSCs/LICs. FTO's contribution to LSC/LIC self-renewal is likely through its positive regulation of *MYC* and *CEBPA* (Su et al., 2018), two genes that play important roles in the maintenance of LSCs/LICs (Li et al., 2014; Ohlsson et al., 2014; Ye et al., 2015; Zhang et al., 2015). FTO KD or inhibition also increased the m^6A abundance in snRNAs, hinting at a role of FTO in RNA alternative splicing (Mauer et al., 2019; Wei et al., 2018). Similar to FTO, m^6A writers (METTL3/14) also target *MYC* and play oncogenic roles in AML (Barbieri et al., 2017; Vu et al., 2017; Weng et al., 2018), likely through distinct mechanisms (Deng et al., 2018c). Thus, it would be interesting to test whether targeting both FTO and an m^6A writer exhibits a synergy in treating AML.

Evidence is emerging that tumor cells utilize immune checkpoints as a major mechanism of immune evasion (Beatty and Gladney, 2015; Dong et al., 2002). Monoclonal antibodies targeting the PD-1/PD-L1/PD-L2 axis have achieved encouraging effects in clinical practice in treating multiple types of solid tumors (Gopalakrishnan et al., 2018; Patnaik et al., 2015; Topalian et al., 2012) but have demonstrated only limited effects in AML (Berger et al., 2008). Here, we show that the expression levels of these genes are very low in human AML cells. In contrast, *LILRB4*, whose activation can promote tumor infiltration and suppress T cell activity (Deng et al., 2018a), is highly expressed in primary AML. Since the endogenous *LILRB4* levels in human primary AML samples (as well as in AML cell lines) are 40- to 50-fold higher than those of *PD-L1* and *PD-L2*, LILRB4 appears to be the major factor that mediates the immune evasion of AML. Interestingly, FTO directly upregulates *LILRB4* expression via an m^6A-dependent mechanism. CS1/CS2 treatment decreased the expression of immune checkpoint genes (especially *LILRB4*) in AML cells, substantially increasing the sensitivity of AML cells to the cytotoxicity of activated T cells. Different from previous studies showing the role of YTHDF1 (an m^6A reader) in the cross-presentation of tumor antigens and the cross-priming of $CD8^+$ T cells (Han et al., 2019) as well as the role of FTO in

(D) Kaplan-Meier survival curves of mice transplanted with primary murine MA9 AML cells treated with free CS1, Micelle_CS1, or CS2.
(E and F) Kaplan-Meier survival curves of AML PDX mouse models (AML, 2016-9) treated with β-CD_CS1 (E) or CS2 (F).
(G and H) *In vivo* bioluminescence imaging (G) and Kaplan-Meier survival curves (H) of xenograft mouse models with human MA9.3ITD cells treated with β-CD_CS1 or CS2.
ns, not significant; p values are derived from log-rank test. See also Figure S5 and Table S1.

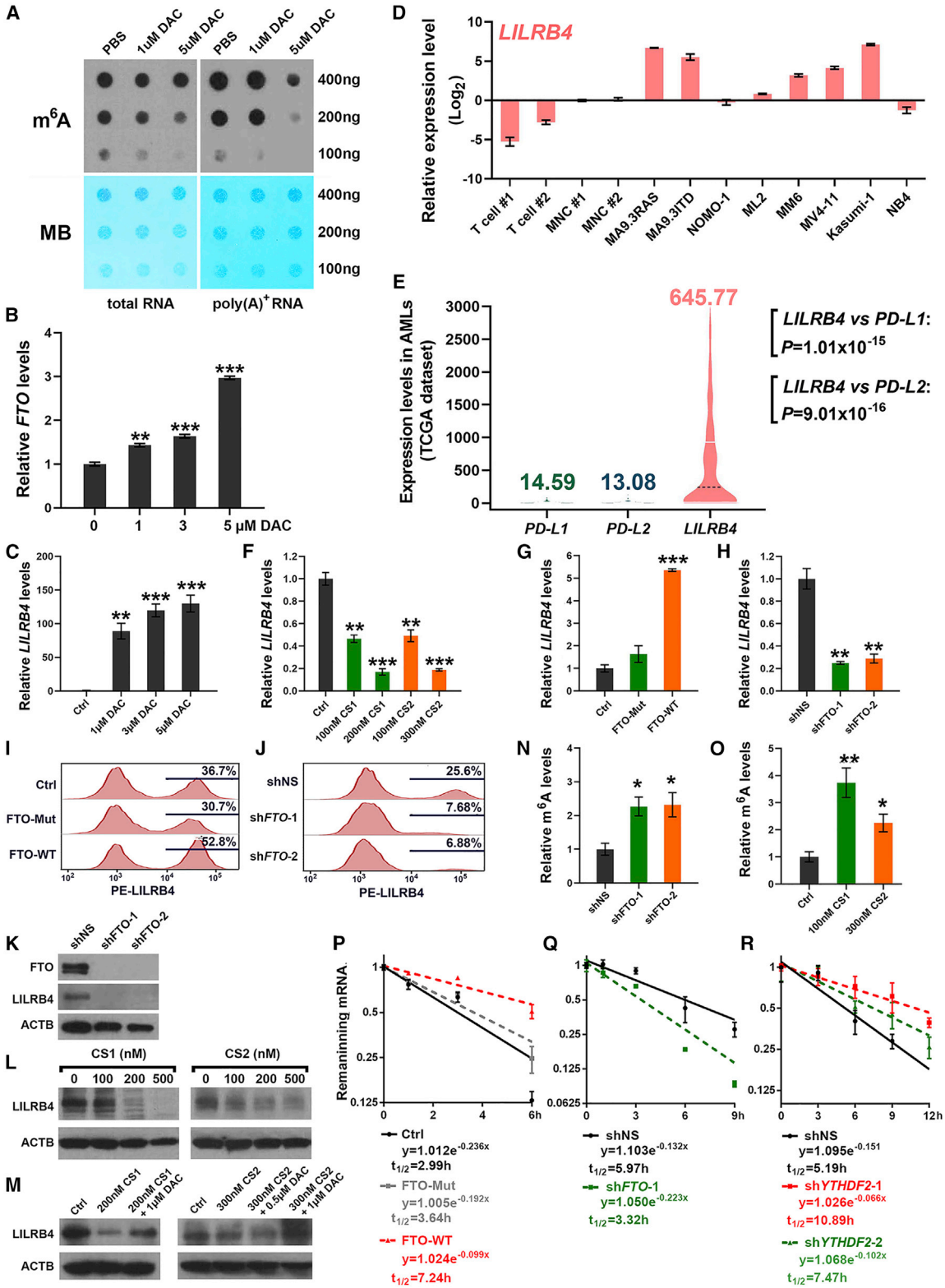

Figure 6. The FTO/m^{6}A Axis Contributes to HMA-Mediated Upregulation of Immune Checkpoint Genes

(A) Global m^{6}A abundance upon DAC or PBS treatment for 48 h in MONOMAC 6 cells.

(B) qPCR analysis of *FTO* level changes in MONOMAC 6 cells upon DAC treatment (48 h).

(C) qPCR analysis of *LILRB4* level changes in NOMO-1 cells upon DAC treatment (48 h).

(legend continued on next page)

promoting melanoma tumorigenesis and anti-PD-1 resistance (Yang et al., 2019), here we demonstrate that by suppressing the expression of intrinsic immune checkpoint genes (especially *LILRB4*) in AML cells, targeting the FTO/m^{6}A axis substantially suppressed immune evasion and sensitized AML cells to T cell cytotoxicity.

In addition, consistent with previous reports (Orskov et al., 2015; Yang et al., 2014), we confirmed that HMA treatment resulted in global upregulation of immune checkpoint genes. Notably, the ascending tendency of *LILRB4* is much more significant than *PD-L1* and *PD-L2* upon DAC treatment. Since the observations that HMA treatment induces upregulation of *PD-1*/*PD-L1*/*PD-L2* (Orskov et al., 2015; Yang et al., 2014), multiple clinical trials are ongoing now to test therapeutic potential of the combinations of HMA with anti-PD-1, PD-L1, or PD-L2 antibodies for AML and MDS treatment (Alfayez and Borthakur, 2018; Daver et al., 2019; Stahl and Goldberg, 2019). However, as *LILRB4* is likely a more critical immune checkpoint gene than the others in AML/MDS, the combinations of FTO inhibitors (or anti-LILRB4 antibody) plus HMAs might be better therapeutic strategies for AML/MDS treatment. Indeed, we have shown that FTO inhibitors exhibit strong synergistic effects with HMAs in treating AML *in vivo*, highlighting the therapeutic potential of this combination in treating myeloid malignancies.

Finally, the potent anti-tumor efficacy and minimal side effects of CS1 and CS2 suggest that that they are highly feasible for clinical application. Further studies are warranted to optimize the compounds to improve their bioavailability, inhibitory effect, and therapeutic efficacy.

Overall, we have identified two potent FTO inhibitors and have demonstrated that targeting the FTO/m^{6}A axis could significantly suppress cancer stem cell self-renewal and immune evasion, highlighting the broad potential of targeting FTO signaling by effective inhibitors (alone or in combination with other therapeutic agents) for cancer therapy. Moreover, our FTO inhibitors can also be used as tool compounds for basic and translational research of FTO and m^{6}A modification.

STAR★METHODS

Detailed methods are provided in the online version of this paper and include the following:

SUPPLEMENTAL INFORMATION

Supplemental Information can be found online at https://doi.org/10.1016/j.ccell.2020.04.017.

ACKNOWLEDGMENTS

We thank Dr. Cai-Guang Yang from Shanghai Institute of Materia Medica, Chinese Academy of Sciences for providing FB23-2 and for his guidance in the NMR analysis. We thank Dr. Mi Deng and Dr. Cheng Cheng Zhang from

(D) qPCR analysis of *LILRB4* in CD3 T cells, healthy MNCs, and AML cell lines.
(E) Expression levels of *PD-L1*, *PD-L2*, and *LILRB4* in the TCGA AML dataset.
(F) qPCR analysis of *LILRB4* level changes upon CS1 or CS2 treatment in MONOMAC 6 cells.
(G and H) qPCR analysis of *LILRB4* level changes upon *FTO* overexpression (G) in NOMO1 cells or *FTO* KD (H) in MONOMAC 6 cells.
(I and J) Flow-cytometry analysis of LILRB4 level changes upon *FTO* overexpression (I) or KD (J) in THP1 cells.
(K and L) Western blot analysis of LILRB4 level changes in MONOMAC 6 cells upon FTO KD (K) or inhibition (L).
(M) Protein levels of LILRB4 in MONOMAC 6 cells with CS1 or CS1 + DAC treatment (left panel), and CS2 or CS2 + DAC treatment (right panel).
(N and O) m^{6}A abundance changes in *LILRB4* mRNA upon FTO inhibition (N) or KD (O) in MONOMAC 6 cells.
(P–R) *LILRB4* mRNA stability changes in AML cells upon *FTO* overexpression (P), *FTO* KD (Q), or *YTHDF2* KD (R).
Mean ± SEM from three independent experiments. *$p < 0.05$; **$p < 0.01$; ***$p < 0.001$. See also Figure S6.

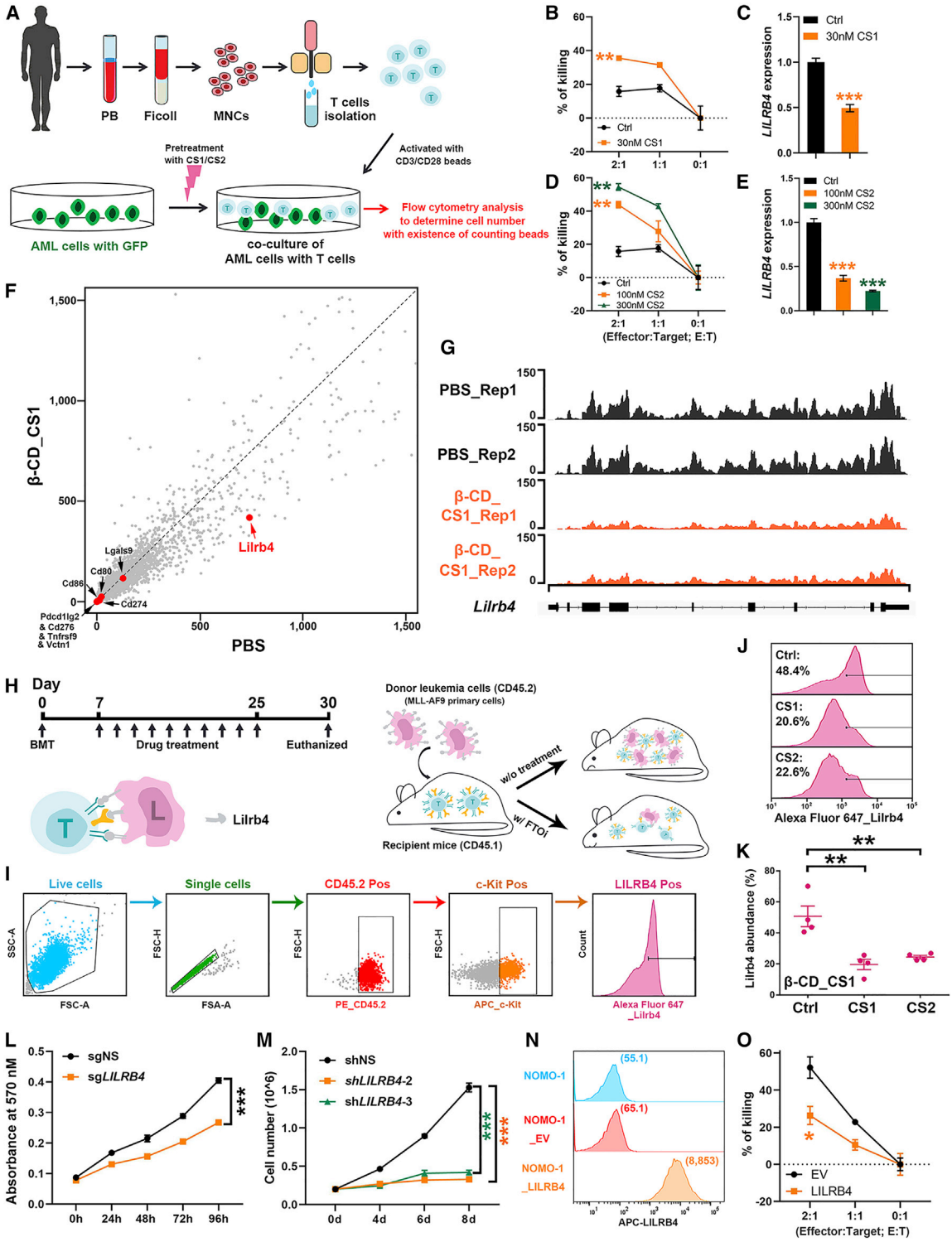

Figure 7. FTO Inhibition Suppressed Immune Evasion by Targeting LILRB4

(A) Schematic of the co-culture assays with T cells and GFP-labeled human AML cells.

(B–E) Effect of CS1 (B) and CS2 (D) on the sensitivity of human AML cells to the cytotoxicity of T cells *in vitro*. MONOMAC 6 cells were pretreated with CS1 or CS2 for 48 h and *LILRB4* levels were validated via qPCR (C and E).

(F) Scatterplot of normalized expression for all genes from RNA-seq with the spleen MNCs of MA9 mice with PBS or CS1 treatment.

(G) Distribution of RNA-seq reads in *Lilrb4* transcript.

(H) Schematic showing the method to assess the effect of FTO inhibition on Lilrb4 expression *in vivo*.

(legend continued on next page)

University of Texas Medical Center for providing the pLVX-ZsGreen and ZsGreen-hLILRB4. We acknowledge the support of the Hematopoietic Tissue Biorepository core at City of Hope Comprehensive Cancer Center, which is supported by the National Cancer Institute of the US National Institutes of Health (NIH) under award number P30CA33572. This work was supported in part by the NIH grants R01 CA243386 (J.C.), R01 CA214965 (J.C.), R01 CA236399 (J.C.), R01 CA211614 (J.C.), R01 DK124116 (J.C.), The Margaret Early Medical Research Trust (R. Su), American Cancer Society Research Scholar grant (Z.L.), NIH R50CA211404 (M.W.), R35CA197628 (M.M.), U10CA180827 (M.M.), R01CA137060 (M.M.), R01CA157644 (M.M.), R01CA172558 (M.M.), and R01CA213138 (M.M.). J.C. is a Leukemia & Lymphoma Society Scholar. M.M. is a Howard Hughes Medical Institute Faculty Scholar.

AUTHOR CONTRIBUTIONS

R. Su and J.C. conceived and designed the project, and supervised the research; R. Su, Y.L., M.G., L.H., M.W., X.D., H.L., Y.H., L.G., C.L., Z.Z., S.R., B.T., Y.Q., X.Q., E.P., J.X., H.Q., W.L., C.S., H.W., H.H., Z.C., X.W., D.H., and J.C. performed experiments and/or data analyses; L.D. performed the bioinformatics analysis; R. Su, M.W., J.S., P.K., B.Z., M.J.O., M.M., G.M., R. Salgia, L.L., A.T.F., Z.L., J.C.M., M.M., D.H., and J.C. contributed reagents/analytic tools and/or grant support; R. Su and J.C. wrote the paper. All authors discussed the results and commented on the manuscript.

DECLARATION OF INTERESTS

A provisional patent was filed, with J.C., R. Su, D.H., X.D., H.L., and J.X. as inventors. J.C. is the scientific founder of Genovel Biotech Corp. and holds equities with the company. A.T.F. has done consultancy work for Celgene, Agios, Astellas, Daiichi Sankyo, and Abbvie, and Celgene and Agios are providing funding for two ongoing clinical trials that A.T.F. is running as investigator-initiated studies.

Received: November 21, 2019
Revised: March 19, 2020
Accepted: April 23, 2020
Published: June 11, 2020

REFERENCES

Alfayez, M., and Borthakur, G. (2018). Checkpoint inhibitors and acute myelogenous leukemia: promises and challenges. Expert Rev. Hematol. *11*, 373–389.

Baell, J.B., and Holloway, G.A. (2010). New substructure filters for removal of pan assay interference compounds (PAINS) from screening libraries and for their exclusion in bioassays. J. Med. Chem. *53*, 2719–2740.

Barbieri, I., Tzelepis, K., Pandolfini, L., Shi, J., Millan-Zambrano, G., Robson, S.C., Aspris, D., Migliori, V., Bannister, A.J., Han, N., et al. (2017). Promoter-bound METTL3 maintains myeloid leukaemia by m(6)A-dependent translation control. Nature *552*, 126–131.

Beatty, G.L., and Gladney, W.L. (2015). Immune escape mechanisms as a guide for cancer immunotherapy. Clin. Cancer Res. *21*, 687–692.

Berger, R., Rotem-Yehudar, R., Slama, G., Landes, S., Kneller, A., Leiba, M., Koren-Michowitz, M., Shimoni, A., and Nagler, A. (2008). Phase I safety and pharmacokinetic study of CT-011, a humanized antibody interacting with PD-1, in patients with advanced hematologic malignancies. Clin. Cancer Res. *14*, 3044–3051.

Boccaletto, P., Machnicka, M.A., Purta, E., Piatkowski, P., Baginski, B., Wirecki, T.K., de Crecy-Lagard, V., Ross, R., Limbach, P.A., Kotter, A., et al. (2018). MODOMICS: a database of RNA modification pathways. 2017 update. Nucleic Acids Res. *46*, D303–D307.

Burris, H.A., 3rd, Raymond, E., Awada, A., Kuhn, J.G., O'Rourke, T.J., Brentzel, J., Lynch, W., King, S.Y., Brown, T.D., and Von Hoff, D.D. (1998). Pharmacokinetic and phase I studies of brequinar (DUP 785; NSC 368390) in combination with cisplatin in patients with advanced malignancies. Invest. New Drugs *16*, 19–27.

Campeau, E., Ruhl, V.E., Rodier, F., Smith, C.L., Rahmberg, B.L., Fuss, J.O., Campisi, J., Yaswen, P., Cooper, P.K., and Kaufman, P.D. (2009). A versatile viral system for expression and depletion of proteins in mammalian cells. PLoS One *4*, e6529.

Chen, B., Ye, F., Yu, L., Jia, G., Huang, X., Zhang, X., Peng, S., Chen, K., Wang, M., Gong, S., et al. (2012). Development of cell-active N^6-methyladenosine RNA demethylase FTO inhibitor. J. Am. Chem. Soc. *134*, 17963–17971.

Chen, H.M., van der Touw, W., Wang, Y.S., Kang, K., Mai, S., Zhang, J., Alsina-Beauchamp, D., Duty, J.A., Mungamuri, S.K., Zhang, B., et al. (2018). Blocking immunoinhibitory receptor LILRB2 reprograms tumor-associated myeloid cells and promotes antitumor immunity. J. Clin. Invest. *128*, 5647–5662.

Cho, H., Gao, J., and Kwon, G.S. (2016). PEG-b-PLA micelles and PLGA-b-PEG-b-PLGA sol-gels for drug delivery. J. Control. Release *240*, 191–201.

Cowan, J.D., Gehan, E., Rivkin, S.E., and Jones, S.E. (1986). Phase II trial of bisantrene in patients with advanced sarcoma: a Southwest Oncology Group Study. Cancer Treat. Rep. *70*, 685–686.

Daver, N., Garcia-Manero, G., Basu, S., Boddu, P.C., Alfayez, M., Cortes, J.E., Konopleva, M., Ravandi-Kashani, F., Jabbour, E., Kadia, T., et al. (2019). Efficacy, safety, and biomarkers of response to azacitidine and nivolumab in relapsed/refractory acute myeloid leukemia: a nonrandomized, open-label, phase II study. Cancer Discov. *9*, 370–383.

de Forni, M., Chabot, G.G., Armand, J.P., Fontana, X., Recondo, G., Domenge, C., Carde, P., Barbu, M., and Gouyette, A. (1993). Phase I and pharmacokinetic study of brequinar (DUP 785; NSC 368390) in cancer patients. Eur. J. Cancer *29A*, 983–988.

Deng, M., Gui, X., Kim, J., Xie, L., Chen, W., Li, Z., He, L., Chen, Y., Chen, H., Luo, W., et al. (2018a). LILRB4 signalling in leukaemia cells mediates T cell suppression and tumour infiltration. Nature *562*, 605–609.

Deng, X., Su, R., Feng, X., Wei, M., and Chen, J. (2018b). Role of N(6)-methyladenosine modification in cancer. Curr. Opin. Genet. Dev. *48*, 1–7.

Deng, X., Su, R., Weng, H., Huang, H., Li, Z., and Chen, J. (2018c). RNA N(6)-methyladenosine modification in cancers: current status and perspectives. Cell Res. *28*, 507–517.

Dobin, A., Davis, C.A., Schlesinger, F., Drenkow, J., Zaleski, C., Jha, S., Batut, P., Chaisson, M., and Gingeras, T.R. (2013). STAR: ultrafast universal RNA-seq aligner. Bioinformatics *29*, 15–21.

Dombret, H., Seymour, J.F., Butrym, A., Wierzbowska, A., Selleslag, D., Jang, J.H., Kumar, R., Cavenagh, J., Schuh, A.C., Candoni, A., et al. (2015). International phase 3 study of azacitidine vs conventional care regimens in older patients with newly diagnosed AML with >30% blasts. Blood *126*, 291–299.

Dong, H., Strome, S.E., Salomao, D.R., Tamura, H., Hirano, F., Flies, D.B., Roche, P.C., Lu, J., Zhu, G., Tamada, K., et al. (2002). Tumor-associated B7-H1 promotes T-cell apoptosis: a potential mechanism of immune evasion. Nat. Med. *8*, 793–800.

Dull, T., Zufferey, R., Kelly, M., Mandel, R.J., Nguyen, M., Trono, D., and Naldini, L. (1998). A third-generation lentivirus vector with a conditional packaging system. J. Virol. *72*, 8463–8471.

Friesner, R.A., Banks, J.L., Murphy, R.B., Halgren, T.A., Klicic, J.J., Mainz, D.T., Repasky, M.P., Knoll, E.H., Shelley, M., Perry, J.K., et al. (2004). Glide: a new approach for rapid, accurate docking and scoring. 1. Method and assessment of docking accuracy. J. Med. Chem. *47*, 1739–1749.

(I) Flow-cytometry analysis of Lilrb4 expression *in vivo*.
(J and K) Representative (J) and statistical summary of (K) Lilrb4 abundance changes in AML blast cells of MA9 mice upon β-CD_CS1 or CS2 treatment.
(L and M) Effects of *LILRB4* KO (L) and KD (M) on cell proliferation in MONOMAC 6 cells.
(N and O) Effect of *LILRB4* overexpression (N) on T cell toxicity (O) in NOMO-1 cells.
Data are presented as Mean ± SEM (B, C, D, E, O) or mean ± SD (K, L, M); n = 3. *p < 0.05; **p < 0.01; ***p < 0.001. See also Figure S7.

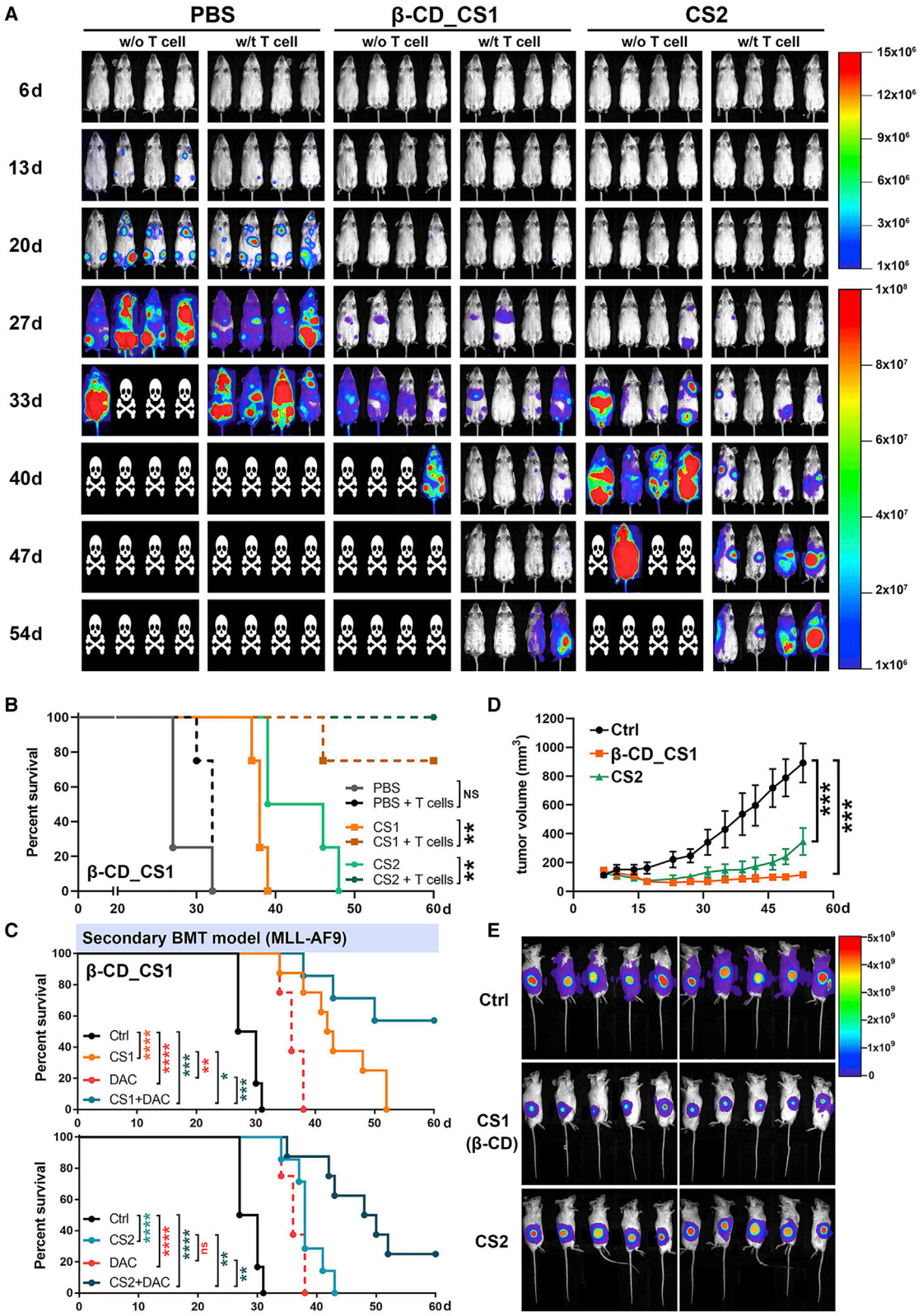

Figure 8. *In Vivo* Effects of FTO Inhibitors on Immunotherapy and Solid Tumors

(A and B) Bioluminescence images (A) and Kaplan-Meier survival curves (B) of NRGS mice with MA9.3ITD AML subjected to treatment with FTO inhibitors and/or activated human T cells.

(legend continued on next page)

Frye, M., Harada, B.T., Behm, M., and He, C. (2018). RNA modifications modulate gene expression during development. Science *361*, 1346–1349.

Gao, M., Deng, J., Chu, H., Tang, Y., Wang, Z., Zhao, Y., and Li, G. (2017). Stereoselective stabilization of polymeric vitamin E conjugate micelles. Biomacromolecules *18*, 4349–4356.

Gopalakrishnan, V., Spencer, C.N., Nezi, L., Reuben, A., Andrews, M.C., Karpinets, T.V., Prieto, P.A., Vicente, D., Hoffman, K., Wei, S.C., et al. (2018). Gut microbiome modulates response to anti-PD-1 immunotherapy in melanoma patients. Science *359*, 97–103.

Han, D., Liu, J., Chen, C., Dong, L., Liu, Y., Chang, R., Huang, X., Liu, Y., Wang, J., Dougherty, U., et al. (2019). Anti-tumour immunity controlled through mRNA m(6)A methylation and YTHDF1 in dendritic cells. Nature *566*, 270–274.

He, W., Zhou, B., Liu, W., Zhang, M., Shen, Z., Han, Z., Jiang, Q., Yang, Q., Song, C., Wang, R., et al. (2015). Identification of a novel small-molecule binding site of the fat mass and obesity associated protein (FTO). J. Med. Chem. *58*, 7341–7348.

Hirayama, F., and Uekama, K. (1999). Cyclodextrin-based controlled drug release system. Adv. Drug Deliv. Rev. *36*, 125–141.

Hu, Y., and Smyth, G.K. (2009). ELDA: extreme limiting dilution analysis for comparing depleted and enriched populations in stem cell and other assays. J. Immunol. Methods *347*, 70–78.

Huang, H., Weng, H., and Chen, J. (2020a). m(6)A modification in coding and non-coding RNAs: roles and therapeutic implications in cancer. Cancer Cell *37*, 270–288.

Huang, H., Weng, H., Deng, X., and Chen, J. (2020b). RNA modifications in cancer: functions, mechanisms, and therapeutic implications. Annu. Rev. Cancer Biol. *4*, 221–240.

Huang, Y., Su, R., Sheng, Y., Dong, L., Dong, Z., Xu, H., Ni, T., Zhang, Z.S., Zhang, T., Li, C., et al. (2019). Small-molecule targeting of oncogenic FTO demethylase in acute myeloid leukemia. Cancer Cell *35*, 677–691.e10.

Huang, Y., Yan, J., Li, Q., Li, J., Gong, S., Zhou, H., Gan, J., Jiang, H., Jia, G.F., Luo, C., and Yang, C.G. (2015). Meclofenamic acid selectively inhibits FTO demethylation of m6A over ALKBH5. Nucleic Acids Res. *43*, 373–384.

Huth, J.R., Mendoza, R., Olejniczak, E.T., Johnson, R.W., Cothron, D.A., Liu, Y., Lerner, C.G., Chen, J., and Hajduk, P.J. (2005). ALARM NMR: a rapid and robust experimental method to detect reactive false positives in biochemical screens. J. Am. Chem. Soc. *127*, 217–224.

Issa, J.P., Garcia-Manero, G., Giles, F.J., Mannari, R., Thomas, D., Faderl, S., Bayar, E., Lyons, J., Rosenfeld, C.S., Cortes, J., and Kantarjian, H.M. (2004). Phase 1 study of low-dose prolonged exposure schedules of the hypomethylating agent 5-aza-2′-deoxycytidine (decitabine) in hematopoietic malignancies. Blood *103*, 1635–1640.

Jafari, R., Almqvist, H., Axelsson, H., Ignatushchenko, M., Lundback, T., Nordlund, P., and Martinez Molina, D. (2014). The cellular thermal shift assay for evaluating drug target interactions in cells. Nat. Protoc. *9*, 2100–2122.

Jia, G., Fu, Y., and He, C. (2013). Reversible RNA adenosine methylation in biological regulation. Trends Genet. *29*, 108–115.

Jia, G., Fu, Y., Zhao, X., Dai, Q., Zheng, G., Yang, Y., Yi, C., Lindahl, T., Pan, T., Yang, Y.G., and He, C. (2011). N^6-methyladenosine in nuclear RNA is a major substrate of the obesity-associated FTO. Nat. Chem. Biol. *7*, 885–887.

Kang, X., Kim, J., Deng, M., John, S., Chen, H., Wu, G., Phan, H., and Zhang, C.C. (2016). Inhibitory leukocyte immunoglobulin-like receptors: immune checkpoint proteins and tumor sustaining factors. Cell Cycle *15*, 25–40.

Krause, D.S., and Van Etten, R.A. (2007). Right on target: eradicating leukemic stem cells. Trends Mol. Med. *13*, 470–481.

Krivtsov, A.V., Twomey, D., Feng, Z., Stubbs, M.C., Wang, Y., Faber, J., Levine, J.E., Wang, J., Hahn, W.C., Gilliland, D.G., et al. (2006). Transformation from committed progenitor to leukaemia stem cell initiated by MLL-AF9. Nature *442*, 818–822.

Ley, T.J., Miller, C., Ding, L., Raphael, B.J., Mungall, A.J., Robertson, A., Hoadley, K., Triche, T.J., Laird, P.W., Baty, J.D., et al. (2013). Genomic and epigenomic landscapes of adult de novo acute myeloid leukemia. N. Engl. J. Med. *368*, 2059–2074.

Li, B., and Dewey, C.N. (2011). RSEM: accurate transcript quantification from RNA-Seq data with or without a reference genome. BMC Bioinformatics *12*, 323.

Li, L., Osdal, T., Ho, Y., Chun, S., McDonald, T., Agarwal, P., Lin, A., Chu, S., Qi, J., Li, L., et al. (2014). SIRT1 activation by a c-MYC oncogenic network promotes the maintenance and drug resistance of human FLT3-ITD acute myeloid leukemia stem cells. Cell Stem Cell *15*, 431–446.

Li, Z., Chen, P., Su, R., Li, Y., Hu, C., Wang, Y., Arnovitz, S., He, M., Gurbuxani, S., Zuo, Z., et al. (2015). Overexpression and knockout of miR-126 both promote leukemogenesis. Blood *126*, 2005–2015.

Li, Z., Weng, H., Su, R., Weng, X., Zuo, Z., Li, C., Huang, H., Nachtergaele, S., Dong, L., Hu, C., et al. (2017). FTO plays an oncogenic role in acute myeloid leukemia as a N(6)-methyladenosine RNA demethylase. Cancer Cell *31*, 127–141.

Lipinski, C.A. (2004). Lead- and drug-like compounds: the rule-of-five revolution. Drug Discov. Today Technol. *1*, 337–341.

Liu, W., Zhou, M., Li, Z., Li, H., Polaczek, P., Dai, H., Wu, Q., Liu, C., Karanja, K.K., Popuri, V., et al. (2016). A selective small molecule DNA2 inhibitor for sensitization of human cancer cells to chemotherapy. EBioMedicine *6*, 73–86.

Lomenick, B., Hao, R., Jonai, N., Chin, R.M., Aghajan, M., Warburton, S., Wang, J., Wu, R.P., Gomez, F., Loo, J.A., et al. (2009). Target identification using drug affinity responsive target stability (DARTS). Proc. Natl. Acad. Sci. U S A *106*, 21984–21989.

Mauer, J., Sindelar, M., Despic, V., Guez, T., Hawley, B.R., Vasseur, J.J., Rentmeister, A., Gross, S.S., Pellizzoni, L., Debart, F., et al. (2019). FTO controls reversible m(6)Am RNA methylation during snRNA biogenesis. Nat. Chem. Biol. *15*, 340–347.

Miller, T.P., Cowan, J.D., Neilan, B.A., and Jones, S.E. (1986). A phase II study of bisantrene in malignant lymphomas. A Southwest Oncology Group Study. Cancer Chemother. Pharmacol. *16*, 67–69.

Myers, J.W., Von Hoff, D.D., Clark, G.M., and Coltman, C.A., Jr. (1984). Phase II clinical trial with bisantrene in patients with advanced refractory small cell lung cancer. Cancer Treat. Rep. *68*, 927–928.

Niu, Y., Lin, Z., Wan, A., Chen, H., Liang, H., Sun, L., Wang, Y., Li, X., Xiong, X.F., Wei, B., et al. (2019). RNA N^6-methyladenosine demethylase FTO promotes breast tumor progression through inhibiting BNIP3. Mol. Cancer *18*, 46.

Noe, D.A., Rowinsky, E.K., Shen, H.S., Clarke, B.V., Grochow, L.B., McGuire, W.B., Hantel, A., Adams, D.B., Abeloff, M.D., Ettinger, D.S., et al. (1990). Phase I and pharmacokinetic study of brequinar sodium (NSC 368390). Cancer Res. *50*, 4595–4599.

Ohlsson, E., Hasemann, M.S., Willer, A., Lauridsen, F.K., Rapin, N., Jendholm, J., and Porse, B.T. (2014). Initiation of MLL-rearranged AML is dependent on C/EBPalpha. J. Exp. Med. *211*, 5–13.

Orskov, A.D., Treppendahl, M.B., Skovbo, A., Holm, M.S., Friis, L.S., Hokland, M., and Gronbaek, K. (2015). Hypomethylation and up-regulation of PD-1 in T cells by azacytidine in MDS/AML patients: a rationale for combined targeting of PD-1 and DNA methylation. Oncotarget *6*, 9612–9626.

(C) Kaplan-Meier survival curves of MA9 AML mouse models upon treatments as indicated.
(D) Tumor growth curves of NSG mice bearing human breast cancer upon treatment with vehicle control, β-CD_CS1, or CS2. Dots represent the mean tumor volume in cubic millimeters ± SD (n = 10).
(E) Representative bioluminescence images of NSG mice at their endpoints.
For survival curves, the p values were calculated using the log-rank test. *$p < 0.05$; **$p < 0.01$; ***$p < 0.001$; ****$p < 0.0001$; NS, not significant. For the tumor growth curve, ***$p < 0.001$ as assayed by one-way ANOVA. See also Figures S7 and S8.

Padariya, M., and Kalathiya, U. (2016). Structure-based design and evaluation of novel N-phenyl-1H-indol-2-amine derivatives for fat mass and obesity-associated (FTO) protein inhibition. Comput. Biol. Chem. *64*, 414–425.

Patnaik, A., Kang, S.P., Rasco, D., Papadopoulos, K.P., Elassaiss-Schaap, J., Beeram, M., Drengler, R., Chen, C., Smith, L., Espino, G., et al. (2015). Phase I study of pembrolizumab (MK-3475; anti-PD-1 monoclonal antibody) in patients with advanced solid tumors. Clin. Cancer Res. *21*, 4286–4293.

Peters, G.J., Kraal, I., and Pinedo, H.M. (1992). In vitro and in vivo studies on the combination of Brequinar sodium (DUP-785; NSC 368390) with 5-fluorouracil; effects of uridine. Br. J. Cancer *65*, 229–233.

Pollyea, D.A., and Jordan, C.T. (2017). Therapeutic targeting of acute myeloid leukemia stem cells. Blood *129*, 1627–1635.

Pratt, C.B., Sinkule, J.A., Etcubanas, E., Douglass, E.C., Crom, D.B., Choi, K., and Avery, L. (1986). Phase I clinical and pharmacokinetic study of bisantrene in refractory pediatric solid tumors. Invest. New Drugs *4*, 149–153.

Rothman, J. (2017). The rediscovery of bisantrene: a review of the literature. Int. J. Cancer Res. Ther. *2*, 1–10.

Salmon, P., and Trono, D. (2007). Production and titration of lentiviral vectors. Curr. Protoc. Hum. Genet., Chapter 12, Unit 12 10.

Sanjana, N.E., Shalem, O., and Zhang, F. (2014). Improved vectors and genome-wide libraries for CRISPR screening. Nat. Methods *11*, 783–784.

Schwartsmann, G., Dodion, P., Vermorken, J.B., ten Bokkel Huinink, W.W., Joggi, J., Winograd, B., Gall, H., Simonetti, G., van der Vijgh, W.J., van Hennik, M.B., et al. (1990). Phase I study of brequinar sodium (NSC 368390) in patients with solid malignancies. Cancer Chemother. Pharmacol. *25*, 345–351.

Singh, B., Kinne, H.E., Milligan, R.D., Washburn, L.J., Olsen, M., and Lucci, A. (2016). Important role of FTO in the survival of rare panresistant triple-negative inflammatory breast cancer cells facing a severe metabolic challenge. PLoS One *11*, e0159072.

Stahl, M., and Goldberg, A.D. (2019). Immune checkpoint inhibitors in acute myeloid leukemia: novel combinations and therapeutic targets. Curr. Oncol. Rep. *21*, 37.

Stewart, S.A., Dykxhoorn, D.M., Palliser, D., Mizuno, H., Yu, E.Y., An, D.S., Sabatini, D.M., Chen, I.S., Hahn, W.C., Sharp, P.A., et al. (2003). Lentivirus-delivered stable gene silencing by RNAi in primary cells. RNA *9*, 493–501.

Su, R., Dong, L., Li, C., Nachtergaele, S., Wunderlich, M., Qing, Y., Deng, X., Wang, Y., Weng, X., Hu, C., et al. (2018). R-2HG exhibits anti-tumor activity by targeting FTO/m(6)A/MYC/CEBPA signaling. Cell *172*, 90–105.e3.

Subramanian, A., Tamayo, P., Mootha, V.K., Mukherjee, S., Ebert, B.L., Gillette, M.A., Paulovich, A., Pomeroy, S.L., Golub, T.R., Lander, E.S., and Mesirov, J.P. (2005). Gene set enrichment analysis: a knowledge-based approach for interpreting genome-wide expression profiles. Proc. Natl. Acad. Sci. U S A *102*, 15545–15550.

Tang, X., Liu, S., Chen, D., Zhao, Z., and Zhou, J. (2019). The role of the fat mass and obesity-associated protein in the proliferation of pancreatic cancer cells. Oncol. Lett. *17*, 2473–2478.

Thorvaldsdottir, H., Robinson, J.T., and Mesirov, J.P. (2013). Integrative Genomics Viewer (IGV): high-performance genomics data visualization and exploration. Brief. Bioinform. *14*, 178–192.

Toh, J.D.W., Sun, L., Lau, L.Z.M., Tan, J., Low, J.J.A., Tang, C.W.Q., Cheong, E.J.Y., Tan, M.J.H., Chen, Y., Hong, W., et al. (2015). A strategy based on nucleotide specificity leads to a subfamily-selective and cell-active inhibitor of N^6-methyladenosine demethylase FTO. Chem. Sci. *6*, 112–122.

Topalian, S.L., Hodi, F.S., Brahmer, J.R., Gettinger, S.N., Smith, D.C., McDermott, D.F., Powderly, J.D., Carvajal, R.D., Sosman, J.A., Atkins, M.B., et al. (2012). Safety, activity, and immune correlates of anti-PD-1 antibody in cancer. N. Engl. J. Med. *366*, 2443–2454.

Vu, L.P., Pickering, B.F., Cheng, Y., Zaccara, S., Nguyen, D., Minuesa, G., Chou, T., Chow, A., Saletore, Y., MacKay, M., et al. (2017). The N^6-methyladenosine (m6A)-forming enzyme METTL3 controls myeloid differentiation of normal hematopoietic and leukemia cells. Nat. Med. *23*, 1369–1376.

Wang, T., Hong, T., Huang, Y., Su, H., Wu, F., Chen, Y., Wei, L., Huang, W., Hua, X., Xia, Y., et al. (2015). Fluorescein derivatives as bifunctional molecules for the simultaneous inhibiting and labeling of FTO protein. J. Am. Chem. Soc. *137*, 13736–13739.

Wang, X., Lu, Z., Gomez, A., Hon, G.C., Yue, Y., Han, D., Fu, Y., Parisien, M., Dai, Q., Jia, G., et al. (2014). N^6-methyladenosine-dependent regulation of messenger RNA stability. Nature *505*, 117–120.

Wei, J., Liu, F., Lu, Z., Fei, Q., Ai, Y., He, P.C., Shi, H., Cui, X., Su, R., Klungland, A., et al. (2018). Differential m(6)A, m(6)Am, and m(1)A demethylation mediated by FTO in the cell nucleus and cytoplasm. Mol. Cell *71*, 973–985.e5.

Weng, H., Huang, H., Wu, H., Qin, X., Zhao, B.S., Dong, L., Shi, H., Skibbe, J., Shen, C., Hu, C., et al. (2018). METTL14 inhibits hematopoietic stem/progenitor differentiation and promotes leukemogenesis via mRNA m(6)A modification. Cell Stem Cell *22*, 191–205.e9.

Wunderlich, M., Mizukawa, B., Chou, F.S., Sexton, C., Shrestha, M., Saunthararajah, Y., and Mulloy, J.C. (2013). AML cells are differentially sensitive to chemotherapy treatment in a human xenograft model. Blood *121*, e90–e97.

Yang, H., Bueso-Ramos, C., DiNardo, C., Estecio, M.R., Davanlou, M., Geng, Q.R., Fang, Z., Nguyen, M., Pierce, S., Wei, Y., et al. (2014). Expression of PD-L1, PD-L2, PD-1 and CTLA4 in myelodysplastic syndromes is enhanced by treatment with hypomethylating agents. Leukemia *28*, 1280–1288.

Yang, S., Wei, J., Cui, Y.H., Park, G., Shah, P., Deng, Y., Aplin, A.E., Lu, Z., Hwang, S., He, C., and He, Y.Y. (2019). m(6)A mRNA demethylase FTO regulates melanoma tumorigenicity and response to anti-PD-1 blockade. Nat. Commun. *10*, 2782.

Yap, H.Y., Yap, B.S., Blumenschein, G.R., Barnes, B.C., Schell, F.C., and Bodey, G.P. (1983). Bisantrene, an active new drug in the treatment of metastatic breast cancer. Cancer Res. *43*, 1402–1404.

Ye, M., Zhang, H., Yang, H., Koche, R., Staber, P.B., Cusan, M., Levantini, E., Welner, R.S., Bach, C.S., Zhang, J., et al. (2015). Hematopoietic differentiation is required for initiation of acute myeloid leukemia. Cell Stem Cell *17*, 611–623.

Yun, S., Vincelette, N.D., Abraham, I., Robertson, K.D., Fernandez-Zapico, M.E., and Patnaik, M.M. (2016). Targeting epigenetic pathways in acute myeloid leukemia and myelodysplastic syndrome: a systematic review of hypomethylating agents trials. Clin. Epigenetics *8*, 68.

Zhang, X., Wei, L.H., Wang, Y., Xiao, Y., Liu, J., Zhang, W., Yan, N., Amu, G., Tang, X., Zhang, L., and Jia, G. (2019). Structural insights into FTO's catalytic mechanism for the demethylation of multiple RNA substrates. Proc. Natl. Acad. Sci. U S A *116*, 2919–2924.

Zhang, Y., Chen, H.X., Zhou, S.Y., Wang, S.X., Zheng, K., Xu, D.D., Liu, Y.T., Wang, X.Y., Wang, X., Yan, H.Z., et al. (2015). Sp1 and c-Myc modulate drug resistance of leukemia stem cells by regulating survivin expression through the ERK-MSK MAPK signaling pathway. Mol. Cancer *14*, 56.

Zheng, G., Cox, T., Tribbey, L., Wang, G.Z., Iacoban, P., Booher, M.E., Gabriel, G.J., Zhou, L., Bae, N., Rowles, J., et al. (2014). Synthesis of a FTO inhibitor with anticonvulsant activity. ACS Chem. Neurosci. *5*, 658–665.

Zheng, G., Dahl, J.A., Niu, Y., Fedorcsak, P., Huang, C.M., Li, C.J., Vagbo, C.B., Shi, Y., Wang, W.L., Song, S.H., et al. (2013). ALKBH5 is a mammalian RNA demethylase that impacts RNA metabolism and mouse fertility. Mol. Cell *49*, 18–29.

STAR★METHODS

KEY RESOURCES TABLE

REAGENT or RESOURCE	SOURCE	IDENTIFIER
Antibodies		
5-Hydroxymethylcytosine (5-hmC) antibody (pAb)	Active Motif	Cat # 39769; RRID: AB_10013602
m^6A (N6-methyladenosine) antibody	Synaptic Systems	Cat# 202003; RRID: AB_2279214
Anti-FTO antibody [EPR6895]	Abcam	Cat# ab124892; RRID: AB_10972698
Anti-ILT-3 antibody	Abcam	Cat# ab229747
GAPDH antibody (0411)	Santa Cruz	Cat# sc-47724; RRID: AB_627678
Goat anti-rabbit IgG H&L (HRP)	Abcam	Cat# ab6721; RRID: AB_955447
Goat anti-mouse IgG H&L (HRP)	Abcam	Cat# ab6789; RRID: AB_955439
β-Actin (8H10D10) Mouse mAb	Cell Signaling Technology	Cat# 3700S; RRID: AB_2242334
Anti-Flag M2 antibody	Sigma-Aldrich	Cat# F3165; RRID: AB_259529
Normal Mouse IgG control antibody	Millipore	Cat# 12-371; RRID: AB_145840
Anti-Human CD33 PE	eBioscience	Cat# 12-0339-42; RRID: AB_10855031
Anti-Human CD45 BV786	BD Horizon	Cat# 563716; RRID: AB_2716864
Anti-Human CD34 FITC	eBioscience	Cat# 11-0349-42; RRID: AB_1518732
Anti-rabbit IgG (H+L), F(ab')2 Fragment (Alexa Fluor 555 Conjugate)	Cell Signaling Technology	Cat# 4413S; RRID: AB_10694110
Anti-Human CD11b PE	eBioscience	Cat# 12-0118-42; RRID: AB_2043799
Anti-Human CD14 APC	eBioscience	Cat# 17-0149-42; RRID: AB_10669167
Anti-Human CD15 APC	eBioscience	Cat# 17-0158-42; RRID: AB_2573137
Anti-Mouse CD45.1 APC	eBioscience	Cat# 17-0453-82; RRID: AB_469398
Anti-Human CD85k (ILT3) APC	eBioscience	Cat# 17-5139-42; RRID: AB_2043854
CD45.2 Monoclonal Antibody (104), PE	eBioscience	Cat# 12-0454-83; RRID:AB_465679
FITC anti-human CD209 antibody	BioLegend	Cat# 330103; RRID: AB_1134057
PE anti-human CD86 antibody	BioLegend	Cat# 374205; RRID: AB_2721632
PE anti-human CD85k (ILT3) antibody	BioLegend	Cat# 333008; RRID:AB_2136645
CD117 (c-Kit) Monoclonal Antibody (2B8), FITC	eBioscience	Cat# 11-1171-82; RRID:AB_465186
Alexa Fluor 647 anti-mouse CD85k (gp49 Receptor) antibody	BioLegend	Cat# 144906; RRID:AB_2562044
CD45.2-Biotin antibody, mouse	Miltenyi Biotec	Cat# 130-101-903; RRID: AB_2660733
Chemicals, Peptides, and Recombinant Proteins		
Recombinant Human FTO protein	Active Motif	Cat# 31572
Recombinant Human ALKBH5 protein	Active Motif	Cat# 31589
Recombinant Tet1 (1418-2136) protein	Active Motif	Cat# 31417
Puromycin dihydrochloride	Sigma-Aldrich	Cat# P8833; CAS: 58-58-2
(2-Hydroxypropyl)-β-cyclodextrin	Sigma-Aldrich	Cat# C0926; CAS: 128446-35-5
Methoxy poly (ethylene glycol)-b-poly (D,L-lactide)	Sigma-Aldrich	Cat# 900661
Hexadimethrine bromide	Sigma-Aldrich	Cat# H9268; CAS: 28728-55-4
Propidium iodide	Sigma-Aldrich	Cat# P4170; CAS: 25535-16-4
bisBenzimide H 33342 trihydrochloride	Sigma-Aldrich	Cat# B2261; CAS: 875756-97-1
Pyronin Y	Sigma-Aldrich	Cat# P9172; CAS: 92-32-0
Pronase from Streptomyces griseus	Roche	Cat# 10165921001
Ammonium iron(II) sulfate hexahydrate	Sigma-Aldrich	Cat# 203505; CAS: 7783-85-9

(*Continued on next page*)

Continued

REAGENT or RESOURCE	SOURCE	IDENTIFIER
α-Ketoglutaric acid	Sigma-Aldrich	Cat# K1128; CAS: 328-50-7
L-Ascorbic acid	Sigma-Aldrich	Cat# A0278; CAS: 50-81-7
Bovine Serum Albumin	Sigma-Aldrich	Cat# A2058; CAS: 9048-46-8
Retinoic acid	Sigma-Aldrich	Cat# R2625; CAS: 302-79-4
5-Aza-2'-deoxycytidine	Sigma-Aldrich	Cat# A3656; CAS: 2353-33-5
Recombinant Human M-CSF	PeproTech	Cat# 300-25
Recombinant Human GM-CSF	PeproTech	Cat# 300-03
Recombinant Human IL-6	PeproTech	Cat# 200-06
Recombinant Human IL-3	PeproTech	Cat# 200-03
Recombinant Human IL-10	PeproTech	Cat# 200-10
Recombinant Human IL-4	PeproTech	Cat# 200-04
Recombinant Human SCF	PeproTech	Cat# 300-07
Recombinant Human TPO	PeproTech	Cat# 300-18
Recombinant Human Flt3-Ligand	PeproTech	Cat# 300-19
DNase I, RNase-free	Thermo Fisher Scientific	Cat# EN0521
D-Luciferin Firefly, potassium salt	Goldbio	Cat# LUCK; CAS: 115144-35-9
G418 Sulfate (50 mg/mL)	Thermo Fisher Scientific	Cat# 10131027; CAS: 108321-42-2
Blasticidin	Invivogen	Cat# ant-bl-1
L-Glutamine (200mM)	Thermo Fisher Scientific	Cat# 25030-081
Ammonium Chloride Solution	STEMCELL Technologies	Cat# 07850
MEM Non Essential Amino Acids Solution (100×)	Thermo Fisher Scientific	Cat# 11-140-050
Sodium Pyruvate (100mM)	Thermo Fisher Scientific	Cat# 11360-070
Insulin, human recombinant zinc solution	Thermo Fisher Scientific	Cat# 12585014
Penicillin Streptomycin	Thermo Fisher Scientific	Cat# 15-140-122
Plasmocin prophylactic	InvivoGene	Cat# ant-mpp
Corning Matrigel Membrane Matrix	Thermo Fisher Scientific	Cat# CB-40234A
ColonyGEL-Mouse Base Medium	Reachbio	Cat# 1201
ColonyGEL – Human Base Medium	Reachbio	Cat# 1101
RIPA Buffer	Sigma-Aldrich	Cat# R0278
Halt Phosphatase Inhibitor Cocktail	Thermo Fisher Scientific	Cat# 78420
Halt Protease Inhibitor Cocktail	Thermo Fisher Scientific	Cat# 78429
Paraformaldehyde powder	Sigma-Aldrich	Cat# 158127
Permeabilization Buffer (10×)	eBioscience	Cat# 00-8333-56
4× Laemmli Sample Buffer	Bio-Rad	Cat# 1610747
RNaseOUT Recombinant Ribonuclease Inhibitor	Thermo Fisher Scientific	Cat# 10777019
Pierce Protein A/G Magnetic Beads	Thermo Fisher Scientific	Cat# 88803
Ficoll Paque Plus	GE Healthcare	Cat# 17-1440-02
CD3 MicroBeads, human	Miltenyi Biotec	Cat# 130-050-101
CD34 MicroBead Kit, human	Miltenyi Biotec	Cat# 130-046-702
CD14 MicroBeads UltraPure, human	Miltenyi Biotec	Cat# 130-118-906
MagniSort Streptavidin Positive Selection Beads	Thermo Fisher Scientific	Cat# MSPB-6003-71
FastDigest BamHI	Thermo Fisher Scientific	Cat# FD0054
FastDigest XbaI	Thermo Fisher Scientific	Cat# FD0684
Dynabeads Human T-Activator CD3/CD28	Thermo Fisher Scientific	Cat# 11161D
Recombinant Human IL-2 Protein	R&D Systems	Cat# 202-IL-010
Absolute Counting Beads	Thermo Fisher Scientific	Cat# C36950

(*Continued on next page*)

Continued

REAGENT or RESOURCE	SOURCE	IDENTIFIER
Critical Commercial Assays		
miRNeasy Mini Kit	Qiagen	Cat# 217004
RNeasy Mini Kit	Qiagen	Cat# 74104
Magna MeRIP m^6A Kit	Millipore	Cat# 17-10499
CellTiter 96 Non-Radioactive Cell Proliferation Assay	Promega	Cat# G4100
PE Annexin V apoptosis Detection Kit	BD Biosciences	Cat# 559763
PolyATract mRNA isolation system IV	Promega	Cat# Z5310
QuantiTect Reverse Transcription Kit	Qiagen	Cat# 205314
Maxima SYBR Green qPCR Master Mix	Thermo Fisher Scientific	Cat# K0253
QIAGEN Plasmid Mini Kit	Qiagen	Cat# 12125
Effectene Transfection Reagent	Qiagen	Cat# 301427
PCR Mycoplasma Detection Kit	Applied Biological Materials	Cat# G238
m^6A Demethylase Assay Kit	Abcam	Cat# ab233489
In-Fusion HD Cloning Plus CE	Takara	Cat# 638916
Deposited Data		
RNA-seq with human AML cells (Raw and analyzed data)	This paper	GEO: GSE136204
RNA-seq with murine AML cells (Raw and analyzed data)	This paper	GEO: GSE145363
Experimental Models: Cell Lines		
293T	ATCC	(CRL-3216); RRID:CVCL_0063
U937	ATCC	(CRL-1593.2); RRID:CVCL_0007
THP-1	ATCC	(TIB-202); RRID:CVCL_0006
MV4-11	ATCC	(CRL-9591); RRID:CVCL_0064
Kasumi-1	ATCC	(CRL-2724); RRID:CVCL_0589
TF-1	ATCC	(CRL-2003); RRID:CVCL_0559
K562	ATCC	(CCL-243); RRID:CVCL_0004
NOMO-1	DSMZ	(ACC-542); RRID:CVCL_1609
MONOMAC 6	DSMZ	(ACC-124); RRID:CVCL_1426
ML-2	DSMZ	(ACC-15); RRID:CVCL_1418
NB4	DSMZ	(ACC-207); RRID:CVCL_0005
ZR75-1	ATCC	(CRL-1500); RRID:CVCL_0588
MDA-MB-231	ATCC	(HTB-26); RRID:CVCL_0062
MA9.3ITD	Dr. James C. Mulloy (CCHMC, Cincinnati, OH)	N/A
MA9.3RAS	Dr. James C. Mulloy (CCHMC, Cincinnati, OH)	N/A
8MGBA	Dr. Ravi Salgia (City of Hope, Duarte, CA)	N/A
A172	Dr. Ravi Salgia (City of Hope, Duarte, CA)	N/A
Capan-1	Dr. Ravi Salgia (City of Hope, Duarte, CA)	N/A
MIAPACA-2	Dr. Ravi Salgia (City of Hope, Duarte, CA)	N/A
Experimental Models: Organisms/Strains		
NRGS mouse	The Jackson Laboratory	Cat# JAX:024099; RRID: IMSR_JAX:024099
NSG mouse	The Jackson Laboratory	Cat# JAX:005557; RRID: IMSR_JAX:005557
NCI B6-Ly5.1/Cr mouse	Charles river	Cat# CRL:564; RRID: IMSR_CRL:564

(*Continued on next page*)

Continued

REAGENT or RESOURCE	SOURCE	IDENTIFIER
Oligonucleotides		
ssRNA with internal m^6A modifiaction 5′-AUUGUCA(m^6A)CAGCAGC-3′	Dharmacon	N/A
DNA oligo with internal 5mC modification 5′-CAG TAA CTG TGG TC/iMe-dC/GGT AAC TGA CTT GCA-3′	Integrated DNA Technologies (IDT)	N/A
DNA Oligos listed in Table S4	Integrated DNA Technologies (IDT)	N/A
Recombinant DNA		
pMIRNA1-FTO	This paper	N/A
pMIRNA1-FTO-Mut	This paper	N/A
pCDH-3×Flag-FTO	This paper	N/A
pCDH-3×Flag-FTO$^{H231A/E234A}$	This paper	N/A
pCDH-3×Flag-FTO$^{K216A/S229A/H231A}$	This paper	N/A
pLenti CMV Puro LUC (w168-1)	Campeau et al., 2009	Addgene plasmid # 17477; RRID: Addgene_17477
pMD2.G	A gift from Dr. Didier Trono	Addgene plasmid # 12259; RRID: Addgene_12259
pMDLg/pRRE	Dull et al., 1998	Addgene plasmid # 12251; RRID: Addgene_12251
pRSV-Rev	Dull et al., 1998	Addgene plasmid # 12253; RRID: Addgene_12253
psPAX2	A gift from Didier Trono	Addgene plasmid # 12260; RRID: Addgene_12260
pLKO.1-shFTO-1	This paper	Table S4
pLKO.1-shFTO-2	Sigma-Aldrich	Cat# TRCN0000246249
pLKO.1-shYTHDF2-1	This paper	Table S4
pLKO.1-shYTHDF2-2	Sigma-Aldrich	Cat# TRCN0000265510
pLKO.1-shLILRB4-2	Sigma-Aldrich	Cat# TRCN0000056863
pLKO.1-shLILRB4-3	Sigma-Aldrich	Cat# TRCN0000056865
pLKO.1 puro	Stewart et al., 2003	Addgene plasmid # 8453
lentiGuide-Puro-sgLILRB4	This paper	Table S4
lentiGuide-Puro	Sanjana et al., 2014	Addgene plasmid # 52963
lentiCas9-Blast	Sanjana et al., 2014	Addgene plasmid # 52962
pLVX-ZsGreen	A gift from Dr. Cheng Cheng Zhang	N/A
ZsGreen- hLILRB4	A gift from Dr. Cheng Cheng Zhang	N/A
Software and Algorithms		
GraphPad Prism	GraphPad	https://www.graphpad.com/scientific-software/prism/
GelAnalyzer	GelAnalyzer	http://www.gelanalyzer.com/
RSEM-1.2.31	Li and Dewey, 2011	https://deweylab.github.io/RSEM/
STAR 2.7	Dobin et al., 2013	https://github.com/alexdobin/STAR
igv-2.3.72g	Thorvaldsdottir et al., 2013	http://software.broadinstitute.org/software/igv/
GSEA-2.2.3	Subramanian et al., 2005	http://software.broadinstitute.org/gsea/index.jsp

RESOURCE AVAILABILITY

Lead Contact

Further information and requests for resources and reagents may be directed to and will be fulfilled by the Lead Contact, Jianjun Chen (jianchen@coh.org).

Materials Availability

All cell lines, plasmids, and other stable reagents generated in this study are available from the Lead Contact with a completed Materials Transfer Agreement.

Data and Code Availability

The RNA-Seq data generated in this study are available at NCBI GEO DataSets under accession number GSE136204 (https://www.ncbi.nlm.nih.gov/geo/query/acc.cgi?acc=GSE136204) and GSE145363 (https://www.ncbi.nlm.nih.gov/geo/query/acc.cgi?acc=GSE145363).

EXPERIMENTAL MODEL AND SUBJECT DETAILS

Leukemia Patients and Healthy Donors Samples

The leukemia patient samples were obtained at the time of newly diagnosis, after treatment, or relapsed, and with informed consent at City of Hope Hospital, Cincinnati Children's Hospital, or Dana-Farber/Harvard Cancer Center in congruence with the protocol approved by the institutional review board (IRB). Characteristics of AML patients were outlined in Table S1. The samples from healthy donors were collected from the healthy donor center in City of Hope Hospital under the IRB protocol approved by the institute. The samples were performed with erythrocytes lysis and the mononuclear cells (MNCs) were cryopreserved in -150°C waiting for further study.

Cell Culture

The leukemia cells, U937, THP1, and MV4-11 were obtained from American Type Culture Collection (ATCC) and cultured in endotoxin-free RPMI1640 supplemented with 10% fetal bovine serum (FBS) (Gemini Bio-Products); K562 (ATCC) was cultured in IMDM with 10% FBS; NOMO-1, ML-2, NB4 were obtained from DSMZ and kept in RPMI1640 with 10% FBS; MONOMAC 6 (DSMZ) was cultured in 90% RPMI 1640 with 10% FBS plus 2 mM L-glutamine, 1 × non-essential amino acids, 1mM sodium pyruvate, and 10μg/ml human insulin;TF-1 (ATCC) was maintained in RPMI1640 with 10% FBS and 2ng/ml GM-CSF; MA9.3ITD (*MLL-AF9* plus *FLT3-ITD*-transformed human $CD34^+$ cord blood) and MA9.3RAS (*MLL-AF9* plus *NRasG12D*-transformed human $CD34^+$ cord blood), established by Dr. James Mulloy (Wunderlich et al., 2013), were maintained in IMDM supplemented with 20% FBS. AML patient-derived primary cells were kept in IDMD supplemented with 20% FBS, 10 ng/ml human cytokines SCF, TPO, FLT3 ligand, IL-3, and IL-6. The glioblastoma cell lines, including 8MGBA and A172 were originally maintained by Dr. David Plas from University of Cincinnati, and cultured in RPMI1640 with 10% FBS. Breast tumor cell lines, including ZR-75-1 and MDA-MB-231, were purchased from ATCC and cultivated in RPMI1640 with 10% FBS. The cell lines from pancreatic cancer cells Capan-1 and MIA PaCa-2 were maintained in RPMI1640 with 10% FBS. All the cells are not among commonly misidentified cell lines, and were tested for mycoplasma contamination annually using a PCR Mycoplasma Detection Kit (G238, Applied Biological Materials Inc.). In order to prevent potential contamination, all the media were supplemented with Penicillin-Streptomycin (15-140-122, Thermo Fisher Scientific) and Plasmocin prophylactic (ant-mpp, InvivoGen) according to the manufacturer's instructions.

Animal Procedures

Human Leukemia Cell Line-Derived Xenograft and PDX Models

NRG-SGM3 (NRGS, RRID: IMSR_JAX:024099) mice were used for both 'human-in-mouse' xeno-transplanation models and PDX models. The mice were originally purchased from the Jackson Laboratory and bred at the specific-pathogen-free core facilities of City of Hope and Cincinnati Children's Hospital according to standard procedures. All animal studies listed below were conducted in accordance with federal and state government guidelines and IACUC protocols approved by City of Hope and Cincinnati Children's Hospital. For each experiment, 6- to 8-week-old mice were used and randomly allocated to each group. For xenograft mouse, 0.1×10^6 MA9.3ITD cells were transplanted into NRGS recipient mice intravenously. Drug treatment was started from 10 days after transplantation. CS2 was administered through intraperitoneal (i.p.) injection at 5mg/kg/day, every other day. CS1 dissolved in saturated β-cyclodextrin (C0926, Sigma-Aldrich) solution was delivered by intravenous injection (i.v.). Successful engraftment was observed following 4 weeks post inoculation displaying a level of about 5% human $CD33^+$ cells in peripheral. To generate PDX mouse models, 1×10^6 AML patient derived BMMNCs were transplanted into NRGS recipient mice intravenously, and drug treatment was started from 7 days later. CS2, FB23-2, and free CS1 were administered through i.p. injection at 5 mg/kg/day, while Micelle (900661, Sigma-Aldrich) packaged CS1 was delivered by i.v. injection at 5mg/kg/day. Both CS1 and CS2 were injected every other day for a total of ten times.

Allogeneic BMT in Immunocompetent Mice

The MA9 cells utilized for secondary BMT were isolated from primary BMT. For primary BMT assay, mouse bone marrow progenitor cells (herein is lineage negative; Lin^-) cells were enriched from 6- to 8-week-old C57BL/6J CD45.2 (B6) mice upon 5-fluorouracil (5-FU) treatment for 5 days with Lineage Cell Depletion Kit (130-090-858, Miltenyi Biotec). The Lin^- progenitor cells were retrovirally transduced with MSCV-Neo-MA9 construct through two rounds of 'spinoculation' as described previously (Li et al., 2015). After 7 days of selection with 0.5mg/ml G418 Sulfate (10131027, Thermo Fisher Scientific) in ColonyGEL (1201, ReachBio Research Lab), the cells were collected and injected into lethally irradiated (960 rads) 8- to 10-week-old B6.SJL (CD45.1, RRID: IMSR_CRL:564) recipient mice with 0.5×10^6 donor cells plus 1×10^6 'helper' cells (freshly isolated from the bone marrow of B6.SJL mice without

irradiation) for each recipient mouse. For secondary BMT assays, primary leukemic mouse bone marrow cells (CD45.2$^+$) were collected and sorted by flow cytometry when the mice developed full-blown AML. The cells were injected into sub-lethally irradiated (570 rads) secondary recipient mice with 0.1x10^6 donor cells per mouse via tail vein injection. One week after BMT, the mice were randomly grouped into CS1, CS2, and control groups. The recipient mice were injected with PBS, 5 mg/kg free CS1, 5 mg/ml Micelle_CS1, and 5 mg/kg CS2, i.p., every other day, for 20 days. As the drug combination study in Figure 8C, DAC (0.2 mg/kg/day, A3656, Sigma-Aldrich) was administrated six times (3 times/week for two continuous weeks) through i.p. injection. For the studies related to immune checkpoint, the recipient mice were not irradiated.

Human Breast Cancer Cell Line-Derived Subcutaneous Xenograft Model

ZR75-1 breast cancer cell line-derived xenograft experiment was performed in 6-8 week old female NSG mice purchased from the Jackson Laboratory (RRID: IMSR_JAX:005557). More information about the generation of the subcutaneous xenograft model is listed below in Method Details.

METHOD DETAILS

Cell Viability and Proliferation Assay

Cell viability and proliferation were determined with CellTiter 96 Non-Radioactive Cell Proliferation Assay (MTT, G4100, Promega). To validate the function of the top 213 compounds enriched from the structure-based virtual screening pipeline, MONOMAC 6 cells were seeded into 96-well plate in the concentration of 10,000 cells/well and treated with 1 μM and 5 μM in triplicates. Per the manufacture's recommendation, 15 μl dye solution was added into the well at indicated time point. After incubation at 37°C for 2-4 hours, 100 μl solubilization/Stop Solution was added to quench the reaction. Finally, the absorbance was recorded at 570 nm on the next day. For the cell proliferation with *FTO* KD stable cells, the indicated AML cells were first infected with pLKO.1-sh*FTO* lentivirus, selected the positive cells with 1 μg/ml puromycin (P8833, Sigma-Aldrich) for one week, and then seeded into 96-well plate upon CS1 and CS2 treatment.

Structure-Based (or Docking-Based) Virtual Screening Pipeline

Briefly, the three-dimensional structure of FTO protein was downloaded from RCSB Protein Data Bank (PDB id 4zs2 (Wang et al., 2015)), and then our in-house developed LiVS (Ligand Virtual Screening Pipeline) (Liu et al., 2016) was employed to screen the NCI Developmental Therapeutics Program (DTP) compound library (containing about 260,000 compounds) *in silico* to identify FTO inhibitor hits (Figures 1A–1C). LiVS method is a multiple-stage and full-coverage pipeline for virtual ligand screening that utilizes the three precision modes (i.e., HTVS, high-throughput virtual screening; SP, standard precision; and XP, extra precision) of Schrödinger Glide software (Friesner et al., 2004) for docking. First, the HTVS precision mode, which is fast but less accurate, was implemented to dock the entire NCI DTP library. The 10,000 top-ranked compounds were next docked and scored by the SP mode. Then the 1,000 top-ranked compounds from SP precision docking were re-docked and re-scored by the XP mode. The 1,000 compounds were further analyzed and filtered by Lipinski's rule of five (Lipinski, 2004), HTS frequent hitter (PAINS) (Baell and Holloway, 2010), protein reactive chemicals such as oxidizer or alkylator (ALARM) (Huth et al., 2005), and maximized the molecule diversity by using UDScore (Universal Diversity Score, developed by us to measure library diversity which is independent of library size). Based on the virtual screening pipeline, we requested the top 370 compounds from NCI DTP and 213 of them are available for experimental study.

Cell Cycle and Apoptosis Assays

In this study, Propidium iodide (PI, P4170, Sigma-Aldrich) DNA staining was chosen to assess the cells located at G0/G1, S, and G2/M stages; while Hoechst 33342 (B2261, Sigma-Aldrich and Pyronin Y (P9172, Sigma-Aldrich) were selected to evaluate cells at G0, G1, and S/G2/M phases. For PI staining, 1 × 10^6 cells were collected, washed once with PBS, and suspended in 1 ml Krishan's buffer supplemented with 0.05 mg/ml PI, 0.1% trisodium citrate, 0.02 mg/ml ribonuclease A, and 0.3% NP-40, incubated at 37°C for 30 minutes and then applied to flow cytometer directly. For Hoechst 33342/Pyronin Y staining, the cells were collected, washed, and resuspended in 1 ml cell culture medium, stained with 10 μg/ml Hoechst 33342 at 37°C for 45 minutes, and further stained with 0.5 μg/ml Pyronin Y for additional 15 minutes at 37°C. The samples were transferred onto ice before subjected to flow cytometry. Cell apoptosis was validated with PE Annexin V Apoptosis Detection Kit I (559763, BD Biosciences) according to the manufacturers' protocol. Cells were washed twice with cold PBS, and then resuspended in 100 μl 1×10^6 cells/ml. Add 5 μl of PE Annexin V and 5 μl 7-AAD to the suspension, gently vortexed the cells, and incubated for 15 min at room tempreture in the dark. After that, apply 400 μl of 1X Binding Buffer to each sample and analyzed by flow cytometry within one hour. Flow cytometry was performed with a BD Fortessa X20 and the results were analyzed with FlowJo V10 software.

In Vivo Bioluminescence Imaging

Prior to *in vivo* bioluminescence imaging, 3rd generation luciferase expression lentivirus was generated by co-transfection of 1.5 μg pLenti CMV Puro LUC plasmid (17477, Addgene) (Campeau et al., 2009), 0.5 μg pMD2.G (12259, Addgene), 0.3 μg pMDLg/PRRE (12251, Addgene), 0.7 μg pRSV-Rev (12253, Addgene) into HEK293T cells in 60 mm cell culture dish with Effectene Transfection Reagent (301427, QIAGEN), and then the leukemia cells or the tumor cells were infected with lentivirus and selected with 1 μg/ml puromycin to stably express luciferase. For *in vivo* bioluminescence imaging, the mice were weighed, injected intraperitoneally with 150 mg/kg D-luciferin (LUCK-2G, Goldbio) in PBS solution, and then anesthetized with isoflurane. The mice were imaged

10 minutes after D-luciferin injection with Lago X (Spectral Instruments Imaging). The bioluminescent signals were quantified using Aura imaging software (Spectral Instruments Imaging). Total flux values were determined by drawing regions of interest, which are identical among the mice in different groups, and are presented in photons/second/cm^2/steradian.

Treatment of AML Xenografts with FTO Inhibitors and/or T Cells

NRG-SGM3 (NRGS) mice were used as recipient mice for human MA9.3ITD AML xenografts subjected to the treatment with FTO inhibitors and/or T cells (Figures 8A–8C). In brief, 0.1×10^6 MA9.3ITD AML cells were resuspended in 200 μl PBS for each mouse and delivered through intravenous injections. All the mice were randomly divided into 6 groups, PBS, T cell, β-CD_CS1, β-CD_CS1 plus T cell, CS2, and CS2 plus T cell. One week post transplantation, the mice were administrated every other day with 5 mg/kg/day β-CD_CS1 or CS2 for 5 times in total. For T cell tretament, each mouse was injected with 5 × 10^6 activated human CD3$^+$ T cells twice after one and two weeks, respectively, post transplantation. Leukemia development and progression were monitored over time by bioluminescence imaging.

In Vivo Solid Tumor Models

Adult NSG mice were utilized for *in vivo* breast cancer subcutaneous xenograft models (Figures 8D and 8E). In this study, 2 × 10^6 ZR75-1 breast cancer cells were collected, resuspended in 100μl 50% matrigel membrane matrix (CB-40234A, Thermo Fisher Scientific) diluted in PBS, and implanted subcutaneously into the flanks of NSG recipient mice on both sides. Tumor was measured for the short and long diameter using a caliper, and the volume was calculated using the formula (short × short × large)/2. Drug treatment began when the tumor size was larger than 100 mm^3. β-cyclodextrin_CS1 (5 mg/kg), CS2 (5 mg/kg) or control vehicle were administrated every other day by i.v. and i.p. injection respectively. Mice receiving CS1 were treated 10 times, while CS2 treated mice were treated 12 times. *In vivo* bioluminescence imaging was performed at the end point. All the mice were euthanized at day 53 after implantation, when the tumors in the control group are around 1,000 mm^3.

Preparation of CS1 mPEG-*b*-PLA Micelle

Methoxy poly(ethylene glycol)-b-poly(D,L-lactide) (mPEG-b-PLA) was purchased from Sigma-Aldrich (900661). The film hydration method was employed to prepare the CS1 loaded polymeric micelle as described previously with some modification (Gao et al., 2017). In brief, CS1 and mPEG-b-PLA were dispersed in chloroform accompanying with sonication, respectively. Then, the two chloroform solutions were well-mixed together via vortex and sonication. After making sure that the mixture was completely dissolved by chloroform, a vacuum-rotary evaporator was employed to evaporate the chloroform and to obtain a CS1-loaded polymer film. The thin film was then hydrated with deionized water, followed by vortex for 2 minutes and sonication for 5 minutes. Finally, the hydrated system was processed by centrifugation for 15 minutes at 5000 rpm to remove the un-encapsulated free CS1. The supernatant was the purified CS1 loaded mPEG-b-PLA micelle.

Serial Colony-Forming Assay

The assay was performed as described previously with some modification (Li et al., 2015). Briefly, the primary murine leukemic cells isolated from bone marrow of AML mice, including MA9 and FLT3ITD/NPM1, were seeded into 35 mm culture dishes (20,000 cells/dish or 10,000 cells/dish) with ColonyGEL plus murine cytokines, including 10 ng/ml IL-3, IL-6, GM-CSF, and 50 ng/ml SCF (Figure S3M). For the colony-forming assay of CD34$^+$ blast cells derived from AML patients (Figure S3L), 20,000 cells were seeded in 1.5 ml ColonyGEL-Human Base Medium (1101, ReachBio Research Lab) in 35 mm culture dish, supplemented with human recombinant 10 ng/ml IL-3, IL-6, GM-CSF and 100 ng/ml SCF. The dishes were incubated at 37°C in a humidified atmosphere of 5% CO_2 for 7 days. Then, colony cells were collected and replated every 7 days for 3 passages. Colony numbers were counted and compared for each passage.

Limiting Dilution Assays

For *in vitro* limiting dilution assays (LDAs), the murine MA9 or FLT3ITD/NPM1Mut AML cells with or without *Fto* knockdown or CS1 treatment were suspended in ColonyGEL medium and plated in 48-well plates at a limiting dilution manner, e.g. 100 cells/well, 50 cells/well, 20 cells/well, 10 cells/well, 5 cells/well, and 1 cell/well. For each dose, 12 wells were included. The number of wells containing spherical colonies was counted after 7 days to estimate stem cell frequency. For *in vivo* LDA, the bone marrow mononuclear cells isolated from MA9 AML mice subjected to PBS, 5 mg/kg β-CD_CS1, or 5 mg/kg CS2 treatment, were injected into sublethally irradiated 8- to 10-week-old B6.SJL (CD45.1) recipient mice via tail vein at a limiting dilution manner, i.e., 1 × 10^6, 1 × 10^5, 1 × 10^4, 1 × 10^3, and 1 × 10^2 donor cells per mouse. The number of recipient mice developed full-blown leukemia within two month post transplantation was counted from each group. ELDA software (Hu and Smyth, 2009) was utilized to evaluate the frequency of LSC/LICs.

Retrovirus and Lentivirus Production

Retrovirus infections of murine progenitor cells were employed as described previously (Li et al., 2015). The retrovirus vectors were transfected into HEK-293T cells using Effectene Transfection Reagent (301427, Qiagen) together with packaging vector pCL-ECO. The retrovirus was collected at 48 and 72 hours post transfection, and transduced into mouse progenitor cells in the presence of 4-8 μg/ml polybrene (H9268, Sigma-Aldrich) for 'spinoculation'. Lentivirus used for overexpression and KD of a specific gene was packaged with pMD2.G, pMDLg/pRRE, and pRSV-Rev (purchased from Addgene) (Dull et al., 1998; Stewart et al., 2003). Briefly, 1.5 μg

pMD2.G, 0.9 μg pMDLg/pRRE, 2.1 μg pRSV-Rev, and 5.4 μg constructs were co-transfected into HEK-293T cells in 100 mm cell culture dish with Effectene Transfection Reagent. The lentivirus particles were harvested at 48 and 72 hours after transfection, concentrated with PEG-it Virus Precipitation Solution (LV810A-1, SBI), and used to infect leukemic cells in the presence of polybrene.

CRISPR-Cas9-Based Knockout of LILRB4 in MONOMAC 6 AML Cells

The MONOMAC 6 cells were infected with Cas9-expressing lentivirus (lentiCas9-Blast) (Sanjana et al., 2014) and single clones were selected with 10 μg/ml blasticidin (ant-bl-1, Invivogen). Then the single clones were infected with sgRNA-expressing lentivirus (lentiGuide-Puro-sgLILRB4) and the sgRNA-infected cells were selected with 1 μg/ml puromycin. Both the Cas9- and sgRNA expressing lentivirus were generated using the second generation package system. In brief, 3 μg expression plasmid, 0.75 μg pMD2.G, and 2.25 μg psPAX2 (psPAX2 was a gift from Dr. Didier Trono) were mixed well and co-transfected into HEK-293T cells in 60 mm cell culture dish with Effectene Transfection Reagent (Salmon and Trono, 2007).

RNA Extraction, cDNA Synthesis, and qPCR

Total RNA samples were isolated with miRNeasy Mini Kit (217004, Qiagen) following the manufacturer's guidelines. The $CD34^+$ and $CD34^-$ cells were isolated from mononuclear cells with CD34 MicroBeads (130-046-702, Miltenyi Biotec). For cDNA synthesis, 200-1,000 ng total RNA or immunoprecipitated RNA samples were used for reverse transcription in 10 μl reaction volume using the QuantiTect Rev. Transcription Kit (205314, Qiagen). Quantitative PCR (qPCR) was performed with Maxima SYBR Green qPCR Master Mix (2X) (K0253, Thermo Fisher) in an AB 7900HT Fast Real-Time PCR system (Applied Biosystem). GAPDH, ACTIN, and/or 28S rRNA were used as endogenous control and each reaction was run in triplicates. All the primers are listed in Table S4.

m^6A Dot Blot Assay and Gene-Specific m^6A Immunoprecipitation

To determine global m^6A abundance, m^6A dot blot assays were employed with total RNA and/or $poly(A)^+$ RNA as described previously (Su et al., 2018). In brief, 50 μl equal amount of RNA samples mixed with 150 μl sample volumes of RNA incubation buffer, followed by denatured at 65°C for 5 minutes. Then 200μl of chilled 20 × SSC buffer was added and mixed well before samples were loaded onto the Amersham Hybond-N+ membrane (RPN303B, GE Healthcare) with a Bio-Dot Apparatus (Bio-Rad). After crosslinking under 254nm UV for 5 minutes, the membrane was stained with methyl blue and the image was captured. The membrane was then washed with 1 × PBST buffer (PBST01-02, Bioland Scientific LLC), blocked with 5% non-fat milk and incubated with rabbit anti-m^6A antibody (1:2000, 202003, Synaptic Systems) overnight at 4°C. After wash three times with PBST, the membrane was incubated with HRP-conjugated goat anti-rabbit IgG (ab6721, Abcam) for 1 hour at room temperature and the membrane was developed with Amersham ECL Prime Western Blotting Detection Reagent (45-010-090, Fisher Scientific). $Poly(A)^+$ RNA was enriched from total RNA with polyATract mRNA isolation system IV (Z5310, Promega). Nuclei were isolated from cells with nuclear isolation buffer (1.28 M sucrose, 40 mM Tris-HCl pH 7.5, 20 mM $MgCl_2$, and 4% Triton X-100) and the nuclear RNA was extracted from nuclei with miRNeasy Mini Kit to evaluate m^6A modification on snRNA. Gene-specific m^6A immunoprecipitation (IP) was employed with Megna MeRIP m^6A kit (17-10499, Millipore) and the RNA was recovered with RNeasy Mini Kit according to the manufacturer's instruction.

Protein Extraction and Western Blot Assay

Total protein was extracted from PBS washed cell pellet, lysed with RIPA buffer (R0278, Sigma-Aldrich) containing 5mM EDTA, 1 × Halt phosphatase inhibitor cocktail (78420, Thermo Fisher Scientific) and 1 × Halt protease inhibitor cocktail (78429, Thermo Fisher Scientific) on ice for 20 minutes, followed by centrifuge at 15,000 rpm at 4°C for 15 minutes. Then the supernatant was collected and the protein concentration was quantified by the BCA method. Western blot assay was performed as described previously (Su et al., 2018). Antibodies used for Western blot were as follows unless otherwise specified: FTO (ab124892, Abcam), GAPDH (sc-47724, Santa Cruz Biotechnology), β-Actin (3700S, Cell Signal Technology), LILRB4 (ab229747, Abcam), Goat anti-rabbit IgG H&L (HRP) (ab6721, Abcam), and Goat anti-mouse IgG H&L (HRP) (ab6789, Abcam).

Flow Cytometry Analysis

Flow cytometry analysis with surface markers was conducted as described previously with some modifications (Su et al., 2018). Retinoic acid (R2625, Sigma-Aldrich) was utilized to induced myeloid differentiation in NB4 cells. Antibodies used included anti-mouse CD45.1 APC (17-0453-82, eBioscience), anti-mouse CD45.2-PE (12-0454-83, Thermo Fisher Scientific), anti-mouse CD117 (c-Kit) FITC (17-1171-82, eBioscience), anti-Human CD33 PE (12-0339-42, Thermo Fisher Scientific), anti-Human CD45 BV786 (563716, BD Horizon), PE anti-mouse/human CD11b antibody (12-0118-42, eBioscience), anti-Human CD15 APC (17-0158-42, eBioscience), anti-Human CD14 APC (17-0149-42, eBioscience), anti-Human LILRB4 PE (333008, BioLegend), anti-Human LILRB4 APC (17-5139-42, eBioscience), anti-human CD209 FITC (330103, BioLegend), anti-human CD86 PE (374205, BioLegend), anti-Mouse Lilrb4 Alexa Fluor 647 (144906, BioLegend), and anti-Human CD34 FITC (11-0349-42, eBioscience).

Intracellular Staining

For intracellular staining with FTO, we first labeled the human primary cells with CD34 surface marker. Then the cells were washed with chilled PBS, re-suspended in 4% paraformaldehyde (158127, Sigma-Aldrich) at a density of 2×10^6 cells/ml, and incubated at 4°C for 20 minutes with rotation. After fixation, the cells were gently re-suspended in 5 × Permeabilization buffer (00-8333-56, eBioscience), and stained with rabbit anti- human FTO (1:100) for 1 hour on ice. Finally, the cells were washed twice

with 1× Permeabilization buffer, incubated with goat anti-rabbit IgG (H+L) (Alexa Fluor 555 Conjugate, 4413S, Cell Signaling Technology) in 5× Permeabilization buffer for 30 minutes at room temperature protected from dark, washed with FACS buffer and resuspended in 200 μl of FACS buffer for analysis.

Nuclear Magnetic Resonance (NMR) Titration

The N-terminal 31 residues truncated FTO protein was purified with modified methods as previously reported (Huang et al., 2015). Briefly, the FTOΔN31 protein was purified by Nickle-affinity chromatography, followed by a gel filtration (Superdex 200) with the phosphate buffer (20 mM sodium phosphate (pH 7.4), 100 mM NaCl). Fractions were collected and concentrated for further analysis. For CS1, samples were composed of 100 μM compound with 10% DMSO in addition of 0, 10 μM and 20 μM FTO, respectively; and for CS2, samples were composed of 200 μM compound with 2% DMSO in addition of 0, 2 μM, 5 μM and 10 μM FTO, respectively (Figures 2E–2H). NMR data acquisition was performed on a Bruker Avance III-600 MHz spectrometer equipped with a cryogenically cooled probe (Bruker biospin, Germany) at 25°C.

Drug Affinity Responsive Targets Stability (DARTS)

To determine the direct binding between small molecule compounds and FTO protein *in cellulo*, DARTS was conducted in MONOMAC 6 AML cells following the published protocol (Lomenick et al., 2009) (Figures 2I–2L). Empty pCDH vector was linearized by XbaI (FD0684, Thermo Fisher Scientific) and BamHI (FD0054, Thermo Fisher Scientific). The ORF of wild-type FTO with 3 × Falg at C-terminal was cloned from pmiRNA1-FTO and then transferred to linearized pCDH vector with In-Fusion HD Cloning. $FTO^{H231A/E234A}$ and $FTO^{K216A/S229A/H231A}$ were generated from pCDH-3 × Falg-FTO with In-Fusion HD Cloning (638916, Takara). The primers used in In-Fusion cloning were listed in Table S4. The plasmids were extracted with QIAGEN Plasmid Mini Kit and validated by Sanger sequencing. The MONOMAC 6 cells were infected with pCDH-3×Flag-FTO, $FTO^{H231A/E234A}$, and $FTO^{K216A/S229A/H231A}$ and positive cells were selected with 1μg/ml puromycin. Then, $\sim 3\times10^7$ stable cells were collected, washed with chilled PBS, and lysed in 600 μl M-PER buffer (78501, Thermo Fisher Scientific) for 10 minutes on ice before subjected to centrifugation. 600 μl of supernatant was transferred into a fresh tube and mixed with one tenth volume of 10×TNC buffer (500 mM Tris-HCl (pH 8.0), 500 mM NaCl, 100 mM $CaCl_2$). The lysates were split into 6 samples by transferring 100 μl into 1.5 ml Eppendorf tubes, incubated with DMSO, CS1 or CS2 at indicated concentrations for 1 hour at room temperature, and then digested with Pronase (1:3000, 10165921001, Roche) for an additional 30 minutes at room temperature. The reaction was quenched by protein inhibitor cocktail and the samples were immediately placed on ice. Finally, Western blotting was performed to determine whether FTO is a direct target of CS1 and CS2. GAPDH was used as a negative control.

Cellular Thermal Shift Assay (CETSA)

To determine whether CS1 or CS2 act as a direct ligand of FTO protein, CETSA was conducted with intact MONOMAC 6 as published previously (Jafari et al., 2014). Briefly, $\sim 10 \times 10^6$ MONOMAC 6 cells in 100 mm dishes were pretreated with 200 nM CS1 or CS2 for 18 hours before subjected to CETSA protocol. The cells from each group were collected, washed once with iced PBS, and re-suspended in 1.5 ml PBS supplemented with protease inhibitor cocktail. The cell suspension was distributed into 12 different 0.2 ml PCR tubes with 100 μl in each tube. The cells were heat shocked in the Bio-Rad T100 Thermal Cycler at indicated temperatures for 3 minutes to denature proteins, and immediately cooled down to room temperature for another 3 minutes. Finally, the samples were subjected to three freeze-thaw cycles with dry ice and a Thermal Cycler set at 25°C to lyse cells, and centrifuged at 20,000 g for 20 min at 4°C to pellet cell debris together with precipitated and aggregated proteins. The supernatant was boiled with 4× Laemmli Sample Buffer (1610747, Bio-Rad) for Western blot. The bands were quantified using Gel-Pro analyzer software and plotted from three biological replicates.

RNA m^6A Demethylation Assay in Cell Free System

To determine whether CS1 and CS2 could directly disturb the m^6A demethylation activity of FTO protein, m^6A demethylase assay was conducted with m^6A demethylase assay kit (ab233489, Abcam) following the manufacturer's protocol with minor modifications. Recombinant FTO protein was purchased from Active Motif (31572). To assess the effects of the top 20 compounds on the enzymatic activity of FTO, 1 μM compound (less than 1% volume) and 0.4 μg FTO protein were utilized for each reaction. While, for the enzymatic reaction of CS1 and CS2, we added 44 μl of final demethylase buffer, 1 μl (0.3 μg) of purified FTO protein, and 5 μl of inhibitor solution with indicated concentration. The strip plates were incubated at 37°C for 90 minutes. For the final signal detection, we added 100 μl of developer solution to each well and incubated at room temperature for 3 minutes away from light before adding 100 μl of stop solution. The absorbance was recorded at 450 nm immediately.

The FTO demethylase activity (OD/h/mg) in each well was determined by the following formula:

The relative inhibition on FTO demethylase was calculated by the following equation:

$$Demethylase\ activity = \frac{[OD(\text{control} - \text{blank}) - OD(\text{inhibitor sample} - \text{blank})]}{\left[\text{Protein Amount}\frac{\mu g}{1000}\right] \times 1.5\ \text{hour}}$$

$$Inhibition\% = \left(1 - \frac{[OD(control - blank) - OD(inhibitor\ sample - blank)]}{[OD(control - blank) - OD(no\ inhibitor\ sample - blank)]}\right) \times 100\%$$

To test the effect of FTO inhibitors on the demethylase activity of the other m^6A eraser protein, ALKBH5, m^6A demethylase assay and m^6A dot blot were performed. The single-stranded RNA with internal m^6A modification (5'-AUUGUCA(m^6A)CAGCAGC-3') were synthesized by GE health, and ALKBH5 protein was purchased from Active Motif (31589). The m^6A demethylase activity assays were conducted as described previously (Su et al., 2018). In brief, a 20 μl reaction mixture containing the indicated concentration of CS1 or CS2, 0.1 nmol ssRNA, 200 nM ALKBH5 protein, 283 μM of $(NH_4)_2(SO_4)_2 \cdot 6H_2O$ (203505, Sigma-Aldrich), 75 μM of α-KG (K1128, Sigma-Aldrich), 2 mM of L-ascorbic acid (A0278, Sigma-Aldrich), 50 μg/ml of bovine serum albumin (BSA A2058, Sigma-Aldrich), and 50 mM of HEPES buffer, pH 7.0 was incubated at 37°C for 3 hours and quenched by 5 mM EDTA followed by thermal inactivation of ALKBH5 for 5 min at 95°C. The ssRNA was precipitated with the addition of one-tenth volumes of 3 M sodium acetate (pH 5.2), glycogen (500 μg/ml, final concentration) and 2.5 volumes of 100% ethanol, and incubated at −80°C overnight. The RNA pellet was resuspended in 10 μl of RNase-free water and then applied to m6A dot blot assay to detect m^6A levels. To avoid the effects of solvent, the volume of compound occupied was less than 1% of the total volume.

DNA 5mC Demethylation Assay and 5hmC Dot Blot in Cell Free System

To assess the effect of FTO inhibitors on the enzymatic activity of methylcytosine dioxygenase, we employed the DNA 5mC demethylation assay with TET1 protein followed by 5hmC dot blot. The DNA oligo with internal 5mC modification (5'-CAG TAA CTG TGG TC/iMe-dC/ GGT AAC TGA CTT GCA-3') was synthesized from Integrated DNA Technologies (IDT) and TET1 protein was purchased from Active Motif (31417). For this assay, 100 μM DNA oligo was incubated with 200 ng/μl TET1 protein in reaction buffer (1 M HEPES PH 8.0, 5 mM $Fe(NH_4)_2(SO_4)_2$, 3 mM 2-oxoglutarate (203505, Sigma-Aldrich), 200 nM L-ascorbic, 10 mM ATP, and 1 M DTT) with the compounds at 37°C for 2 hours. The DNA oligos were purified and 5hmC dot blot assay was conducted to determine the 5hmC levels with 5hmC antibody (39769, Active Motif) as described previously (Su et al., 2018).

Cross-Linking Immunoprecipitation and qPCR (CLIP-qPCR)

CLIP-qPCR was utilized to validate the interactions between FTO and its target mRNAs. Briefly, cells in 150 mm culture plates at 80% confluence were washed once with ice-cold PBS, cross-linked by UV with 150 mJ/cm^2 (254 nm), and harvested by trypsinization. The nuclear fraction was isolated with freshly prepared nuclear isolation buffer (1.28 M sucrose, 40 mM Tris-HCl pH 7.5, 20 mM $MgCl_2$, 4% Triton X-100), lysed in RNA immunoprecipitation (RIP) buffer (150 mM KCl, 25 mM Tris pH 7.4, 5 mM EDTA, 0.5 mM DTT, 0.5% NP40) with freshly added 100 U/ml RNAase inhibitor (10777019, Thermo Fisher Scientific) and 1 × protease inhibitors for sonication. For each reaction, 50 μl Protein A/G magnetic beads (88803, Thermo Fisher Scientific) were added to pre-clear nuclear lysates. In the meantime, Flag (F3165, Sigma-Aldrich) antibody and negative control IgG antibody (12-371, Millipore) were conjugated to Protein A/G magnetic Beads by incubation for 4 hours at 4°C. The conjugated beads were washed three times with RIP buffer, incubated with pre-cleared nuclear extract at 4°C overnight. After three washes with RIP buffer, the beads were incubated with RNase-free DNase I for 15 minutes at 37°C, and Proteinase K for 15 minutes at 37°C before quenched by QIAzol lysis reagent (79306, Qiagen). The input RNA and immunoprecipitated RNA were recovered by QIAzol extraction, and dissolved in 12 μl RNase-free water. 4 μl purified RNA from each group was used for reverse transcription and qPCR.

Co-culture Assay with AML Cells and T Cells

For the co-culture assays, peripheral blood mononuclear cells (PBMNCs) were isolated from healthy donor peripheral blood samples through Ficoll separation (Ficoll Paque Plus, GE17-1440-02, GE Health), and CD3 T cells were enriched from PBMNCs with CD3 MicroBeads (130-050-101, Miltenyi Biotec). The CD3 T cells were kept in RPMI 1640 with CD3/CD28 Dynabeads (11161D, Thermo Fisher Scientific) and 50 U/ml recombinant Human IL-2. In the meantime, AML cells were infected with pmiRNA1 lentivirus and GFP^+ cells were selected. After treated with indicated concentration of CS1, CS2, and DMSO for 48 hours, the GFP^+ cells were collected and resuspended in fresh medium. The pretreated AML cells (40,000 cells/well) were mixed with CD3 T cells at indicated ratios and co-cultured in 48-well plates for 12-16 hours. After that, the cells were collected and mixed with absolute counting beads (C36950, Thermo Fisher Scientific). The number of GFP^+ cells was determined through flow cytometry analysis FlowJo V10 Software.

Generation of Human Dendritic Cells and Macrophages

Both human dendritic cells and macrophages are derived from $CD14^+$ PBMNCs. In brief, the PBMNCs were enriched from peripheral blood samples of healthy donors and $CD14^+$ cells were separated from PBMNCs via magnetic beads sorting with CD14 microbeads accordingly (130-118-906, Miltenyi Biotec). The $CD14^+$ cells were differentiated into dendritic cells with 50 ng/ml GM-CSF and 500 U/ml IL-4 for 7 days; while the cells were differentiated into macrophages with 50 ng/ml M-CSF and 25 ng/ml IL-10 for 7 days. All the cells were maintained in RPMI 1640 with 10% FBS. The dendritic cells and macrophages were confirmed by CD209 and CD86, respectively. Then the dendritic cells and macrophages were treated with CS1 and CS2 for 48 hours.

Isolation of Spleen MNCs from PBS and CS1 Treated MLL-AF9 (MA9) Mice

MA9 primary leukemic mouse bone marrow cells ($CD45.2^+$) were collected and sorted by flow cytometry when the mice developed full-blown AML. The cells were injected into sub-lethally irradiated (320 rads) secondary recipient mice with 5×10^4 donor cells per mouse via tail vein injection. One week after BMT, the mice were randomly divided into CS1 and control groups. The recipient mice were injected with PBS control and 5mg/kg CS1 i.p. every other day for 20 days. Spleens were removed from mice at the end point, and homogenized into a single-cell suspension using RPMI 1640 supplemented with 2% FBS. Red blood cells were lysed using ammonium chloride (07850, STEMCELL Technologies), washed with cold PBS. Cell pellets were then resuspended in 45 μl pre-cold MACS buffer (0.5% BSA and 2mM EDTA in PBS) per 1×10^7 total cells. Biotin-labeled CD45.2 (130-101-903, Miltenyi Biotec) were added to the cells and incubated for 10 minutes in the refrigerator (2−8°C). Cells were subsequently washed with MACS buffer and resuspended in MACS buffer (1×10^8 cells/mL). Streptavidin microbeads (MSPB-6003-71, Thermo Fisher Scientific) were added and the cell mixture was incubated at room temperature for 10 minutes. Cells were washed again and resuspended in 500 μl MACS buffer and then isolated with the MACS separation Columns. After collecting the $CD45.2^+$ cells, total RNA was extracted using miRNeasy Mini Kit and polyA RNA was enriched for RNA sequencing.

RNA Sequencing and Data Analysis

Total RNA samples were isolated from cells upon CS1, CS2 treatment and *FTO* KD with miRNeasy Mini Kit for sequencing. RNA concentration was measured by NanoDrop 1000 (Thermo Fisher Scientific, Waltham Massachusetts, US) and RNA integrity was determined using Bioanalyzer (Agilent). Each RNA sample was spiked in with an appropriate amount of either Mix1 or Mix2 according to Life Technologies' guidelines which would lead to about 1% of the total number of RNA-Seq reads mapping to the 92 ERCC control sequences, assuming the mRNA fraction in the total RNA is 2%. Library construction of 300 ng total RNA for each sample was made using KAPA Stranded mRNA-Seq Kit (Illumina Platforms) (Kapa Biosystems, Wilmington, USA) with 10 cycles of PCR amplification. Libraries were purified using AxyPrep Mag PCR Clean-up kit (Thermo Fisher Scientific). Each library was quantified using a Qubit fluorometer (Life Technologies) and the size distribution assessed using the 2100 Bioanalyzer (Agilent Technologies, Santa Clara, USA). Sequencing was performed on an Illumina® Hiseq 2500 (Illumina, San Diego, CA, USA) instrument using the TruSeq SR Cluster Kit V4-cBot-HS (Illumina®) to generate 51 bp single-end reads sequencing with v4 chemistry. Quality control of RNA-Seq reads was performed using FastQC. Each group contains 3-4 replicates. Reads were trimmed for adaptor sequence, masked for low-complexity or low-quality sequence by Cutadapt, and then aligned to reference genome GRCh38 by STAR (Dobin et al., 2013). The expressions of the genes were calculated using RSEM (Li and Dewey, 2011), $p < 0.05$ was set as the threshold of the differential expressions. The reads distributed in a specific transcript were displayed by IGV (Thorvaldsdottir et al., 2013). Hierarchical cluster analysis was generated by R package cluster. Gene Set Enrichment Analysis (GSEA) and hallmark gene sets in Molecular Signatures Database (MSigDB) (Subramanian et al., 2005) were hired to calculate enriched pathways.

QUANTIFICATION AND STATISTICAL ANALYSIS

Data were analyzed with GrapPad Prism 7 and were presented as mean ± SEM or mean ± SD as indicated. Two-tailed Student's t test was used to compare the means between groups as indicated; $p < 0.05$ was considered significant. Kaplan-Meier survival curves were plotted with GraphPad Prism 7 and the p values were calculated using the log-rank test. For Western blot results, representative figures from three biological replicates were shown. Densitometry analysis of the bands from Western blot was performed with GelAnalyzer.

Cancer Cell, Volume *38*

Supplemental Information

Targeting FTO Suppresses Cancer Stem Cell Maintenance and Immune Evasion

Rui Su, Lei Dong, Yangchan Li, Min Gao, Li Han, Mark Wunderlich, Xiaolan Deng, Hongzhi Li, Yue Huang, Lei Gao, Chenying Li, Zhicong Zhao, Sean Robinson, Brandon Tan, Ying Qing, Xi Qin, Emily Prince, Jun Xie, Hanjun Qin, Wei Li, Chao Shen, Jie Sun, Prakash Kulkarni, Hengyou Weng, Huilin Huang, Zhenhua Chen, Bin Zhang, Xiwei Wu, Mark J. Olsen, Markus Müschen, Guido Marcucci, Ravi Salgia, Ling Li, Amir T. Fathi, Zejuan Li, James C. Mulloy, Minjie Wei, David Horne, and Jianjun Chen

Supplemental Information

Targeting FTO suppresses cancer stem cell maintenance and immune evasion

Rui Su, Lei Dong, Yangchan Li, Min Gao, Li Han, Mark Wunderlich, Xiaolan Deng, Hongzhi Li, Yue Huang, Lei Gao, Chenying Li, Zhicong Zhao, Sean Robinson, Brandon Tan, Ying Qing, Xi Qin, Emily Prince, Jun Xie, Hanjun Qin, Wei Li, Chao Shen, Jie Sun, Prakash Kulkarni, Hengyou Weng, Huilin Huang, Zhenhua Chen, Bin Zhang, Xiwei Wu, Mark J. Olsen, Markus Müschen, Guido Marcucci Ravi Salgia, Ling Li, Amir T. Fathi, Zejuan Li, James C. Mulloy, Minjie Wei, David Horne, Jianjun Chen

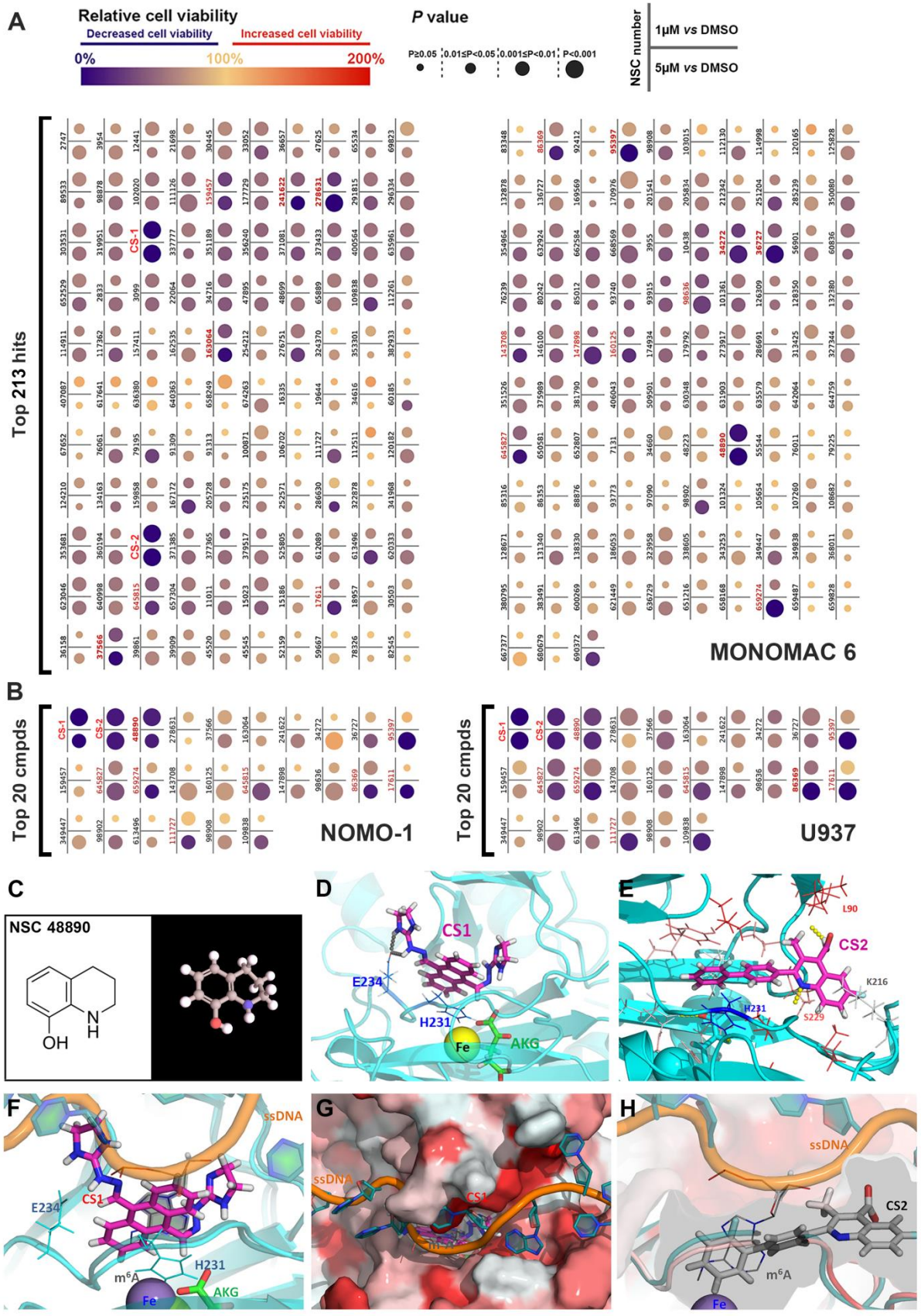
A
Relative cell viability
Decreased cell viability
Increased cell viability
0%
100%
200%
P value
P≥0.05
0.01≤P<0.05
0.001≤P<0.01
P<0.001
NSC number
1μM vs DMSO
5μM vs DMSO
Top 213 hits
MONOMAC 6
B
Top 20 cmpds
NOMO-1
Top 20 cmpds
U937
C
NSC 48890
OH
N
H
D
CS1
E234
H231
Fe
AKG
E
L90
CS2
K216
H231
S229
F
ssDNA
CS1
E234
H231
m6A
Fe
AKG
G
ssDNA
CS1
H
ssDNA
CS2
m6A
Fe

Figure S1. The effects of top FTO inhibitor hits on cell viability in AML cells as well as the docking pose of the top hits with FTO protein, Related to Figure 1

(A) The effects of the top 213 hits (among the 370 top hits identified by the virtual screening, only 213 were available from NCI) on the viability of human MONOMAC 6 AML cells. The cells were treated with DMSO, 1 μM or 5 μM compounds (with indicated NSC numbers) for 48 hours and the relative cell viability was assessed by MTT assays and normalized to DMSO control. As the heat bar, 101%-200% represents increase in cell viability; while 0%-99% indicates decrease in cell viability. For a given compound, the left number represents its NSC number. The upper and lower dots represent the relative cell viability upon treatment with 1 μM and 5 μM individual compounds, respectively. The diameter of the circle represented the p value from 1 μM compound *vs.* DMSO or 5 μM compound *vs.* DMSO. Each experiment was repeated in triplicates; *P* value was derived from *t* test between DMSO group and drug-treated group.

(B) Validation of the inhibitory effects of the top 20 hits on cell viability in two additional human AML cell lines with high FTO expression, NOMO-1 (left panel) and U937 (right panel). All the cells were treated with 1 μM or 5 μM compounds for 48 hours.

(C) The 2D structure (left panel) and 3D conformer (right panel) of the third compound (NSC 48890).

(D) CS1 forms salt-bridge and hydrogen bonds (shown as grey dots) with E234, and strong π-stacking interaction with H231 of FTO. The catalytic iron atom (yellow ball) and α-ketoglutarate (AKG, green sticks) at the bottom of catalytic pocket are also displayed.

(E) CS2 forms salt-bridge and hydrogen bonds with H231, S229, and K216 of FTO protein.

(F) Occupancy of CS1 at the location of m^6A in the catalytic pocket of FTO protein.

(G) Docking pose of CS1 with FTO protein. According to the structure, CS1 could block the entrance of nucleotide oligos into the catalytic pocket of FTO.

(H) Occupancy of CS2 in the catalytic pocket of FTO protein.

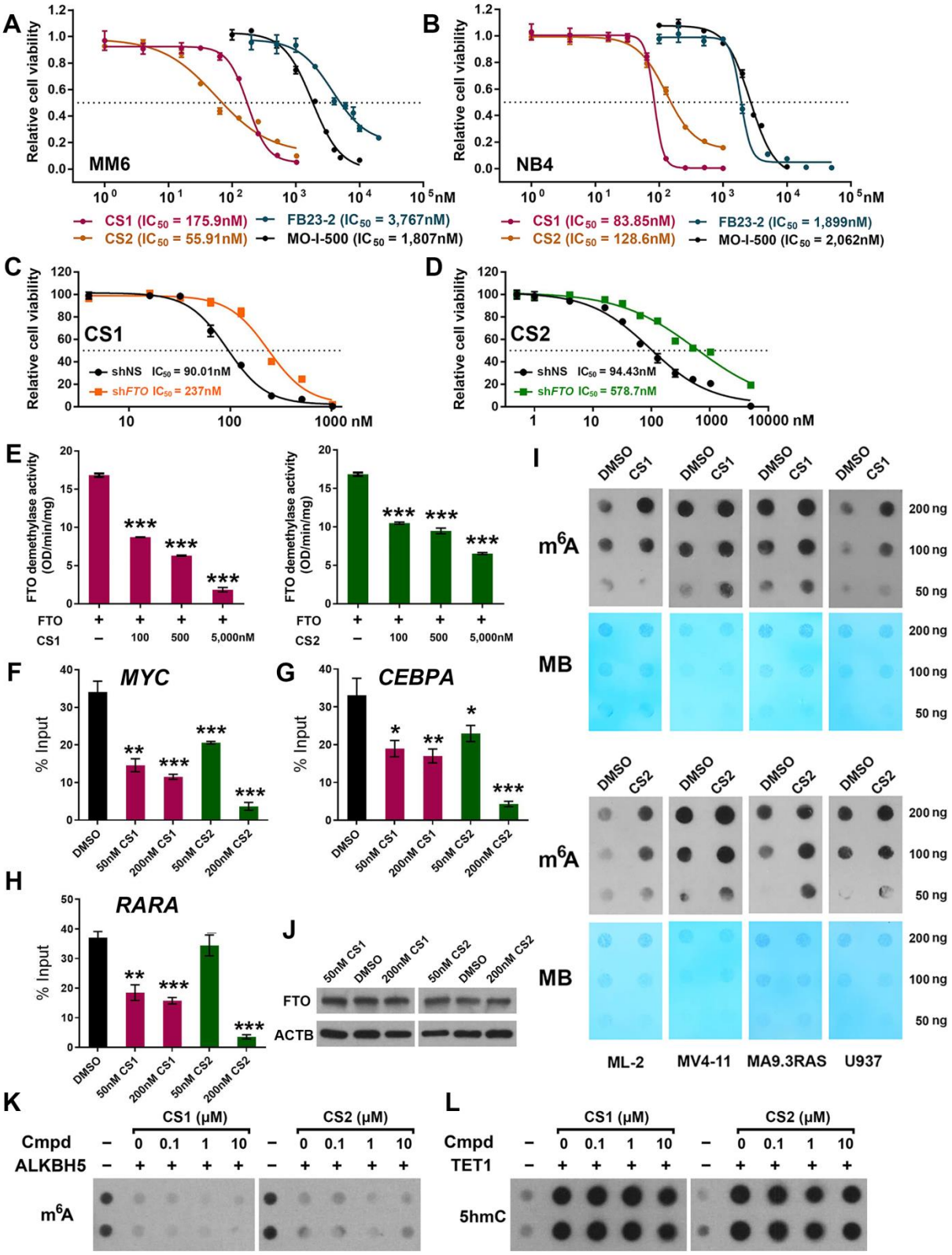

Figure S2. The anti-leukemic effects of CS1 and CS2 are FTO-dependent, Related to Figure 2

(A and B) The IC_{50} values of our in-house FTO inhibitors (CS1 and CS2) and two reported FTO inhibitors (FB23-2 and MO-I-500) on inhibiting cell viability in MONOMAC 6 (A) and NB4 (B) AML cells.

(C and D) Knockdown of *FTO* (sh*FTO*-1) decreased the sensitivity of human AML cells (NOMO-1) to CS1 (C) or CS2 (D) treatment.

(E) The effect of CS1 (left panel) or CS2 (right panel) treatment on enzymatic activity of FTO protein as detected by *in vitro* (cell–free) m^6A demethylation assays.

(F-H) The changes of FTO protein enrichment on its target mRNAs, *MYC* (F), *CEBPA* (G), and *RARA* (H), after CS1 or CS2 treatment as detected by CLIP-qPCR in HEK-293T cells. The cells were treated with 200 nM CS1 or CS2 for 24 hours.

(I) Global m^6A abundance of poly(A)+ RNA isolated from CS1- (upper panel) or CS2 (lower panel) -treated AML cell lines. All the cells were treated with 100nM CS1 or 500nM CS2 for 72 hours.

(J) Protein levels of FTO in HEK-293T cells upon CS1, CS2 or vehicle control treatment for 24 hours.

(K) The effects of CS1 and CS2 treatments on the m^6A demethylase activity of ALKBH5 protein as detected by m^6A demethylation and dot blot assays in a cell-free system.

(L) The effects of CS1 and CS2 treatments on the demethylase activity of TET1 protein as detected by DNA 5hmC demethylation and dot blot assays in a cell-free system.

Values are mean ± SEM, n =3 independent experiments. Two-tailed student *t*-test were used (*, $p < 0.05$; **, $p < 0.01$; ***, $p < 0.001$).

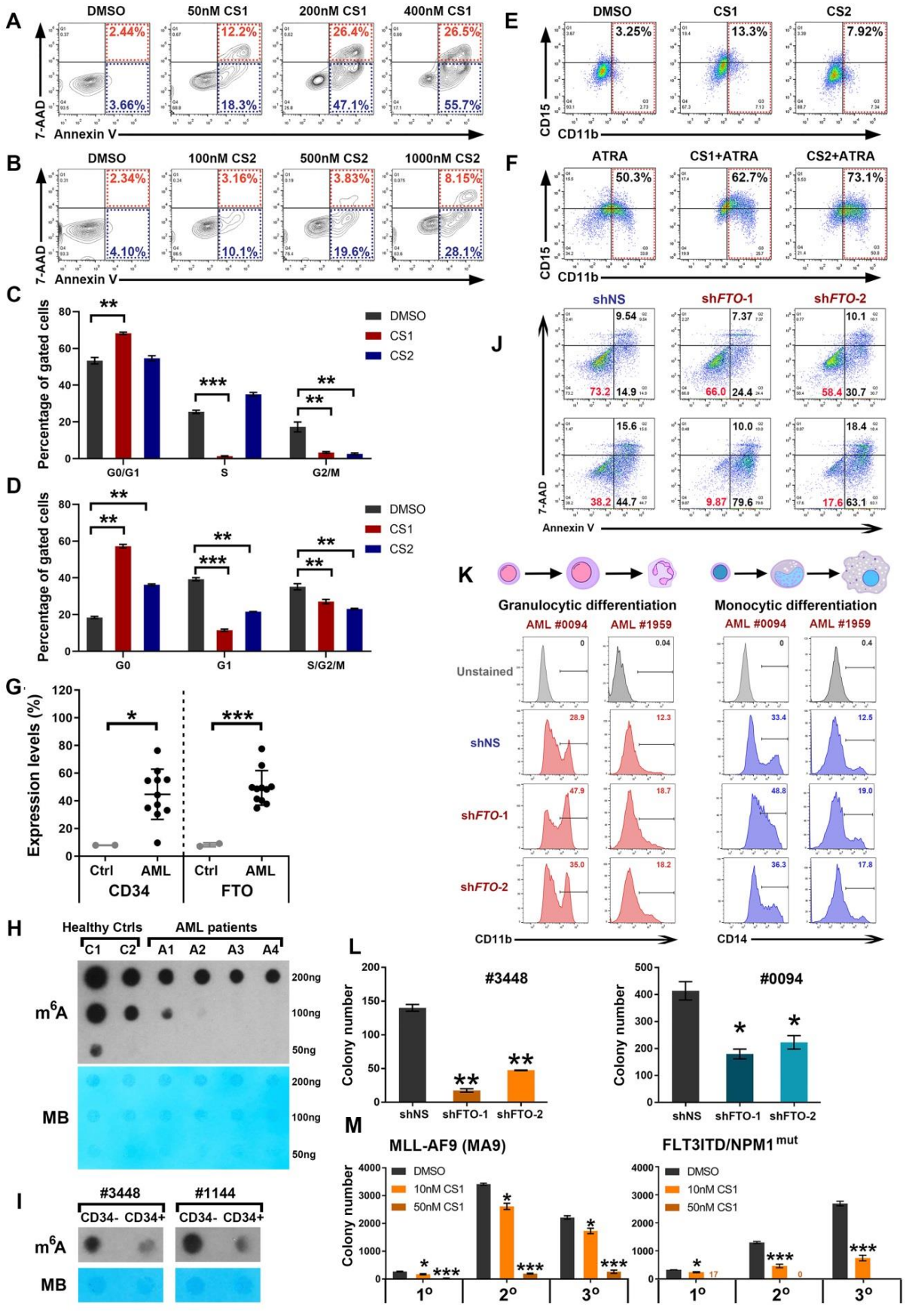
A
DMSO
50nM CS1
200nM CS1
400nM CS1
2.44%
12.2%
26.4%
26.5%
3.66%
18.3%
47.1%
55.7%
7-AAD
Annexin V
B
DMSO
100nM CS2
500nM CS2
1000nM CS2
2.34%
3.16%
3.83%
8.15%
4.10%
10.1%
19.6%
28.1%
C
Percentage of gated cells
DMSO
CS1
CS2
G0/G1
S
G2/M
D
G0
G1
S/G2/M
E
DMSO
CS1
CS2
3.25%
13.3%
7.92%
CD15
CD11b
F
ATRA
CS1+ATRA
CS2+ATRA
50.3%
62.7%
73.1%
J
shNS
shFTO-1
shFTO-2
9.54
7.37
10.1
73.2
14.9
66.0
24.4
58.4
30.7
15.6
10.0
18.4
38.2
44.7
9.87
79.6
17.6
63.1
K
Granulocytic differentiation
Monocytic differentiation
AML #0094
AML #1959
Unstained
shNS
shFTO-1
shFTO-2
CD11b
CD14
G
Expression levels (%)
Ctrl
AML
CD34
FTO
H
Healthy Ctrls
AML patients
C1
C2
A1
A2
A3
A4
m6A
MB
200ng
100ng
50ng
I
#3448
#1144
CD34-
CD34+
L
#3448
#0094
Colony number
shNS
shFTO-1
shFTO-2
M
MLL-AF9 (MA9)
FLT3ITD/NPM1 mut
DMSO
10nM CS1
50nM CS1
1°
2°
3°

Figure S3. The effects of FTO knockdown or inhibition on apoptosis, myeloid differentiation, and self-renewal of LSCs/LICs, Related to Figure 3

(A and B) The effects of CS1 (A) or CS2 (B) treatment on apoptosis in NOMO-1 AML cells. The cells were treated with indicated concentrations of inhibitors for 48 hours.

(C and D) Statistical results for the effects of CS1 and CS2 on cell cycle as detected by PI staining (C) and Hoechst 33342/Pyronin Y staining (D) in NOMO-1 cells.

(E and F) The effect of CS1 or CS2 treatment on myeloid differentiation without (E) or with 200 nM ATRA (F) in NB4 AML cells. The cells were treated with 50 nM CS1 or 100 nM CS2 for 48 hours.

(G) The levels of CD34 and FTO in healthy control and AML patients. The expression of surface CD34 and intracellular FTO were detected by flow cytometry. Healthy controls represent the bone marrow mononuclear cells (BMMNCs) from healthy donors; AML patient samples are BMMNCs from AML patients.

(H) Global m^6A levels of total RNA from the two healthy controls and four AML patient samples (A1: #1144; A2: #3448; A3: #18044; and A4: #2212).

(I) Global m^6A levels of total RNA enriched from $CD34^-$ and $CD34^+$ populations of human primary AML BMMNCs.

(J) Knockdown of *FTO* induced apoptosis in $CD34^+$ blast cells derived from AML patients during granulocytic differentiation (upper panel) or monocytic differentiation (lower panel).

(K) Knockdown of *FTO* promoted G-CSF induced granulocytic differentiation (left panel) and M-CSF induced monocytic differentiation (right panel) of $CD34^+$ blast cells derived from AML patients.

(L) Effects of *FTO* knockdown on the colony-formation capability of $CD34^+$ blast cells derived from AML patients.

(M) The effects of FTO inhibitor treatment on the colony-formation/replating capacity of primary murine AML cells, MLL-AF9 (AF9) (left panel) or FLT3ITD/$NPM1^{mut}$ (right panel) AML cells. Three passages of replating were conducted.

All the *in vitro* experiments were performed at least two times. Data are represented as mean ± SEM. *, $p < 0.05$; **, $p < 0.01$; ***, $p < 0.001$ as assayed by two-tailed student *t*-test.

See also Table S1.

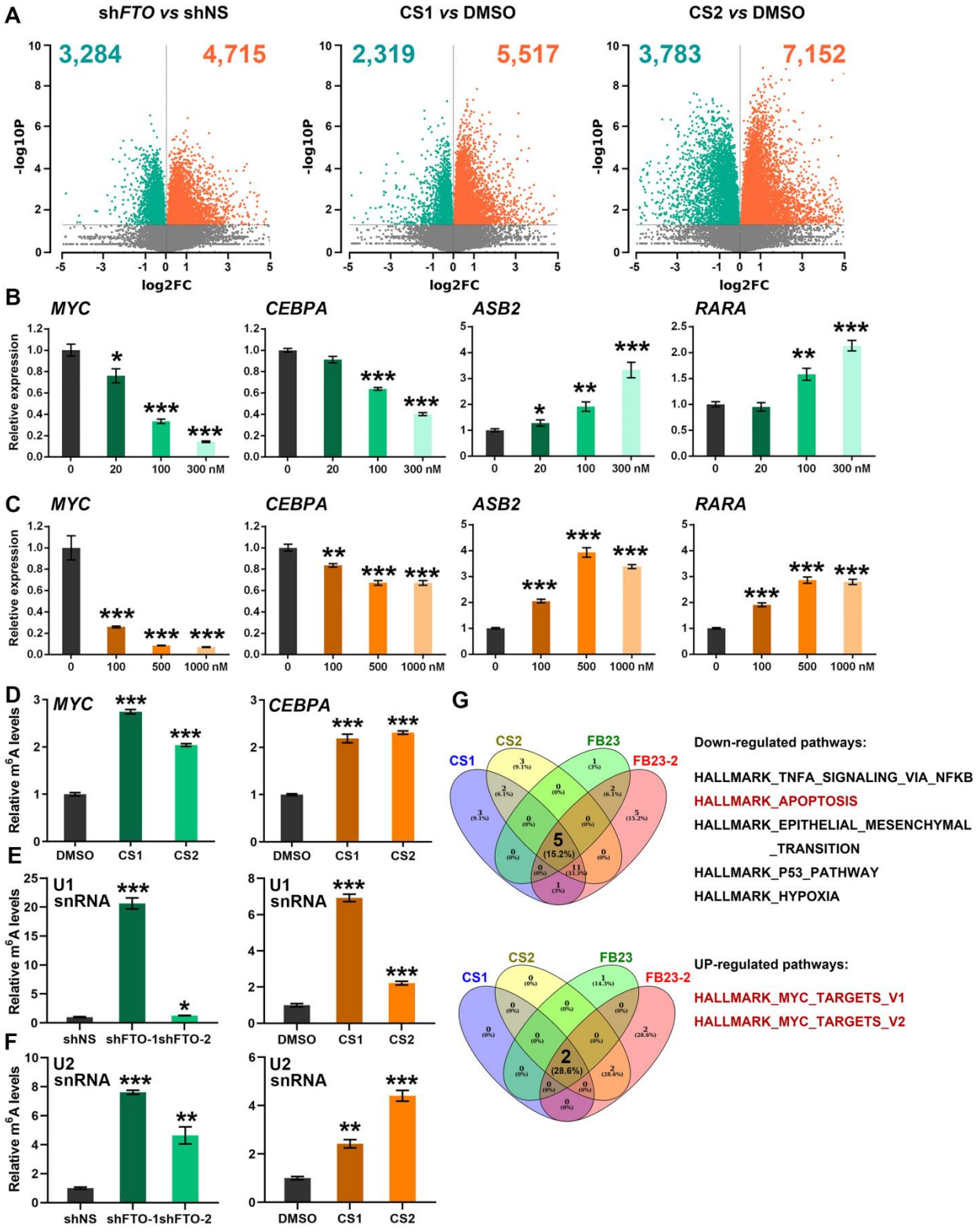

Figure S4. Identification of genes and pathways affected by FTO knockdown and inhibition, Related to Figure 4

(A) Distributions of differential expression levels of core enriched genes in FTO knockdown, CS1 or CS2 treated NOMO-1 cells compared to control cells, respectively. The significantly increased (orange) or decreased (green) genes ($p < 0.05$) are highlighted.

(B) CS1 treatment resulted in gradual decrease of *MYC* and *CEBPA*, as well as increase of *ASB2* and *RARA*. NOMO-1 cells were treated with DMSO, 20, 100, and 300 nM CS1 for 48 hours.

(C) Bar graphs presenting the relative expression of *MYC*, *CEBPA*, *ASB2*, and *RARA* in NOMO-1 cells subjected to DMSO, 100, 500, and 1000 nM CS2 treatment for 48 hours.

(D) The relative m^6A level changes of *MYC* and *CEBPA* mRNA in MONOMAC 6 cells upon CS1 or CS2 treatment. The cells were treated with 100 nM CS1 or 300 nM CS2 for 48 hours.

(E and F) The relative m^6A level changes of U1 (E) or U2 (F) snRNA in MONOMAC 6 cells upon *FTO* knockdown (left panels) or FTO inhibition (right panels). For FTO inhibition, the cells were treated with 200 nM CS1 or 300 nM CS2 for 48 hours.

(G) The overlapped signal pathways induced by CS1, CS2, FB23, and FB23-2 treatment. The core-enriched genes from 'Apoptosis', 'MYC targets V1', and 'MYC targets V2' were listed in Table S2.

Values are mean ± SEM of n =3 independent experiments. Two-tailed student *t*-test was used (*, $p < 0.05$; **, $p < 0.01$; ***, $p < 0.001$).

See also Table S2.

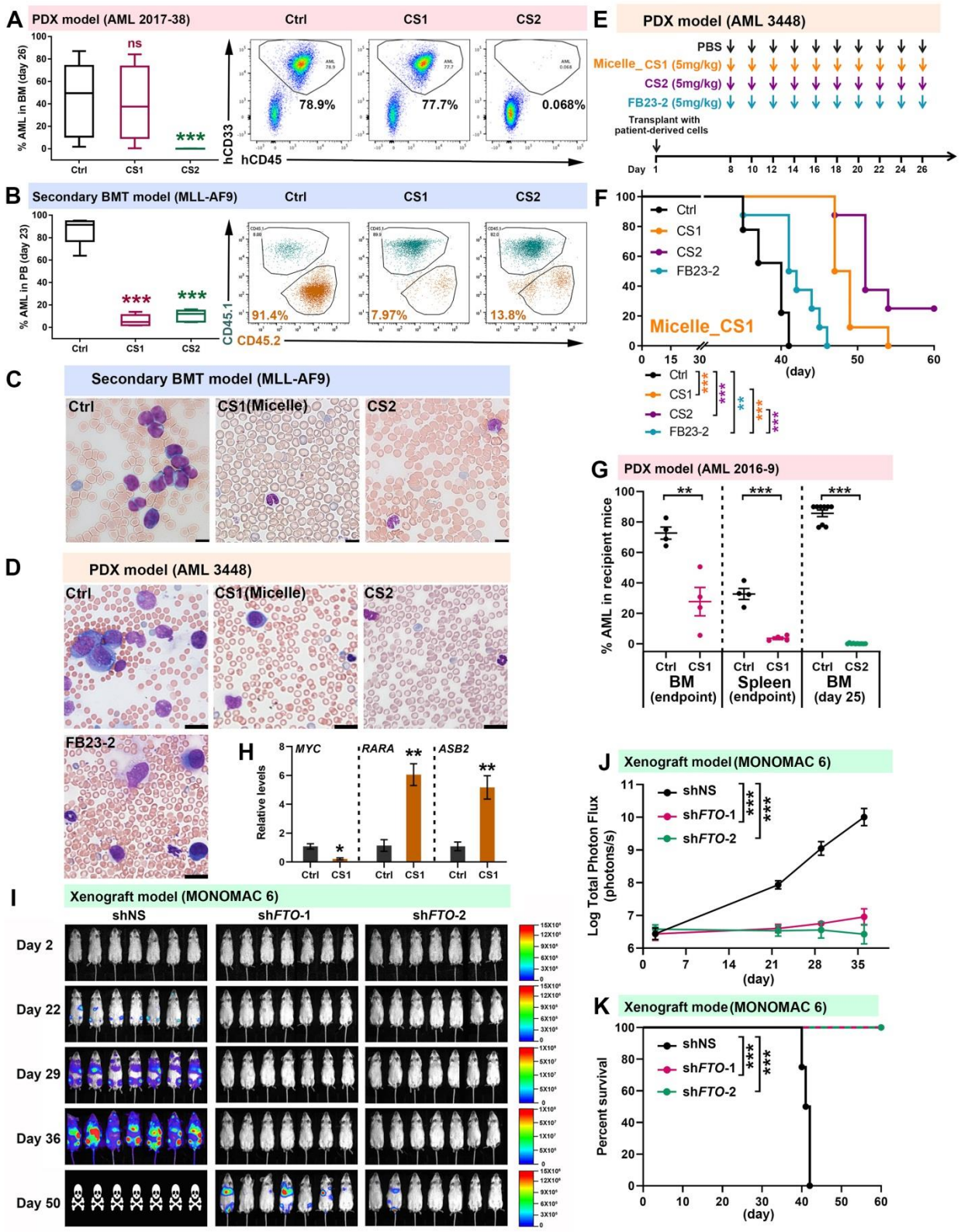

Figure S5. Both FTO inhibition and knockdown suppressed leukemia progression *in vivo*, Related to Figure 5

(A) Engraftment of human AML cells in bone marrow (BM) of patient-derived xeno-transplantation (PDX) recipient mice (NRGS) after treatment with free CS1 or CS2 (5 mg/kg once every other day for 10 times), or vehicle control in PDX mouse model with AML 2017-38. The BM samples were collected on day 26 post xeno-transplantation. The hCD45 and hCD33 double positive cells were utilized to determine the engraftment of human AML cells in recipient mice, and representative flow cytometry data were shown.

(B) Engraftment of murine CD45.2 MA9 AML cells in the peripheral blood (PB) of recipient CD45.1 mice after treatment with Micelle_CS1 and CS2 in the secondary BMT model. The PB samples were collected on day 23 after transplantation. The CD45.2 positive cells were utilized to determine the engraftment of leukemic MA9 cells in recipient mice, and representative flow cytometry data were shown.

(C) Wright-Giemsa staining of PB smears from secondary BMT mice (PB collected on day 29 post transplantation) after the treatment with Micelle_CS1, CS2 or vehicle control. The bar represents 20 μm.

(D) Wright-Giemsa staining of PB smears from PDX (AML 3448) recipient mice (PB collected at their end points) after the treatment with Micelle_CS1, CS2, FB23-2, or vehicle control. The bar represents 20 μm.

(E and F) Diagram of drug treatment (E) and Kaplan-Meier survival curves (F) of PDX with AML 3448 subjected to CS1, CS2, and FB23-2. 1×10^6 MNCs isolated from BM of the AML patient were xeno-transplanted into each individual NRGS recipient mice, and the mice were treated with vehicle control (PBS), CS2, or FB23-2 by i.p., or treated with Micelle_CS1 by i.v.., starting from day 8 post xeno-transplantation.

(G) Engraftment of AML 2016-9 cells in the BM and spleen of NRGS recipient mice upon β-CD_CS1, CS2 or vehicle control treatment. The engraftment of donor AML cells was assessed by flow cytometry with hCD33 and hCD45 antibodies.

(H) The relative expression levels of *MYC*, *RARA*, and *ASB2* in the BMMNCs of PDX model (AML 2016-9) with PBS or CS1 treatment.

(I) Pseudo color bioluminescence images of NRGS mice xeno-transplanted with human MONOMAC 6 AML cells (with or without *FTO* knockdown). Radiance is defined as "photons/second/cm^2/steradian".

(J) Total flux (photons/sec) of the NRGS mice xeno-transplanted with MONOMAC 6 upon *FTO*

knockdown. Signal intensity was quantified from each animal in Figure S5I.

(K) Kaplan-Meier survival curves of xenograft mouse model with MONOMA 6 cells upon FTO knockdown.

For A, B, G, H, and J, **, $p < 0.01$; ***, $p < 0.001$; ns, not significant, as assessed by two-tailed student *t*-test. For survival curves in F and K, the p values were calculated with the log-rank test; **, $p < 0.01$; ***, $p < 0.001$.

See also Table S1

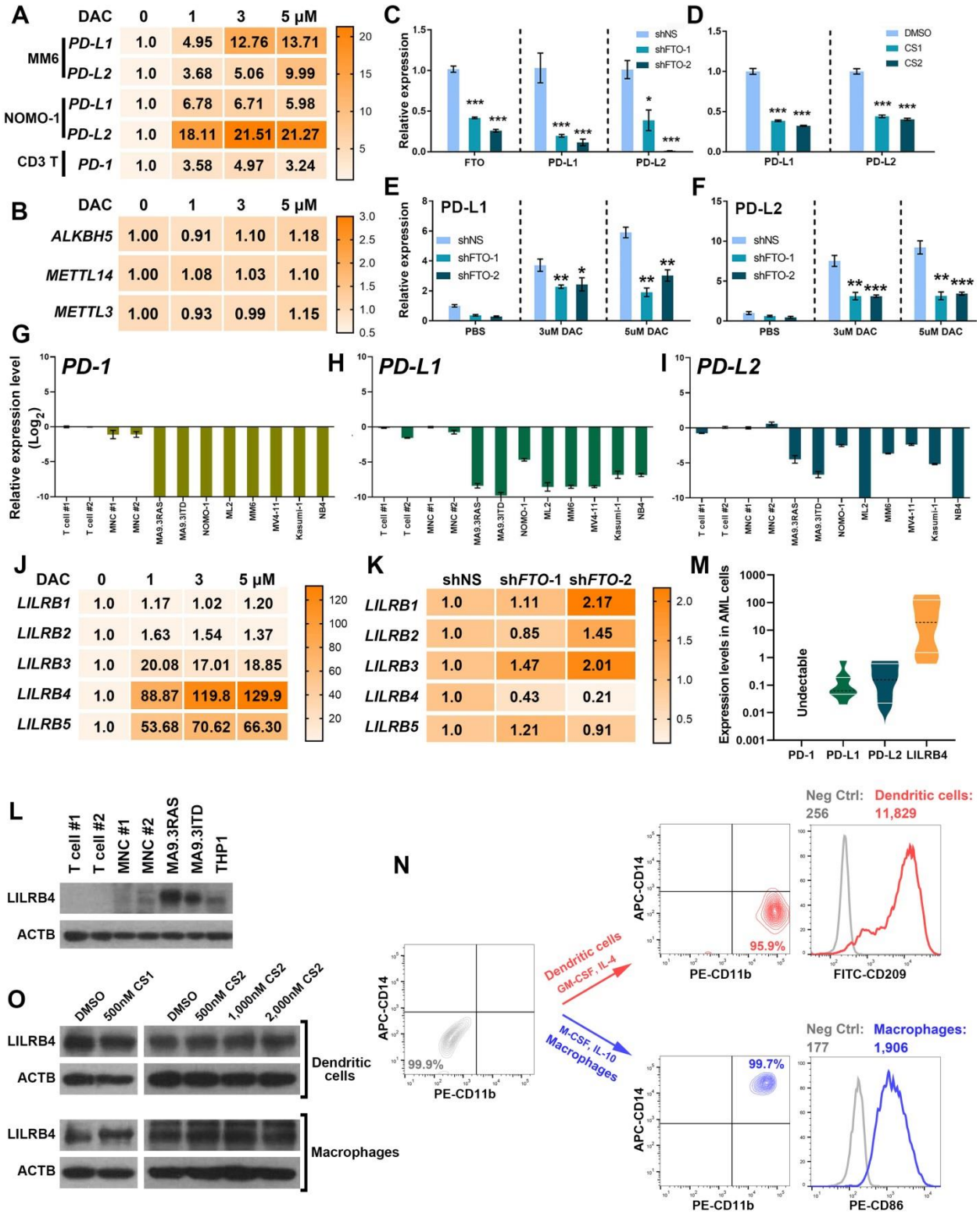

Figure S6. Expression of immune checkpoint genes in AML cells and antigen-presenting cells, Related to Figure 6

(A) Expression level changes of *PD-L1, PD-L2,* and *PD-1* upon DAC treatment for 72 hours in human MONOMAC 6 (MM6) and NOMO-1 AML cells (for *PD-L1* and *PD-L2*), or in human normal CD3 T cells (for *PD-1*).

(B) Expression level changes of *ALKBH5*, *METTL14*, and *METTL3* in MONOMAC 6 cells upon DAC treatment for 48 hours.

(C and D) Expression level changes of *FTO*, *PD-L1* and *PD-L2* in NOMO-1 cells upon FTO knockdown (C), or CS1 or CS2 treatment (D) as detected by qPCR.

(E and F) Expression level changes of *PD-L1* (E) and *PD-L2* (F) in NOMO-1 cells (with or without *FTO* knockdown) upon DAC treatment.

(G-I) Relative expression levels of *PD-1* (G), *PD-L1* (H), and *PD-L2* (I) in CD3 T cells, healthy MNCs, and AML cell lines as detected by qPCR, with *ACTIN* as endogenous control. The expression levels of *PD-1* in CD3 T cells, as well as those of *PD-L1* and *PD-L2* in MNC #1, were set as 1, and then the given gene's levels in other samples were normalized accordingly; then all the values were $\log_2$ transformed. Values lower than -10 shown in G and I indicate that the expression level of the given gene in the relevant samples is below detectable limits (Ct value larger than 35 in the qPCR assay).

(J) Heat map showing the relative expression level changes of the *LILRB* family members in NOMO-1 AML cells upon DAC treatment for 72 hours.

(K) Heat map showing the expression level changes of the *LILRB* family members in NOMO-1 AML cells upon *FTO* knockdown.

(L) Protein levels of LILRB4 in normal T cells, normal MNCs, and AML cells.

(M) Expression levels of *PD-1*, *PD-L1*, *PD-L2*, and *LILRB4* in the human AML cell lines (shown in G-I) as detected by qPCR. The ($2^{-\Delta Ct}$*10,000) values were shown.

(N) Generation of dendritic cells and macrophages from CD14+ PBMNCs.

(O) Protein levels of LILRB4 in dendritic cells and macrophages with or without CS1 or CS2 treatment for 72 hours.

Values are mean ± SD of n =3 independent experiments. Two-tailed student *t*-test was used for statistical analyses. *, $p < 0.05$; **, $p < 0.01$; ***, $p < 0.001$.

A

Gene	PBS	CS1
Lilrb4	741.24	418.54
Lgals9	127.4	116.735
Cd80	22.71	24.685
Cd86	13.55	9.685
Cd274 (Pdl1)	12.925	6.18
Pdcd1lg2 (Pdl2)	0.565	0.395
Tnfrsf9	0.54	0.01
Cd276	0.13	0.145
Vtcn1	0.035	0.01

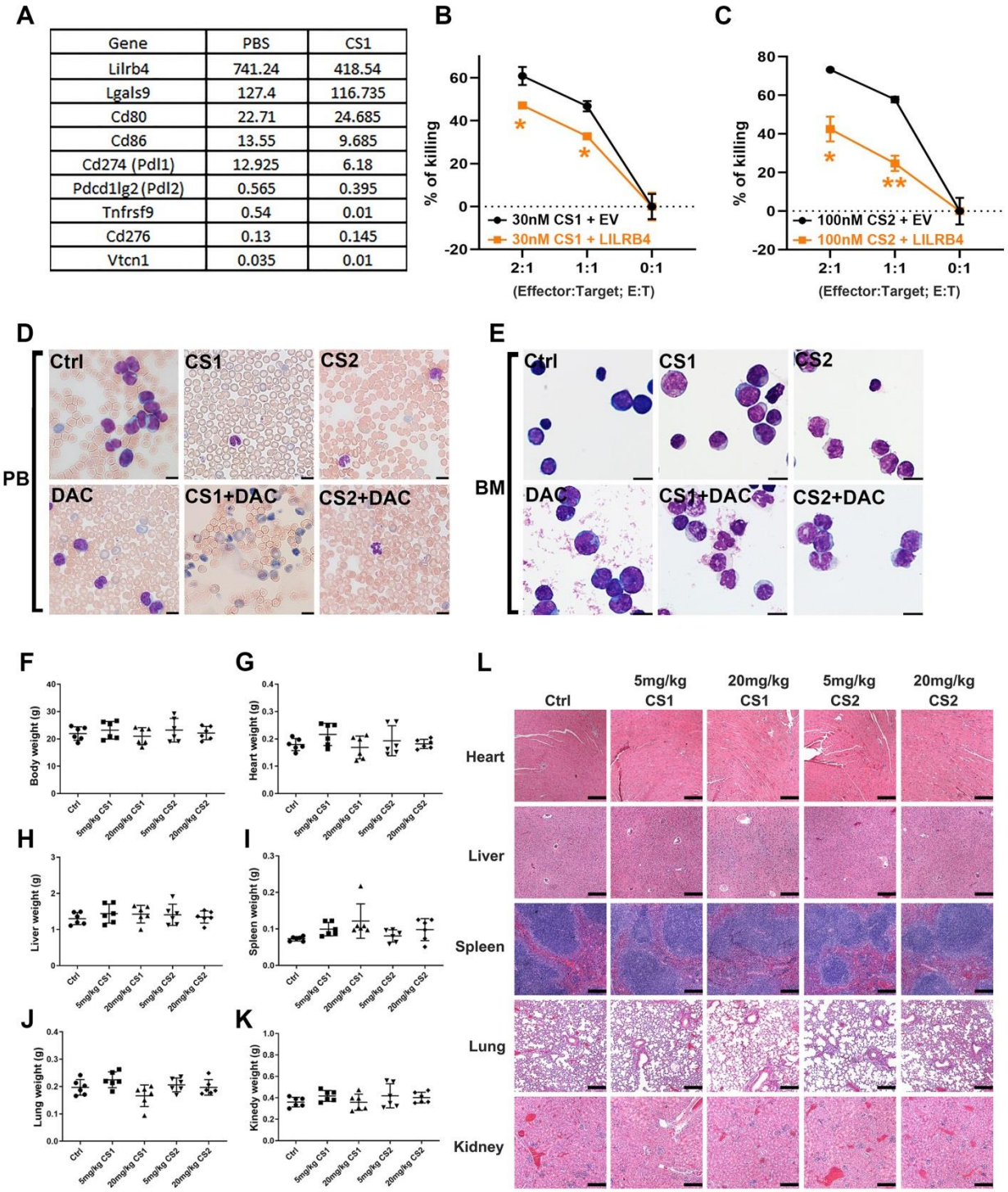

Figure S7. The effects of FTO inhibitors on immune response and the toxicity of FTO inhibitors, Related to Figures 7 and 8

(A) The normalized expression of immune checkpoint genes in the $CD45.2^+$ spleen MNCs isolated from MA9 AML-bearing (B6.SJL; CD45.1) mice after treatment with PBS or β-CD_CS1.

(B and C) The effects of LILRB4 on T cell killing of NOMO-1 cells pre-treated with CS1 (B) or CS2 (C).

(D and E) Wright-Giemsa staining of PB smears (D) and BM smears (E) collected from secondary BMT AML mice treated with CS1, CS2, DAC, CS1+DAC, CS2+DAC, or vehicle control. Scale bar represents 10 μm.

(F-K) The weight of whole body (F), heart (G), liver (H), spleen (I), lung (J) and kidney (K) of C57BL/6 mice from drug toxicity test. For this assay, the C57BL/6 mice (6 mice/group) were treated with PBS, 5mg/kg β-CD_CS1, 20mg/kg β-CD_CS1, 5mg/kg CS2, or 20mg/kg CS2 following the same strategy in AML treatment (i.e., treated every other day for a total of 10 times). All the mice were euthanized simultaneously 10 days after the full treatment.

(L) Haemotoxylin and Eosin (H&E) staining of the organs from vehicle control-, CS1-, and CS2-treated groups. Scale bar represents 200 μm.

For B and C, values are mean ± SEM. Two-tailed student *t*-test was used for statistical analyses. *, $p < 0.05$; **, $p < 0.01$.

See also Table S3.

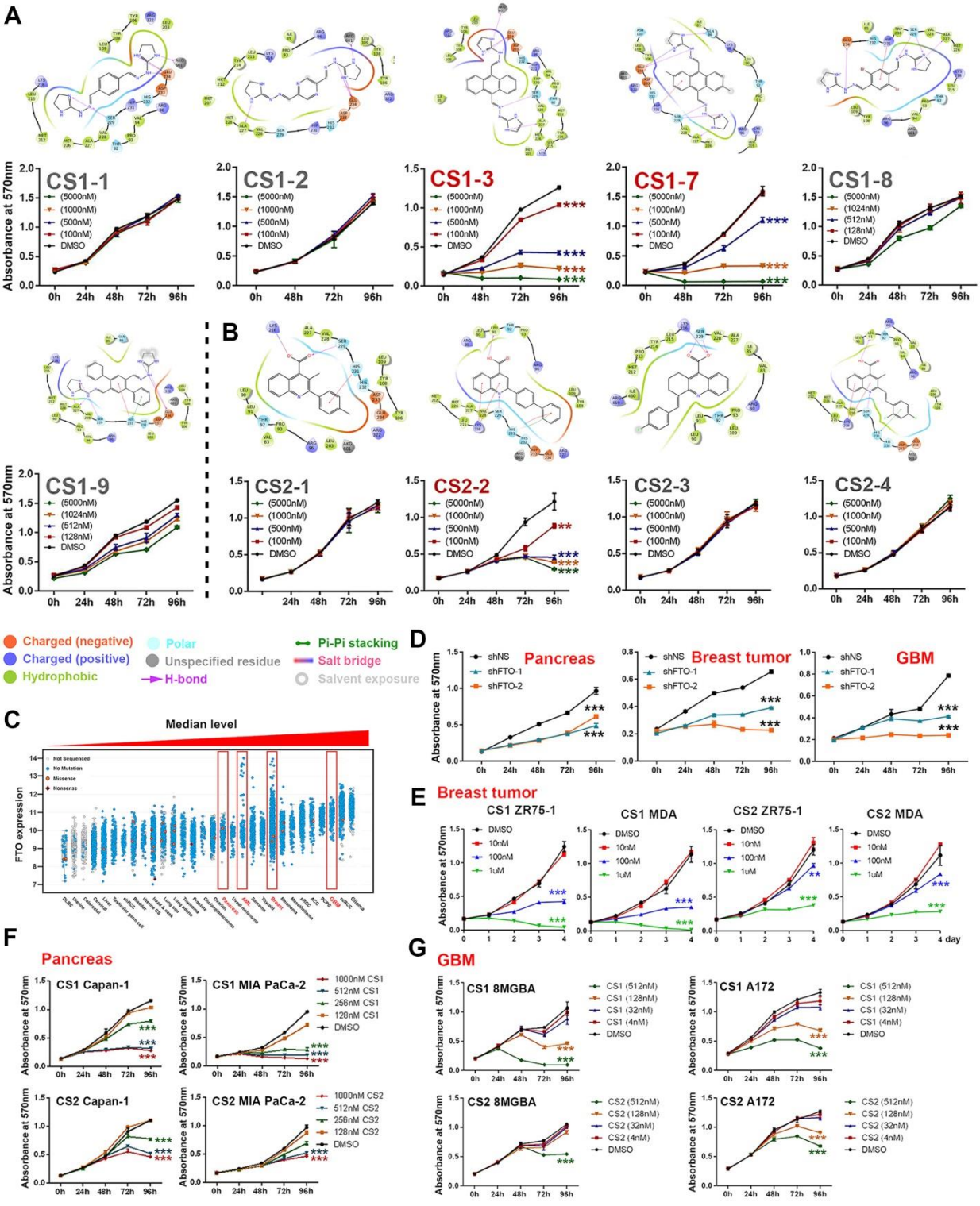

Figure S8. The SAR study of CS1 and CS2, and the anti-tumor effects of FTO inhibitors in solid tumors, Related to Figure 8

(A) The 2D ligand interaction diagrams for the six synthesized CS1 analogs (upper panel) and

also their effects on the growth/proliferation of MONOMAC 6 AML cells (lower panel).

(B) The 2D ligand interaction diagrams for the four synthesized CS2 analogs (upper panel) and also their effects on the growth/proliferation of MONOMAC 6 AML cells (lower panel).

(C) Expression levels of *FTO* in various types of cancers (adopted from cBioPortal for Cancer Genomics (http://www.cbioportal.org/)). pRCC, Papillary Renal Cell Carcinoma; DLBC, Diffuse Large B-cell Lymphoma; GBM, Glioblastoma Multiforme; ACC, Adrenocortical Carcinoma; PCPG, Pheochromocytoma and Paraganglioma; ccRCC, Renal Clear Cell Carcinoma; chRCC, Chromophobe Renal Cell Carcinoma.

(D) The effects of *FTO* knockdown on cell growth/proliferation of human solid tumor cell lines, including MIA PaCa-2 (pancreatic cancer), MDA-MB-231 (MDA, breast cancer), and A172 (GBM).

(E-G) The effects of CS1 and CS2 treatments on the growth/proliferation of breast cancer cells (E), pancreatic cancer cells (F), and GBM cells (G).

Values are mean ± SEM of n =3 independent experiments. Two-tailed student *t*-test was used (**, $p < 0.01$; ***, $p < 0.001$).